CHARACTERIZATION OF MICROPOROSITIES AND LOAD-INDUCED INTERSTITIAL FLUID MOVEMENT IN NORMAL AND OSTEOPENIC BONE

by

CESARE CIANI

A dissertation submitted to the Graduate Faculty in Engineering in partial fulfillment of the requirements for the degree of Doctor of Philosophy, The City University of New York
2008

This manuscript has been read and accepted for the Graduate Faculty in Engineering satisfaction of the dissertation requirement for the degree of Doctor of Philosophy

Date	Professor Susannah P. Fritton, Ph.D. Chair of Examining Committee
Date	Professor Mumtaz Kassir, Ph.D. Executive Officer

Stephen C. Cowin, Ph.D.

Ali M. Sadegh, P.D.

Sheldon Weinbaum, Ph.D.

Stephen B. Doty, Ph.D.

Supervision Committee

THE CITY UNIVERSITY OF NEW YORK

Abstract

CHARACTERIZATION OF MICROPOROSITIES AND LOAD-INDUCED INTERSTITIAL FLUID MOVEMENT IN NORMAL AND OSTEOPENIC BONE

By

Cesare Ciani

Advisor: Professor Susannah P. Fritton

It is believed that load-induced bone interstitial fluid flow activates osteocytes, which are involved in the perception and transduction of external mechanical stimuli. Interstitial bone fluid movement induced by external loads also enhances the metabolic exchange of nutrients and waste products in the lacunar-canalicular network surrounding osteocytes. In the present work three experimental studies are presented to increase our understanding of the interstitial fluid pathway and the effect of load-induced fluid flow on bone. To clarify bone's interstitial fluid pathway, the reported ability of the tracer ferritin to form halo-shaped labeling in the mineralized matrix around blood vessels was challenged and proven to be an artifact originated by histological processing techniques. Bone interstitial space and fluid movement was then characterized to determine the effect that conditions such as osteoporosis and external loading might provoke. Using a new staining technique to characterize bone interstitial space, we found that the lacunar-canalicular porosity of cancellous bone in the proximal tibia and the canalicular diameter of ovariectomized (OVX) rats were greater compared to control (CTRL). We also detected microstructural changes in the rat proximal tibia following OVX and found that higher mineralized bone regions had a more disconnected canalicular network, while

lower mineralized bone regions had higher canalicular density. Finally, the combined effect of OVX and application of an external non-invasive mechanical load resulted in enhancement of injected tracer transported to osteocyte lacunae in the cancellous bone of the rat proximal tibia. The increased tracer movement may be related not only to the applied loading, but also to the canalicular widening occurring after the development of osteopenia due to OVX. The increased lacunar-canalicular porosity might disrupt the tethers between the osteocyte and the lacunar-canalicular wall, resulting in a reduced capability of estrogen-depleted animals to respond to mechanical stimuli. The bone microporosity measurements, the effect of ovariectomy and loading on transport through the lacunar-canalicular network, along with the ferritin findings will contribute to a better understanding of the effect of osteoporosis on bone morphology and on the efficiency of bone's mechanosensory system.

ACKNOWLEDGMENT

The last seven years spent at The City College of New York and at Hospital for Special Surgery have been the most exciting of my life. I have grown scientifically and personally, realizing myself as researcher, husband and father.

For these reasons I want to thank and express timeless gratitude to my mentor, Professor Susannah Fritton, who has been always been professionally impeccable and she made feel like I never left home. She is simply the best! A special thank also to my other mentor, Doctor Stephen Doty, who taught me and lead through the difficult process of becoming a real scientist.

Last but not least, I want to thank my family, la mia mamma (my mum), il mio babbo (my dad), e mia sorella barella (my syster), for being always near me. A special thank to my wife, Francesca, and my son, Giulio, whose have always sustained me with their strength and love.

Table of Contents

List of Tables

List of Illustrations and Diagrams

Chapter 1

Introduction

1.1. Bone Structure, Porosities, and Function

Bones are porous, composite, and extremely dense connective tissues that, in various shapes and sizes, constitute the skeleton (Figure 1-1). The composite nature of bone, a blend of proteins embedded in mineral crystals, makes it one of the hardest structures in the body, providing elasticity and both strength and resilience. There are two types of bone: cortical or compact bone and trabecular or cancellous bone. Cancellous bone (20% of the total bone mass) is a complex mesh of short and parallel struts that help bone maintain its shape. It is found in the epiphyseal and metaphyseal regions of long bones and in the interior of short bones. Cortical bone is present in every bone of the body and functions as a protective outer shell and also provides strength in the bone regions more subjected to bending (Figure 1-2).

The turnover for these two types of bone, a process associated with bone resorption and deposition, depends upon several factors such as hormone levels, age, gender, and external stimuli; it is realized by the four cell types that live in bone tissue: osteoclasts, osteoblasts, osteocytes and bone lining cells. Osteoclasts are giant cells dedicated to bone resorption, while osteoblasts are the cells primarily involved in bone formation. During the formation of new bone, some osteoblasts are trapped in the secreted collagen apatite matrix and become osteocytes. Osteocytes are the only cells completely embedded in the mineralized bone matrix, and they seem to be the best candidates for the preservation of tissue health by sensing and transducing external stimuli (e.g., the presence or absence of mechanical loading) via signals that can initiate either bone formation or resorption [1, 2]. Bone lining cells are former osteoblasts present on all bone surfaces. They have been proposed to regulate bone fluid and flux of ions between the vascular canals and the

interstitial fluid in the lacunar-canalicular system; they have also been proposed to be responsible for activating bone remodeling in response to signals from osteocytes or hormones and to be involved in the mechanotransduction of external stimuli in cancellous bone [3-7].

The basic element of cortical bone in many animals is the osteon, also called the Haversian system, although some animals (e.g., rats, mice) present only primary bone structure and consequently do not have secondary osteons. However, primary bone and osteonal bone have many similar features (Figure 1-3). An osteon is a concentric structure of lamellae of approximately 100-150 μm in radius [8-10] often running approximately parallel to the long axis of the bone, with a semi-permeable outer limit called the cement line that delineates the boundary of the osteon. At the center of each osteon there is a vascular canal, also referred to as the Haversian canal, filled with interstitial fluid and containing one or more blood vessels and nerves.

In osteonal bone, osteocytes are contained in lacunae located in a circumferential fashion in different lamellae around the Haversian canal. Lacunae are connected to each other by tunnels, called canaliculi, whose function is to host the osteocyte processes (Figure 1-3a). In primary bone, which lacks the highly organized structure of osteonal bone, blood vessels and osteocytes are more randomly distributed throughout the bone, with the former still connected via the canalicular system, which drains into vascular pores similar to Haversian canals (Figure 1-3b). This terrific network of canaliculi allows the osteocytes to communicate with each other via gap junctions located at the tips of the osteocyte processes (Figure 1-4).

The bone hierarchical architecture gives rise to three different levels of porosity, namely the vascular porosity, the lacunar-canalicular porosity, and the collagen-apatite porosity of the mineralized matrix. Even though most of the struts of trabecular bone lack the larger porosity, they are surrounded by a rich blood environment, the bone marrow, which provides the same function of Haversian canals in osteons. The vascular porosity is associated with the blood vessel dimension, and it is the largest of the three bone porosities, with reported dimensions of 20 - 50 μm in diameter for both primary and secondary bone [8]. The lacunar-canalicular porosity includes the space surrounding the osteocytes in the lacunae and the canaliculi (order 100 nm) [11]. Within the canaliculi tethering elements and conical structures that protrude from the canalicular wall keep the osteocyte processes in position, connecting them to the canalicular wall and preventing them from collapsing [12-14]. The fiber matrix spacing is believed to be approximately 7 - 8 nm, similar to the surface glycocalyx on endothelial cells, and the fiber matrix has been proposed to work as a sieve, allowing only molecules smaller than the pore diameter to pass through it [13, 15, 16]. The smallest bone porosity is the collagen–apatite porosity associated with the space between the collagen fibers and the crystallites of mineral apatite. The dimensions of this porosity have not been well characterized, and there is contradictory evidence from tracer studies as to whether molecules smaller than 10 nm can pass into the mineralized matrix [17-22]. The vascular and the lacunar-canalicular porosities are filled with mobile interstitial fluid, while it is believed that the water in the collagen-apatite porosity is bound to calcium crystals and for this reason is fixed to the mineral matrix [23, 24].

Bone porosity has a significant effect on the mechanical and physical properties of bone, with small changes in porosity inducing significant changes in the material properties, such as stiffness and strength, for both compact and cancellous bone [25-28]. Measurements of human, canine, and rat bone have found the vascular porosity to range from 1.5 to 6% and the lacunar-canalicular porosity to range from 2 to 5%, with the overall cortical bone porosity estimated to be approximately 9% [29, 30]. However, recent studies quantifying the 3-D microstructure of the osteocyte lacunar-canalicular system observed that the lacunar-canalicular network is quite extensive in the mineralized bone volume, raising the possibility that previous studies might have underestimated the interstitial fluid porosity [31, 32]. Accurate porosity measurements are important for determining realistic bone permeability values that can be used in poroelastic models that assess the response of bone to mechanical loading.

1.2. Bone Interstitial Fluid Flow

The role of interstitial fluid flow in the process of bone adaptation is still unclear and not well characterized. When bone is mechanically loaded fluid pressure gradients are induced through bone pores, creating a load-induced interstitial fluid displacement throughout bone porosities [33]. The movement of load-induced interstitial fluid in the lacunar-canalicular porosity is thought to play an important role in bone's mechanosensory system either by activating bone cells via shear stresses [2, 13, 34] or, as revealed in more recent studies, by cytoskeletal deformations induced by the deflection of the physical attachments that connect osteocyte processes to the canalicular walls [12, 14, 35]. In addition, interstitial fluid flow grants exchange of nutrients and solutes and

transports metabolic waste products from the osteocytes embedded in the lacunar-canalicular network [36].

To demonstrate mass transport in the lacunar-canalicular system, several groups have performed experiments involving the injection of different sized tracers in vivo. This method gives an indirect measurement of bone porosity by tracking the injected molecules via histological preparation of bone samples. Many different tracers such as procion red (300-400 Da, diameter < 1 nm), reactive red (1470 Da, diameter ~1 nm), microperoxidase (1860 Da, diameter ~2 nm), horseradish peroxidase (40 kDa, diameter ~6 nm), bovine serum albumin (67 kDa, diameter ~7 nm), ferritin (440 kDa, diameter ~12 nm), and different sized dextrans (range 300 Da - 2000 kDa, diameter ~1 nm - 60 nm) have been used to determine the pore dimensions of the lacunar-canalicular and collagen-apatite porosities (Table 1-1) [17-22, 37-43]. However, the different results among the investigations are still a cause of debate. Knothe Tate et al. [19] and Tami et al. [21] report that two very small tracers, procion red and microperoxidase, behave differently. Knothe Tate et al. [19] found the smaller of the two molecules, procion red, confined to the lacunar-canalicular porosity, while the larger microperoxidase formed discrete bands within the collagen-apatite porosity. Tami et al. [21] instead showed that procion red was able to penetrate the collagen-apatite porosity. In similar studies Knothe Tate et al. [18] and Wang et al. [22] report the presence of small tracers (< 3 nm) only in the vascular and lacunar-canalicular porosities, confirming the results described by the visualization of horseradish peroxide and microperoxidase by Doty and Schofield [40], Tanaka and Sakano [42], Dillaman et al. [39], and Ayasaka et al. [37].

Even more controversial are the results from experiments using ferritin as a tracer. Our previous tracer studies indicate that ferritin injected into rats is confined to the bone blood vessels and does not pass into the collagen-apatite porosity [22]. However, other investigators have shown that ferritin forms halo-shaped labeling that appears to enter the mineralized matrix around blood vessels, along with appositional fronts along the bone surfaces (Figure 1-5) [20, 38, 41, 44]. This ferritin labeling is widely used to explain normal interstitial fluid movement in bone: the halos are said to demonstrate bulk centrifugal interstitial fluid movement away from a highly pressurized vascular porosity, and the appositional fronts are said to demonstrate centrifugal interstitial fluid movement from the medullary canal to the periosteal surface [20, 34, 38, 39, 41, 44-46].

Injection of different sized tracers has also become a valuable methodology to study the differences in solute transport when a mechanical load is applied to bone. This method allows the application of different types of loading at different frequencies to mimic different loading situations, and at the same time provides the tracking of the solutes subjected to the load. Recent in vivo experiments have studied how tracers move in the different bone porosities during a load application [18, 21, 44]. These studies, where one limb is cyclically loaded while the contralateral limb serves as control, need to be clarified and verified because of the conflicting results regarding similar sized tracer distribution. Mak et al. [44] did not report the presence of ferritin (~ 12 nm diameter) in the canalicular porosity, but they did report the presence of ferritin halos in the mineralized matrix, for both the loaded and unloaded limbs, showing an increase of the ferritin transudation distance from the blood vessels for the loaded limb. Knothe Tate et al. (2000) showed a load enhancement of small tracer transport (procion red, ~ 1 nm

diameter, and microperoxidase, ~ 2 nm diameter), resulting in a higher number of labeled lacunae when comparing loaded and unloaded limbs. The tracer distribution was reported to be loading mode dependent as well, decreasing with increasing the loading frequency. Tami et al. [21] reported a qualitative increase of the labeled osteocyte lacunae for the loaded limb when compared to the unloaded; the study also presented a molecular sieve cut-off for the lacunar-canalicular porosity for probes bigger than 10 kDa (approximately 5 nm in diameter).

Because of the contradictory evidence in the literature regarding different sized tracers studies and to demonstrate the real fluid pathway through bone porosities, it is necessary to study more accurately the movement of ferritin in bone, and further delineate bone interstitial fluid flow in vivo to determine the largest size molecule that can penetrate the lacunar-canalicular porosity (in the range of 6 - 12 nm). In addition the tracer injection technique can be used to evaluate the tracer distribution in osteoporotic animal models, providing direct information about the influence and effect that osteoporosis has on bone interstitial fluid displacement.

1.3. Bone Cell-Fluid Flow Interaction

As proposed by Weinbaum et al. [13], osteocytes are believed to be coated with a matrix of proteoglycan, which is thought to be fundamental for the mechanotransduction of load-induced fluid flow (Figure 1-6). Accurately developed hierarchical models have been used to demonstrate that the fluid movement in the canalicular network induces a deflection of the transverse fibers and conical protrusions that link the processes to the canalicular wall [12], and a partial reorganization of the actin filaments in the osteocyte processes should occur.

In vitro experiments have applied fluid flow to bone cells, both osteoblasts and osteocytes, to study how interstitial fluid flow affects these cells [47-50]. Ajubi et al. [47] tested the production of PGE_2 for osteocytes and osteoblasts derived from fetal chick calvariae with normal and disrupted actin filaments, when a pulsating fluid flow with maximal intensity of 5 dyn/cm^2 was applied. After 5 minutes of pulsating flow osteocytes and osteoblasts with intact actin filaments showed an increase of PGE_2 production of 4.5 fold and 1.3 fold higher than the control cells, respectively. The disruption of the actin filaments prevented the production of PGE_2 for both cell types when subjected to pulsating fluid flow, leading to the conclusion that actin filaments are actively involved in bone mechanotransduction. In a similar study, Pavalko et al. [50] analyzed the role in mechanical signaling of actin filaments and their attachment to integrins in osteoblast-like cells subjected to a constant flow rate of 12 dyn/cm^2. After being subjected to fluid shear stress for 1 hour, the actin filaments of osteoblasts became highly organized into thicker and more abundant stress fibers, and the production of the enzyme COX-2 increased 2.7-fold. The disruption of actin filaments inhibited the expression of COX-2 and the ability to induce reorganization of the actin filaments. The results of this experiment, the enhanced expression of the enzyme COX-2, correlated with changes in the organization of the cytoskeleton actin filaments, sustaining the hypothesis that the reorganization of actin filaments plays a critical role in the mechanotransduction of fluid shear stress. Kamioka et al. [49] studied actin binding proteins (e.g., α-actin, myosin, fimbrin) of osteocytes and osteoblasts with and without exposure to fluid flow. For a period of 30 minutes, cells were exposed to a steady fluid flow that produced a constant shear stress of 12 dyn/cm^2. The stress produced by the fluid flow stimulated in the

osteoblasts a reorganization of fimbrin at the end of the stress fiber, which appeared to be linear and thicker when compared to the controls. Also osteoblasts treated with fluid flow underwent contraction and lost contact with neighboring cells. Interestingly, osteocytes did not show any morphological change even after being exposed to shear-induced fluid flow.

The results of the studies just examined do not specify if the glycocalyx, the gel-like fiber matrix proposed to cover the surface of osteocytes and osteoblasts, has a role in bone mechanotransduction. The importance of this gel-like fiber matrix was investigated by Reilly [51]. MC3T3-E1 osteoblastic cells and MLO-Y4 osteocytic cells, coated and depleted of the glycocalyx fiber matrix, were subjected to oscillating fluid flow; the transient increases in intracellular calcium and PGE_2 release were both examined. The results of these experiments indicated the effective presence of a proteoglycan coat on both cell types, and that the depleted cells were unable to increase the production of prostaglandin E_2 when subjected to shear stress via fluid flow. The release of intracellular calcium increased in response to the fluid flow, but its production was not dependent upon the presence of the glycocalyx on the cell surfaces. This work is important because it shows the effective presence of a gel-like fiber structure, similar to the endothelial cell glycocalyx matrix, on the surface of osteocytes and osteoblasts, and confirms the hypothesized role of the hyaluronic acid rich glycocalyx coating matrix in the mechanotransduction pathway.

1.4. Osteoporosis and Animal Model of Osteoporosis

Osteoporosis is a clinical condition characterized by skeletal fragility that affects women more than men, in which the normal bone remodeling process is skewed toward bone resorption, with a net decreased bone mass balance. Currently in the U.S. 8 million women and 2 million men suffer from osteoporosis [www.nof.org], and approximately half of women and one-fourth of men aged 50 years or older will experience an osteoporosis-related fracture within their lifetime [52]. The most common cause of osteoporosis is the reduced presence of estrogen that women experience during menopause. The bone resorption is upregulated by the capability of estrogen to regulate cytokines needed to recruit osteoclasts, the bone resorbing cells.

The need to find a remedy for osteoporosis spurred the creation of several animal models that attempt to mimic this bone condition. An animal model of postmenopausal bone loss has to be identified as an animal where the characteristics of bone loss and the pathogenesis of the osteoporosis condition mimic those expressed by postmenopausal women as close as possible. A variety of animal models, such as primates, dogs, rats and mice, rabbits, and sheep, have been used in the study of osteoporosis, and every species has shown strengths and weaknesses.

Dogs have generally been used as a model for the human skeleton because of the secondary osteonal structure, and their capacity of Haversian remodeling. However, despite these skeletal characteristics, the dog model of osteoporosis has been demonstrated to be not completely reliable, showing bone loss and no bone changes following ovariectomy [53-55]. Sheep, on the contrary, have lately become a very interesting model for osteoporosis. They posses skeletal turnover similar to humans, and

respond to ovariectomy with a significant decline of the iliac crest cancellous bone volume as well as bone loss in the lumbar vertebrae [56, 57].

The rat provides a useful and well-established model to investigate the effect ovariectomy produces in bone. This type of animal can only develop osteopenia via surgical removal of the ovaries, but the resulting changes in bone architecture and bone loss are very similar to those experienced by women in their initial period of osteoporosis development, such as greater loss of cancellous than cortical bone, medullary area expansion, and resorption exceeding formation [58, 59]. In the first five weeks following ovariectomy rats experience a very rapid loss of trabecular bone of the proximal tibia that is associated with an increased rate of bone growth in the longitudinal direction [60]. The number of osteoclasts and osteoblasts is increased, inducing bone resorption and formation, and bone mineral density and ash weight is reduced [60-63]. The non-uniform bone loss experienced in rats after ovariectomy confirms that cancellous bone loss is higher than cortical bone loss, and that bone resorption is site specific, with the proximal tibial metaphysis being the location showing the most consistent loss [63-65]. The tibial epiphysis is also sensitive to estrogen withdrawal, showing a net high bone turnover rate as initial response to estrogen deficiency, followed by a slow cancellous bone loss [65, 66]. All of the just mentioned characteristics expressed in osteopenic rat bone, along with the convenience in terms of money and space and the response to osteoporosis treatments comparable to the responses obtained with humans, make the rat one of the best animals to be used as a model for osteoporosis [60, 67].

1.5. Confocal Laser Scanning Microscopy and its Application to Bone

The principal function of a microscope is to transform an object into an image several degrees of magnification larger. Historically, the classic method to image objects has been to use light bright field microscopy (LM) and wide-field epifluorescence microscopy, an LM system equipped with a mercury lamp used to image fluorescent samples. Both systems incorporate a complex arrangement of lenses that allows a maximum resolution on the order of light waves, approximately 500 nm. The limited resolution of the system and the necessity to image samples at higher magnification to better resolve details spurred active development in the microscopy field [68].

In conventional wide-field epifluorescence microscopy a mercury lamp is used to illuminate uniformly, throughout the thickness of the sample, a large area of a specimen. Using thick specimens this imaging technique produces blurred images with reduced contrast and resolution resulting from the detected light coming from the out-of-focus volumes above and below the plane of focus. To reduce these problems it is possible to use thin or ultra-thin sections, or to take advantage of Confocal Laser Scanning Microscopy (CLSM) technology [68].

The primary asset that CLSM offers is the ability to produce optical sections throughout the whole thickness of an opaque sample containing information from only one focal plane, eliminating the out-of-focus reflected light, and producing crisp images (Figure 1-7). This is possible by using a laser beam passing through an objective numerical aperture before reaching a point inside the specimen plane of focus. The fluorescence light originated by the laser and specimen interaction goes back and it is collected as focal point at the detector after passing through a pinhole. The pinhole

location in front of the detector has the function to reject the out-of-focus light information, so that only the region of the specimen that is in focus is detected.

Hard tissue, such as bone and teeth, is one of the many biological tissues where CLSM has found success in its application. CLSM has been used to visualize bone microcracks developed during cyclic fatigue loading, and the association of microdamage with bone interstitial fluid flow [69, 70]. Wang et al [71] developed a very interesting model to visualize bone in situ and to measure solute transport in the bone lacunar-canalicular system detecting fluorescent dye present in individual osteocyte lacunae.

1.6. Scanning Electron Microscopy and its Application to Bone

Although CLSM has shown the excellent capability of producing crisp and detailed images, the best resolution offered is approximately 200 nm. Higher resolution images can be achieved using an electron beam, which offers resolution of the order of electron waves down to the single digit angstrom (Å). Scanning Electron Microscopy (SEM) employs accelerated electrons usually emitted by an electron gun composed of a tungsten filament. These electrons are then focused by condenser lenses into a beam with a very fine focal spot size, 0.4 nm to 5 nm (Figure 1-8). The electron beam is then scanned across the specimen with the consequent release of many different signals [72].

The most common image modalities collect the secondary electrons, and the backscattered electrons. Secondary electrons are low energy electrons, generated from the sample after the energetic passage of the electrons beam. Because of their low energy these electrons are emitted from the atoms occupying the very proximal surface region of the sample. Backscattered electrons are high energy electrons of the electron beam, which

have experienced collisions with the sample and then have been reflected from the surface they entered. The high contrast of backscattered images reflects the atomic number of the elements in the sample, so for this reason backscattered electrons are used to determine contrast between areas with different chemical composition. Bombarding the surface specimen with high energy electrons also produces the emission of X-rays whose energy and characteristic wavelength can be collected and measured to accurately determine the nature and quantity of different elements present in the specimen [72].

The high resolution, the capability of topographic and morphologic imaging, and the possibility of determining element composition and crystallographic information of the sample make scanning electron microscopy a useful tool for imaging bone. This technique has been used to analyze trabecular bone morphology and three-dimensional structure as well as the structure of bone in an osteoporotic animal model [73-76]. In the last two decades scanning electron microscopy has been used to observe the bone-implant interface, and important aspects related to this interface, such as fracture surface analysis and bone implant surface detachment [77].

1.7 Overview of Dissertation Research

To address some of the unresolved issues presented in this introductory chapter, four experimental studies that investigate bone?s interstitial fluid flow pathway and determine the effect that conditions such as osteoporosis and external load produce on interstitial fluid movement.are presented. In Chapter 2 we challenge the reported ability of the tracer ferritin to form halo-shaped labeling in the mineralized matrix around blood vessels, which has been used to explain normal interstitial fluid movement in bone. Chapter 3 describes a new histological staining technique developed to delineate bone

interstitial fluid space using high-resolution confocal microscopy imaging. In Chapter 4 we use the new staining technique to delineate, visualize, and quantify cortical and cancellous bone microporosities of normal and osteopenic rats. Finally, in Chapter 5 we analyze the effect that external loads produce on interstitial fluid movement in normal and osteopenic bone and discuss the possible role increased microporosities may play in the mechanosensory system of osteoporotic bone.

1.8 References

[1] Burger EH, Klein-Nulend J. Mechanotransduction in bone--role of the lacuno-canalicular network. Faseb J 1999;13 Suppl: S101-12.

[2] Klein-Nulend J, van der Plas A, Semeins CM, Ajubi NE, Frangos JA, Nijweide PJ, Burger EH. Sensitivity of osteocytes to biomechanical stress in vitro. Faseb J 1995;9: 441-5.

[3] Chow JW, Wilson AJ, Chambers TJ, Fox SW. Mechanical loading stimulates bone formation by reactivation of bone lining cells in 13-week-old rats. J Bone Miner Res 1998;13: 1760-7.

[4] Hauge EM, Qvesel D, Eriksen EF, Mosekilde L, Melsen F. Cancellous bone remodeling occurs in specialized compartments lined by cells expressing osteoblastic markers. J Bone Miner Res 2001;16: 1575-82.

[5] Miller SC, de Saint-Georges L, Bowman BM, Jee WS. Bone lining cells: structure and function. Scanning Microsc 1989;3: 953-60; discussion 960-1.

[6] Norimatsu H, Yamamoto T, Ozawa H, Talmage RV. Changes in calcium phosphate on bone surfaces and in lining cells after the administration of parathyroid hormone or calcitonin. Clin Orthop Relat Res 1982: 271-8.

[7] Rubinacci A, Villa I, Dondi Benelli F, Borgo E, Ferretti M, Palumbo C, Marotti G. Osteocyte-bone lining cell system at the origin of steady ionic current in damaged amphibian bone. Calcif Tissue Int 1998;63: 331-9.

[8] Cooper RR, Milgram JW, Robinson RA. Morphology of the osteon. An electron microscopic study. J Bone Joint Surg Am 1966;48: 1239-71.

[9] Cowin SC. Bone poroelasticity. J Biomech l1999;32: 217-38.

[10] Mohsin S, Taylor D, Lee TC. Three-dimensional reconstruction of Haversian systems in ovine compact bone. Eur J Morphol 2002;40: 309-15.

[11] You LD, Weinbaum S, Cowin SC, Schaffler MB. Ultrastructure of the osteocyte process and its pericellular matrix. Anat Rec A Discov Mol Cell Evol Biol 2004;278: 505-13.

[12] Wang Y, McNamara LM, Schaffler MB, Weinbaum S. A model for the role of integrins in flow induced mechanotransduction in osteocytes. Proc Natl Acad Sci U S A 2007;104: 15941-6.

[13] Weinbaum S, Cowin SC, Zeng Y. A model for the excitation of osteocytes by mechanical loading-induced bone fluid shear stresses. J Biomech 1994;27: 339-60.

[14] You L, Cowin SC, Schaffler MB, Weinbaum S. A model for strain amplification in the actin cytoskeleton of osteocytes due to fluid drag on pericellular matrix. J Biomech 2001;34: 1375-86.

[15] Cowin SC, Weinbaum S, Zeng Y. A case for bone canaliculi as the anatomical site of strain generated potentials. J Biomech 1995;28: 1281-97.

[16] Squire JM, Chew M, Nneji G, Neal C, Barry J, Michel C. Quasi-periodic substructure in the microvessel endothelial glycocalyx: a possible explanation for molecular filtering? J Struct Biol 2001;136: 239-55.

[17] Ciani C, Doty SB, Fritton SP. Mapping bone interstitial fluid movement: displacement of ferritin tracer during histological processing. Bone 2005;37: 379-87.

[18] Knothe Tate ML, Knothe U. An ex vivo model to study transport processes and fluid flow in loaded bone. J Biomech 2000;33: 247-54.

[19] Knothe Tate ML, Knothe U, Niederer P. Experimental elucidation of mechanical load-induced fluid flow and its potential role in bone metabolism and functional adaptation. Am J Med Sci 1998;316: 189-95.

[20] Montgomery RJ, Sutker BD, Bronk JT, Smith SR, Kelly PJ. Interstitial fluid flow in cortical bone. Microvasc Res 1988;35: 295-307.

[21] Tami AE, Schaffler MB, Knothe Tate ML. Probing the tissue to subcellular level structure underlying bone's molecular sieving function. Biorheology 2003;40: 577-90.

[22] Wang L, Ciani C, Doty SB, Fritton SP. Delineating bone's interstitial fluid pathway in vivo. Bone 2004;34: 499-509.

[23] Neuman WF, Neuman MW. The chemical dynamics of bone. Chigago; 1958.

[24] Neuman WF, Toriba TY, Mulrvan BJ. The surface chemistry of bone. J Am Chem Soc 1953;75: 4239-4242.

[25] Martin RB. Determinants of the mechanical properties of bones. J Biomech 1991;24 Suppl 1: 79-88.

[26] McCalden RW, McGeough JA, Barker MB, Court-Brown CM. Age-related changes in the tensile properties of cortical bone. The relative importance of changes in porosity, mineralization, and microstructure. J Bone Joint Surg Am 1993;75: 1193-205.

[27] Schaffler MB, Burr DB. Stiffness of compact bone: effects of porosity and density. J Biomech 1988;21: 13-6.

[28] Yeni YN, Brown CU, Wang Z, Norman TL. The influence of bone morphology on fracture toughness of the human femur and tibia. Bone 1997;21: 453-9.

[29] Li GP, Bronk JT, An KN, Kelly PJ. Permeability of cortical bone of canine tibiae. Microvasc Res 1987;34: 302-10.

[30] Morris MA, Lopez-Curto JA, Hughes SP, An KN, Bassingthwaighte JB, Kelly PJ. Fluid spaces in canine bone and marrow. Microvasc Res 1982;23: 188-200.

[31] Sugawara Y, Kamioka H, Honjo T, Tezuka K, Takano-Yamamoto T. Three-dimensional reconstruction of chick calvarial osteocytes and their cell processes using confocal microscopy. Bone 2005;36: 877-83.

[32] Beno T, Ciani C, Doty SB, Fritton SP. Structural measurements of osteocyte lacunae and canaliculi using confocal microscopy. In: Proceedings of the 2005 Summer Bioengineering Conference abstract 92348; 2005.

[33] Qin YX, Kaplan T, Saldanha A, Rubin C. Fluid pressure gradients, arising from oscillations in intramedullary pressure, is correlated with the formation of bone and inhibition of intracortical porosity. J Biomech 2003;36: 1427-37.

[34] Hillsley MV, Frangos JA. Bone tissue engineering: the role of interstitial fluid flow. Biotechnol Bioeng 1994;43: 573-81.

[35] Han Y, Cowin SC, Schaffler MB, Weinbaum S. Mechanotransduction and strain amplification in osteocyte cell processes. Proc Natl Acad Sci U S A 2004;101: 16689-94.

[36] Piekarski K, Munro M. Transport mechanism operating between blood supply and osteocytes in long bones. Nature 1977;269: 80-2.

[37] Ayasaka N, Kondo T, Goto T, Kido MA, Nagata E, Tanaka T. Differences in the transport systems between cementocytes and osteocytes in rats using microperoxidase as a tracer. Arch Oral Biol 1992;37: 363-9.

[38] Dillaman RM. Movement of ferritin in the 2-day-old chick femur. Anat Rec 1984;209: 445-53.

[39] Dillaman RM, Roer RD, Gay DM. Fluid movement in bone: theoretical and empirical. J Biomech 1991;24 Suppl 1: 163-77.

[40] Doty SB, Schofield BH. Electron microscopic localization of hydrolytic enzymes in osteoclasts. Histochem J 1972;4: 245-58.

[41] Qin L, Mak AT, Cheng CW, Hung LK, Chan KM. Histomorphological study on pattern of fluid movement in cortical bone in goats. Anat Rec 1999;255: 380-7.

[42] Tanaka T, Sakano A. Differences in permeability of microperoxidase and horseradish peroxidase into the alveolar bone of developing rats. J Dent Res 1985;64: 870-6.

[43] Quintana C, Cowley JM, Marhic C. Electron nanodiffraction and high-resolution electron microscopy studies of the structure and composition of physiological and pathological ferritin. J Struct Biol 2004;147: 166-78.

[44] Mak AF, Qin L, Hung LK, Cheng CW, Tin CF. A histomorphometric observation of flows in cortical bone under dynamic loading. Microvasc Res 2000;59: 290-300.

[45] Kelly PJ, Montgomery RJ, Bronk JT. Reaction of the circulatory system to injury and regeneration. Clin Orthop Relat Res 1990: 275-88.

[46] Winet H. A bone fluid flow hypothesis for muscle pump-driven capillary filtration: II. Proposed role for exercise in erodible scaffold implant incorporation. Eur Cell Mater 2003;6: 1-10; discussion 10-1.

[47] Ajubi NE, Klein-Nulend J, Nijweide PJ, Vrijheid-Lammers T, Alblas MJ, Burger EH. Pulsating fluid flow increases prostaglandin production by cultured chicken osteocytes--a cytoskeleton-dependent process. Biochem Biophys Res Commun 1996;225: 62-8.

[48] Jiang JX, Cherian PP. Hemichannels formed by connexin 43 play an important role in the release of prostaglandin E(2) by osteocytes in response to mechanical strain. Cell Commun Adhes 2003;10: 259-64.

[49] Kamioka H, Sugawara Y, Honjo T, Yamashiro T, Takano-Yamamoto T. Terminal differentiation of osteoblasts to osteocytes is accompanied by dramatic changes in the distribution of actin-binding proteins. J Bone Miner Res 2004;19: 471-8.

[50] Pavalko FM, Chen NX, Turner CH, Burr DB, Atkinson S, Hsieh YF, Qiu J, Duncan RL. Fluid shear-induced mechanical signaling in MC3T3-E1 osteoblasts requires cytoskeleton-integrin interactions. Am J Physiol 1998;275: C1591-601.

[51] Reilly GC, Haut TR, Yellowley CE, Donahue HJ, Jacobs CR. Fluid flow induced PGE2 release by bone cells is reduced by glycocalyx degradation whereas calcium signals are not. Biorheology 2003;40: 591-603.

[52] Chrischilles EA, Butler CD, Davis CS, Wallace RB. A model of lifetime osteoporosis impact. Arch Intern Med 1991;151: 2026-32.

[53] Martin RB, Butcher RL, Sherwood LL, Buckendahl P, Boyd RD, Farris D, Sharkey N, Dannucci G. Effects of ovariectomy in beagle dogs. Bone 1987;8: 23-31.

[54] Snow GR, Anderson C. The effects of 17 beta-estradiol and progestagen on trabecular bone remodeling in oophorectomized dogs. Calcif Tissue Int 1986;39: 198-205.

[55] Snow GR, Karambolova KK, Anderson C. Bone remodeling in the lumbar vertebrae of young adult beagles. Am J Vet Res 1986;47: 1275-7.

[56] Turner AS, Alvis M, Myers W, Stevens ML, Lundy MW. Changes in bone mineral density and bone-specific alkaline phosphatase in ovariectomized ewes. Bone 1995;17: 395S-402S.

[57] Turner AS, Mallinckrodt CH, Alvis MR, Bryant HU. Dual-energy X-ray absorptiometry in sheep: experiences with in vivo and ex vivo studies. Bone 1995;17: 381S-387S.

[58] Frost HM, Jee WS. On the rat model of human osteopenias and osteoporoses. Bone Miner 1992;18: 227-36.

[59] Wronski TJ, Dann LM, Scott KS, Cintron M. Long-term effects of ovariectomy and aging on the rat skeleton. Calcif Tissue Int 1989;45: 360-6.

[60] Wronski TJ, Lowry PL, Walsh CC, Ignaszewski LA. Skeletal alterations in ovariectomized rats. Calcif Tissue Int 1985;37: 324-8.

[61] Jordan VC, Phelps E, Lindgren JU. Effects of anti-estrogens on bone in castrated and intact female rats. Breast Cancer Res Treat 1987;10: 31-5.

[62] Kalu DN, Liu CC, Hardin RR, Hollis BW. The aged rat model of ovarian hormone deficiency bone loss. Endocrinology 1989;124: 7-16.

[63] Turner RT, Vandersteenhoven JJ, Bell NH. The effects of ovariectomy and 17 beta-estradiol on cortical bone histomorphometry in growing rats. J Bone Miner Res 1987;2: 115-22.

[64] Wronski TJ, Walsh CC, Ignaszewski LA. Histologic evidence for osteopenia and increased bone turnover in ovariectomized rats. Bone 1986;7: 119-23.

[65] Westerlind KC, Wronski TJ, Ritman EL, Luo ZP, An KN, Bell NH, Turner RT. Estrogen regulates the rate of bone turnover but bone balance in ovariectomized rats is modulated by prevailing mechanical strain. Proc Natl Acad Sci U S A 1997;94: 4199-204.

[66] Ke HZ, Jee WS, Ito H, Setterberg RB, Li M, Lin BY, Liang XG, Ma YF. Greater bone formation induction occurred in aged than young cancellous bone sites. Bone 1993;14: 481-5.

[67] Wronski TJ, Dann LM, Horner SL. Time course of vertebral osteopenia in ovariectomized rats. Bone l1989;10: 295-301.

[68] Pawley JB. Handbook of Biological Confocal Microscopy. Wisconsin: Springer; 1995.

[69] Colopy SA, Benz-Dean J, Barrett JG, Sample SJ, Lu Y, Danova NA, Kalscheur VL, Vanderby R, Jr., Markel MD, Muir P. Response of the osteocyte syncytium adjacent to and distant from linear microcracks during adaptation to cyclic fatigue loading. Bone 2004;35: 881-91.

[70] Muir P, Sample SJ, Barrett JG, McCarthy J, Vanderby R, Jr., Markel MD, Prokuski LJ, Kalscheur VL. Effect of fatigue loading and associated matrix microdamage on bone blood flow and interstitial fluid flow. Bone 2007;40: 948-56.

[71] Wang L, Wang Y, Han Y, Henderson SC, Majeska RJ, Weinbaum S, Schaffler MB. In situ measurement of solute transport in the bone lacunar-canalicular system. Proc Natl Acad Sci U S A 2005;102: 11911-6.

[72] Schatten H, Pawley JB. Biological Low Voltage Field Emission Scanning Electron Microscopy. 2007.

[73] Boyde A, Hobdell M. Scanning electron microscopy of bone. Calcif Tissue Res 1968: Suppl:4-4B.

[74] Miller SC, Wronski TJ. Long-term osteopenic changes in cancellous bone structure in ovariectomized rats. Anat Rec 1993;236: 433-41.

[75] Rohanizadeh R, LeGeros RZ, Bohic S, Pilet P, Barbier A, Daculsi G. Ultrastructural properties of bone mineral of control and tiludronate-treated osteoporotic rat. Calcif Tissue Int 2000;67: 330-6.

[76] Whitehouse WJ, Dyson ED, Jackson CK. The scanning electron microscope in studies of trabecular bone from a human vertebral body. J Anat 1971;108: 481-96.

[77] Davies JE, Baldan N. Scanning electron microscopy of the bone-bioactive implant interface. J Biomed Mater Res 1997;36: 429-40.

[78] Ciani C, Doty SB, Fritton SP. Transport of different sized probes into bone's lacunar-canalicular porosity. In: Transactions of the 51st Meeting of the Orthopedic Research Society; 2005. p. 1644.

[79] da Vinci L, O'Malley CD. Leonardo on the Human Boby. Dover: Courrier Dover Publications; 1983.

[80] Jee WSS. The skeletal tissues, in Cells and Tissue Biology, A Textbook of Histology. Baltimore: Urban and Schwarzenberg; 1988.

[81] Chicago LU. Stritch School of Medicine website. In.

[82] Zeiss. Confocal Laser Scanning Microscopy. In; 2007.

[83] University P. Radiological & Environmental Management www.purdue.edu/REM/rs/sem.htm.

Tracer	Study	Animal	Porosity		
			VP	LCP	CAP
Procion Red	[19]	Rat (young and adult)	Y	Y	N
	[18]	Rat	Y	Y	NS
	[21]	Rat	Y	Y	Y
Reactive Red	[22]	Rat	Y	Y	N
Microperoxidase	[42]	Rat alveolar bone	Y	Y	N
	[37]	Rat alveolar bone	Y	Y	N
	[19]	Rat (young and adult)	NS	NS	Y
	[18]	Rat	Y	Y	N
	[22]	Rat	Y	Y	N
Horseradish peroxidase	[40]	Rat	Y	Y	N
	[42]	Rat alveolar bone	Y	Y	N
	[39]	Rat	Y	Y	NS
	[19]	Rat (young and adult)	Y	Y	NS
	[22]	Rat	Y	Y	N
Bovine Serum Albumin	[78]	Rat	Y	Y	Y
Ferritin	[38]	Chick (2-day-old)	Y	NS	H
	[20]	Dog	Y	NS	H
	[41]	Goat	Y	NS	H
	[44]	Goat	Y	NS	H
	[17]	Rat	Y	N	N
	[22]	Rat	Y	N	N
Dextran 300 Da	[21]	Rat	Y	Y	Y
Dextran 3 kDa	[21]	Rat	Y	Y	NS
Dextran 10 kDa	[21]	Rat	Y	Y	N
Dextran 70 & 250 kDa	[78]	Rat	Y	Y	Y
Dextran 70 & 2000 kDa	[21]	Rat	Y	N	N

Table 1-1. Different tracers used in in vivo studies to estimate the bone porosities. The letters Y (yes) and N (no) indicate whether a particular tracer was found in each of the three bone porosities, the vascular porosity (VP), lacunar-canalicular porosity (LCP) or collagen-apatite porosity (CAP). H indicates the presence of "halos," and NS indicates penetration into the particular porosity was not specified.

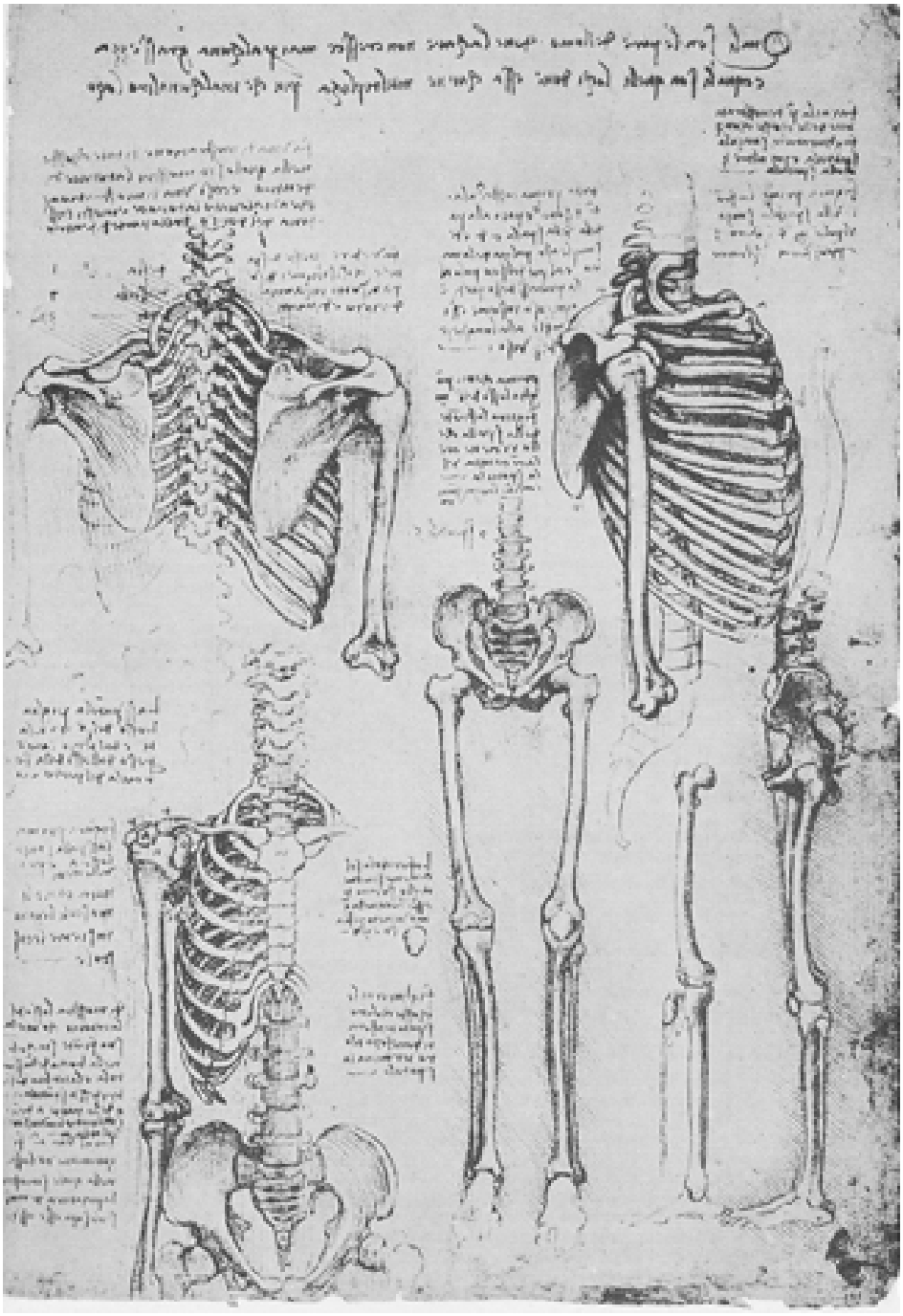

Figure 1-1. Different sizes and shapes of human bones [79].

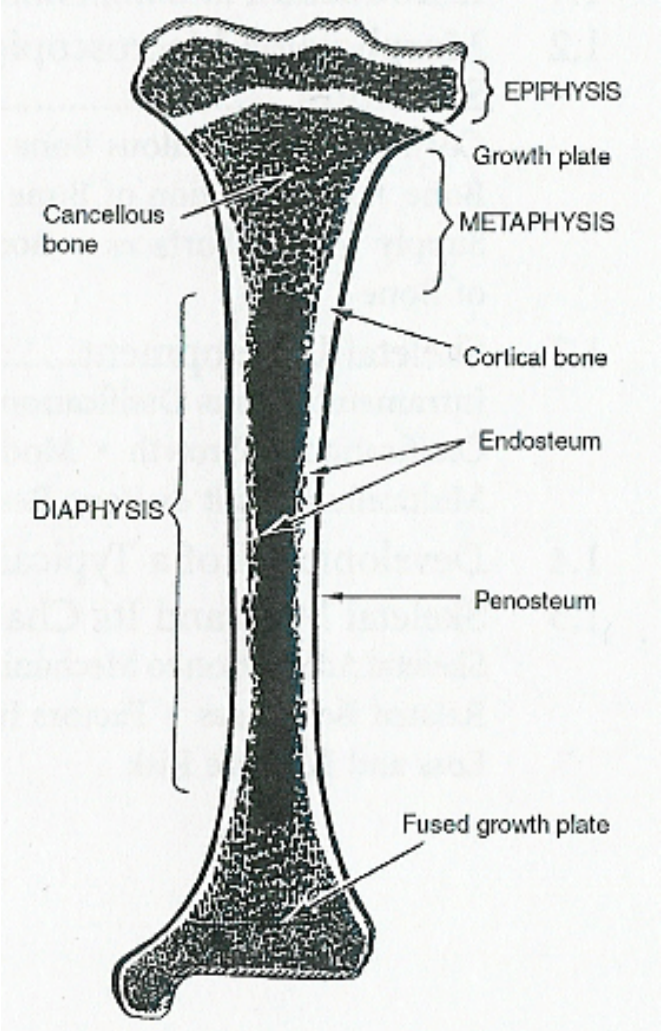

Figure 1-2. Schematic diagram of a tibia [80].

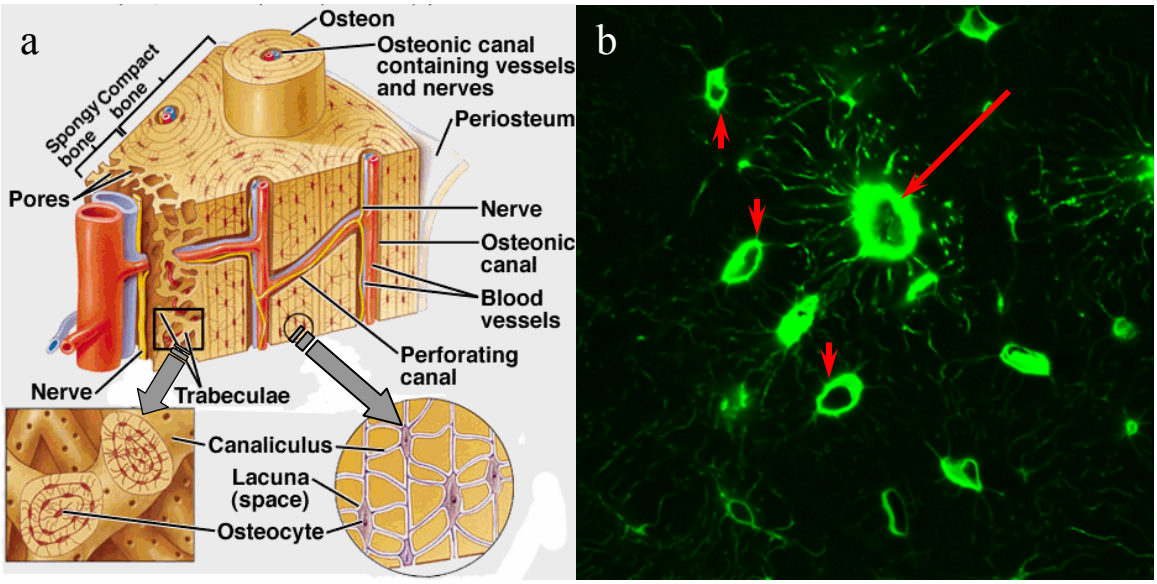

Figure 1-3. Human secondary bone, or osteonal bone (a, from the Owensboro Community & Technical College website) and primary bone (b, from rat) are very similar. They have the same types of porosities, and the dimensions governing these porosities are of the same order of magnitude. (b) Blood vessel and osteocyte lacunae are indicated by long and short arrows, respectively.

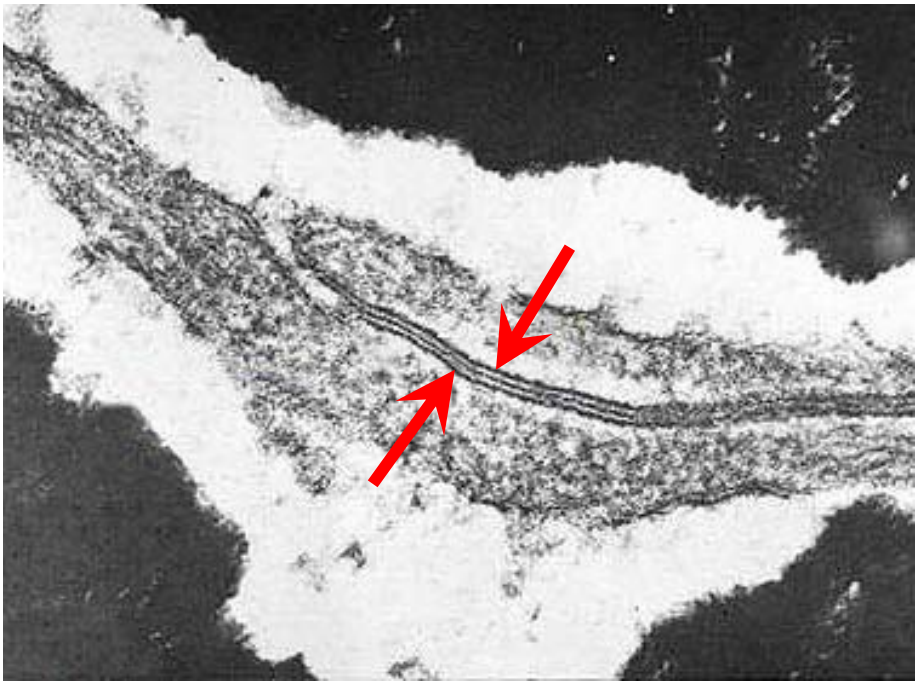

Figure 1-4. Communication system between two neighboring osteocytes. The dark lines (indicated by the red arrows), show the location of the gap junctions between the tip of the osteocyte processes [81].

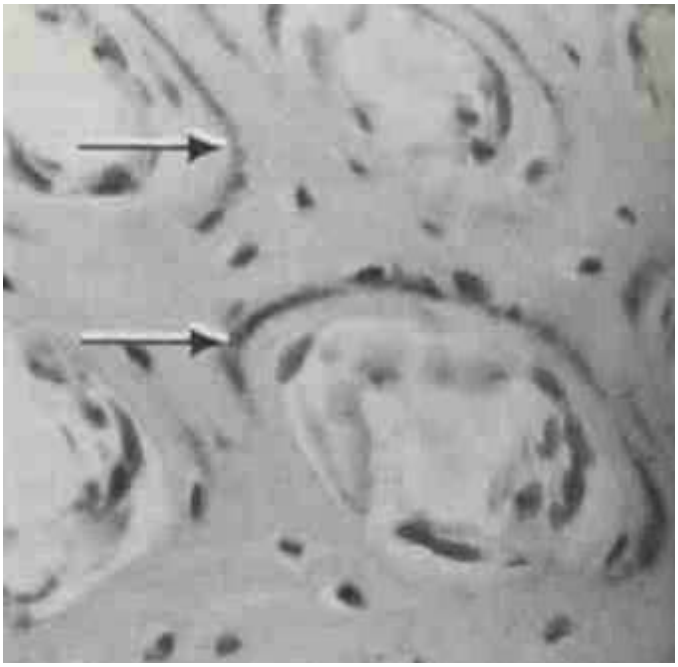

Figure 1-5. Ferritin halo-shaped labeling (**H**) surrounding the vascular canal (**C**) [38].

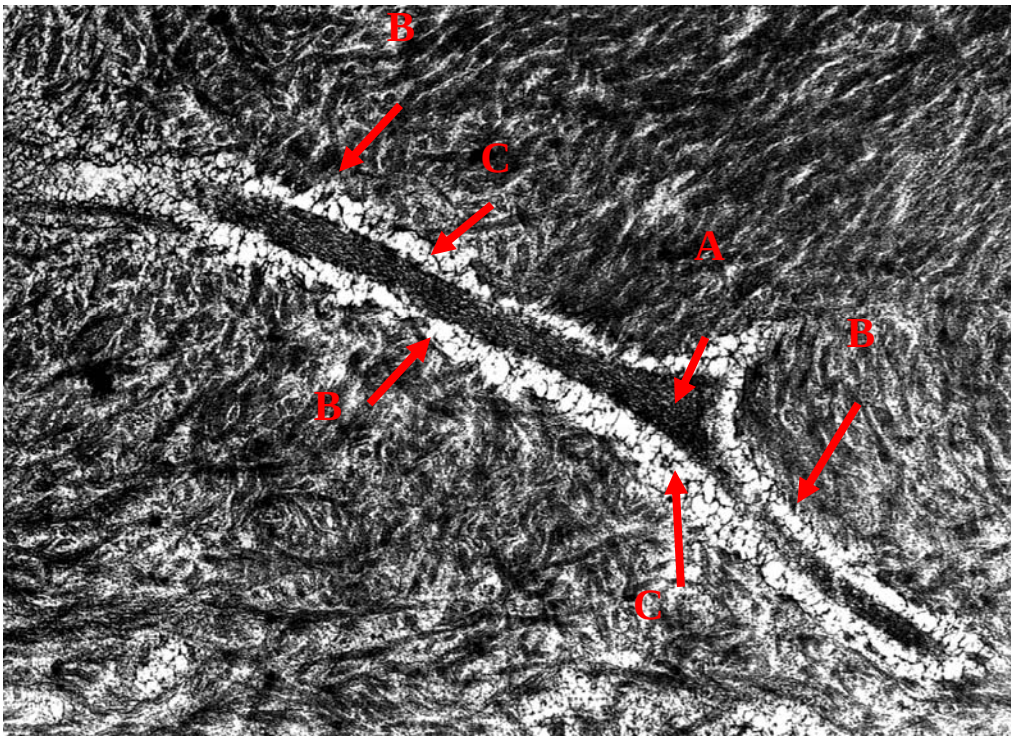

Figure 1-6. TEM picture of a osteocyte process (A), canalicular wall (B), transverse elements connecting the process to the canalicular wall (C), and pericellular matrix filling the annular space (D).

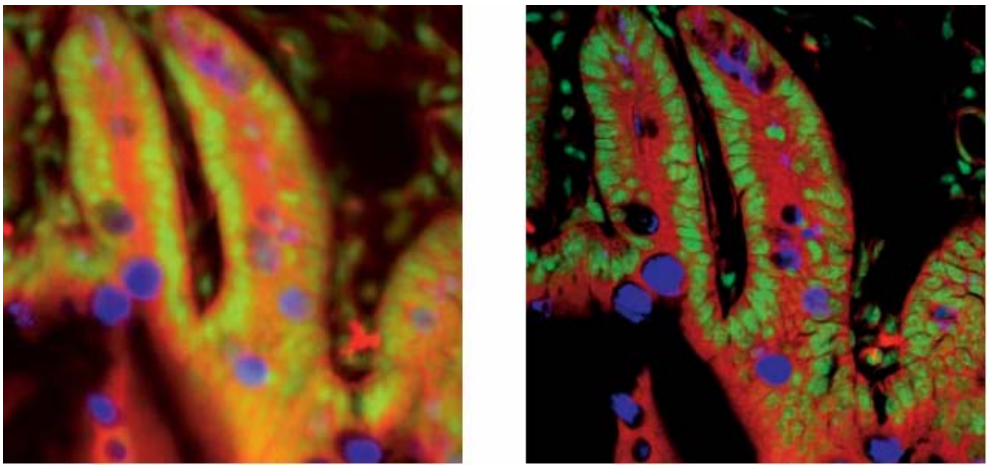

Figure 1-7. Non-confocal (left) and confocal (right) image of a triple-labeled mouse intestine section. Notice the crisp details of the confocal image (right) compared to the blurred image obtained with epifluorescent microscope (left) [82].

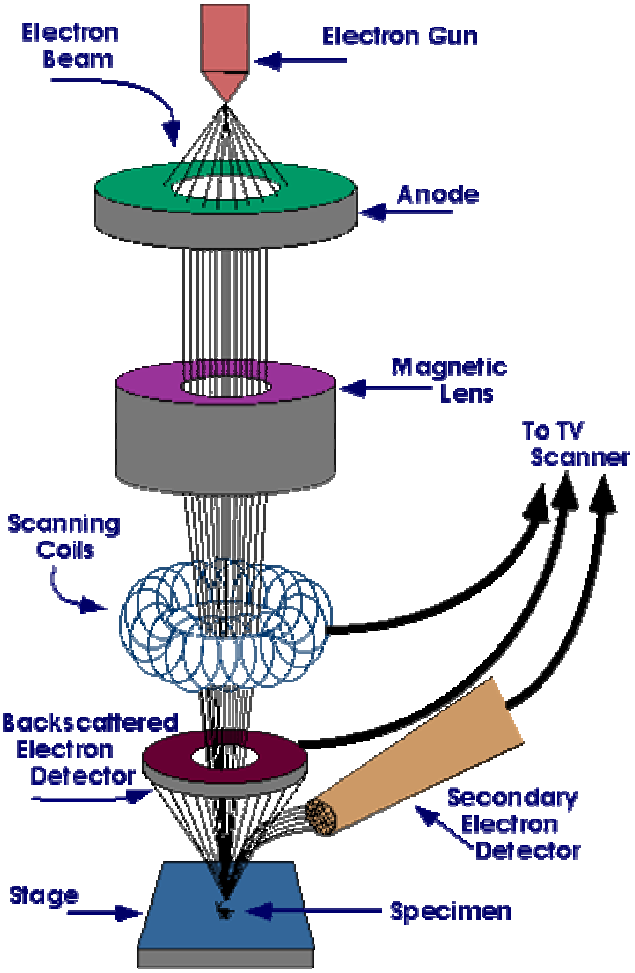

Figure 1-8. Principles of scanning electron microscopy [83].

Chapter 2

Mapping Bone Interstitial Fluid Movement: Displacement of Ferritin Tracer During Histological Processing

Mapping Bone Interstitial Fluid Movement: Displacement of Ferritin Tracer During Histological Processing

Cesare Ciani[1], Stephen B. Doty[2], Susannah P. Fritton[1*]

[1]Department of Biomedical Engineering, City College of New York / CUNY, New York, NY 10031
[2]Research Division, Hospital for Special Surgery, New York, NY 10021

*Corresponding author

Mailing address:
Department of Biomedical Engineering
City College of New York
Convent Avenue at 138th Street
New York, NY 10031

212-650-5213 (voice); 212-650-6727 (fax)
fritton@ccny.cuny.edu

This study was supported by research grants from the NIH (NIAMS, AR46429) and the Whitaker Foundation (RG-01-0440).

Abstract

Bone interstitial fluid flow is thought to play a fundamental role in the mechanical stimulation of bone cells, either via shear stresses or cytoskeletal deformations. Recent evidence indicates that osteocytes are surrounded by a fiber matrix that may be involved in the mechanotransduction of external stimuli as well as in nutrient exchange. In our previous tracer studies designed to map how different sized molecules travel through the bone porosities we found that injected ferritin was confined to blood vessels and did not pass into the mineralized matrix. However, other investigators have shown that ferritin forms halo-shaped labeling that enters the mineralized matrix around blood vessels. This labeling is widely used to explain normal interstitial fluid movement in bone; in particular, it is said to demonstrate bulk centrifugal interstitial fluid movement away from a highly pressurized vascular porosity. In addition, appositional ferritin fronts are said to demonstrate centrifugal interstitial fluid movement from the medullary canal to the periosteal surface. The purpose of this study was to investigate the conflicting ferritin labeling results by evaluating the role of different histological processes in the formation of ferritin "halos." Ferritin was injected into the rat vasculature and allowed to circulate for five minutes. Samples obtained from tibiae were reacted for different times with Perl's reagent and then were either paraffin-embedded or sectioned with a cryostat. Halo-like labeling surrounding vascular pores were found in all groups, ranging from 1.2 – 3.9% for the samples treated with the shortest histological processes (unembedded, frozen sections) to 5.6 – 15% for the samples treated with the longest histological processes (paraffin-embedded sections). These results indicate that different histological processing methods are able to create ferritin "halos," with some processing methods

allowing more redistribution of the ferritin tracer than others. Based on these results and the fact that "halo" labeling has not been found with any other tracer, as we seek to further delineate the movement of interstitial fluid and the role it plays in bone mechanotransduction, we believe that ferritin "halo" labeling should not be used to demonstrate physiological bone interstitial fluid flow.

Keywords

bone permeability, physiological transport, bone metabolism, osteocyte, lacunar-canalicular porosity

Introduction

Interstitial fluid flow is thought to play an important role in bone's mechanosensory system by activating bone cells via shear stresses [9,12,25] or cytoskeletal deformations [27]. Bone interstitial fluid flow is also believed to aid in delivering nutrients and transporting metabolic waste products from the bone cells [17]. To better understand interstitial fluid movement in bone, techniques using markers or tracers such as procion red (300-400 Da, diameter < 1 nm), reactive red (1470 Da, diameter ~1 nm), microperoxidase (1860 Da, diameter ~2 nm), horseradish peroxidase (40 kDa, diameter ~6 nm), ferritin (440 kDa, diameter ~12 nm [20], and different sized dextrans (range 300 Da - 2000 kDa, diameter ~1 nm - 60 nm) have been used to map how different sized molecules travel through the various porosities in bone [1,5,8,13-16,19,22-24].

The architecture of cortical bone has three levels of porosity: the vascular porosity, the lacunar-canalicular porosity, and the collagen-apatite porosity of the mineralized matrix. The vascular porosity of animals without a secondary osteonal structure, such as rats and mice, consists of primary canals and transverse canals; this porosity is the largest of the three bone porosities (order 20 μm [2]). The lacunar-canalicular porosity is formed by the space surrounding the osteocytes in the lacunae and canaliculi (order 100 nm [28]). Within the canaliculi a pericellular fiber matrix is believed to keep the osteocyte processes in position, connecting them to the canalicular wall [25,27] and preventing them from collapsing [28]. The fiber matrix spacing is believed to be approximately 7-8 nm, similar to the surface glycocalyx on endothelial cells, and the fiber matrix has been proposed to work as a sieve, allowing only molecules smaller than the pore diameter to pass through [3,21,25]. Lastly, the smallest bone porosity is the collagen-apatite porosity

associated with the space between the collagen fibers and the crystallites of mineral apatite. The dimensions of this porosity have not been well characterized, and there is contradictory evidence from tracer studies as to whether molecules < 10 nm can pass into the mineralized matrix [22,24].

Our previous tracer studies indicate that ferritin injected into rats is confined to the bone blood vessels and does not pass into the mineralized matrix [24]. However, other investigators have shown that ferritin forms halo-shaped labeling that appears to enter the mineralized matrix around blood vessels, along with appositional fronts along the bone surfaces [5,15,16,19]. This ferritin labeling is widely used to explain normal interstitial fluid movement in bone: the halos are said to demonstrate bulk centrifugal interstitial fluid movement away from a highly pressurized vascular porosity, and the appositional fronts are said to demonstrate centrifugal interstitial fluid movement from the medullary canal to the periosteal surface [5,6,9-11,15,16,19,26]. These previous studies suggest that ferritin may be small enough to pass through the canalicular pores and possibly through the collagen-apatite pores in the mineralized matrix.

The contradictory ferritin findings and the fact that ferritin is the only tracer that has demonstrated "halo" labeling around blood vessels pushed us to investigate in further detail the movement of ferritin in the bone porosities. Based on our previous work with ferritin, our hypothesis was that the halo-shaped ferritin labeling found by other investigators was the result of histological processing methods. In this study we evaluated the role of different histological processing steps in the formation of ferritin "halos."

Methods

In vivo injection of Type I horse spleen ferritin (440 kDa, diameter ~12 nm, Sigma, St. Louis, MO) was performed on male Sprague Dawley rats (n=5, 320-340g, 10-11 weeks old). An additional animal (n=1, 280g, 9 weeks old) was injected with saline buffer solution as control. Permission for this in vivo study was granted by the Institutional Animal Care and Use Committee at the Hospital for Special Surgery. Rats were first anaesthetized via an intraperitoneal injection of a mixture of ketamine (80 mg/kg body weight) and xylazine (5 mg/kg body weight). The left jugular vein was then exposed surgically and a 25G5/8 needle attached to a 3-ml syringe was inserted into the vein to inject a bolus of tracer solution. Our previous experiments showed that ferritin was best detected if injected at a dosage of at least 150 mg/100 g of body weight [24]. We concentrated the ferritin solution using Amicon Ultra-4 centrifugal filter devices (100,000 molecular weight cutoff, Millipore, Billerica, MA), from 85 mg/ml to a final solution of 309 mg/ml. The final concentrated ferritin solution was delivered at 190 mg/100 g of body weight with a total volume of 2 ml. After the tracer was injected (injection time 2 minutes), it was allowed to freely circulate for 5 minutes. The rats were then sacrificed with carbon dioxide inhalation and both tibiae and femora were harvested. Femora were put immediately in Karnovsky's fixative (3% glutaraldehyde, 3% paraformaldehyde in 0.2 M sodium potassium phosphate), while tibiae were cut at the mid-diaphysis into two parts and then placed in Karnovsky's fixative.

From each injected animal, one 6-mm block was cut from the right tibia, while from the left tibia five 2-mm blocks were cut using a diamond blade saw (Buehler, Lake Bluff, IL) (Figure2-1). All the samples were placed in Perl's reagent (1:1 solution of 2% HCl and 2% potassium ferrocyanide), which allowed potassium ferrocyanide to combine with

the ferric ion to form the characteristic end product Prussian Blue that enables visualization of the ferritin under light microscopy.

Histological Processing of Bone Groups

The goal of this study was to determine if different histological processing methods affect the production of ferritin "halos." Six different histological processes were performed to determine if a particular processing method would be able to transport ferritin into the mineralized matrix (Table 2-1). These processing methods were similar to or variations of the methods used in our previous ferritin study [24] as well as previous studies where the movement of ferritin into the mineralized matrix produced a characteristic "halo" of blue stain around the blood vessels [5,16]. The six blocks taken from each animal were divided into two groups and each group was labeled according to its major histological process: the first group (two blocks) was designated PARA (for paraffin embedding), while the second group (4 blocks) was designated FROZ (for frozen section, no embedding).

Paraffin-embedded Samples (blocks PARA3, PARA8): After 48 hours in Karnovsky's fixative the samples PARA3 and PARA8 were put in Perl's reagent for 3 or 8 hours, respectively. They were then decalcified in 10% nitric acid for 5 days (samples PARA3) or in citrate formic acid [18] for 8 days (samples PARA8) [5,16]. Samples were placed in a series of graded alcohol (50%, 70%, 95%, and 100%), then xylene, and then were embedded in paraffin. Thin sections (5-7 μm thick) were cut using a microtome (Reichert-Jung 2030, Germany), dried overnight in an oven, deparaffinized,

counterstained with hematoxolin to achieve a pink background, and coverslipped with mounting media (Richard-Allan Scientific, Kalamazoo, MI).

Frozen, Unembedded Samples (blocks FROZ1, FROZ3, FROZ8, FROZ24): After 48 hours in Karnovsky's fixative the samples were put in Perl's reagent for 1 hour (samples FROZ1), 3 hours (samples FROZ3), 8 hours (samples FROZ8), or 24 hours (samples FROZ24). The blocks FROZ1 and FROZ3 were decalcified in 10% nitric acid for 24 hours while FROZ8 and FROZ24 samples could be immediately cut without being further decalcified. The blocks were embedded in OCT medium (Tissue Tek) to provide support during cryosectioning. Thin cross-sections (10-15 μm thick) were cut from the blocks using a cryostat (Model OTF 5030, Bright Instrument Company, England). The sections were then counterstained using 0.1% acid fuchsin for 15 seconds to achieve a pink background, rinsed briefly in distilled water, and coverslipped with aqueous mounting media (Biomeda Corp., Foster City, CA).

To determine mineral content in the samples, the von Kossa treatment was performed on femur specimens. Two-mm thick specimens were cut from the femur mid-diaphysis using the diamond blade saw and put in Karnovsky's fixative for 24 hours. They were then placed in Perl's reagent for 1, 3, 5, 8, or 24 hours and embedded in PMMA. Thin cross sections (5-10 μm) were cut from each block and analyzed under light microscopy to qualitatively measure the mineralized area of the section. The mineral distribution is visualized by the brown/black color resulting from the reaction of the mineral present in the section and the silver nitrate in the von Kossa solution. A high degree of mineralization results in very black sections, while demineralized sections do

not present the characteristic black color. Sections partially mineralized show a varying degree of black according to the mineral content.

To further investigate the Perl's action we placed a 3-mm block from the control animal injected with saline solution into freshly made Perl's solution for 3 hours. In addition, a 3-mm block from the control animal was placed in Perl's reagent in which a sample from a ferritin-injected animal had previously been placed and reacted for 8 hours. This control sample was left in the previously used Perl's solution for 24 hours.

Microscopic Imaging and Data Analysis

To analyze the tracer distribution in the bone, one cross-section was chosen from each animal for each treatment. Sections with a complete cross-sectional area and little cutting damage were chosen for analysis. The sections were analyzed under routine light microscopy (Nikon Microphot-FXA, Japan). For each section we counted the total number of blood vessels (*N.Bv*), the number of blood vessels labeled with ferritin (*N.Bv.La*), the number of osteocytes labeled with ferritin (*N.Ot.La*), and the number of "halos" surrounding blood vessels (*N.Ha*). The data were collected using the BIOQUANT image analysis system (BIOQUANT Image Analysis Corp., Nashville, TN), and images of each halo were recorded. The means and standard deviations of the measurements were calculated for each histological process. When counting the blood vessels no distinction was made between blood vessels cut longitudinally or in cross section. Halos were identified as both total or partial well-defined ferritin lines around blood vessels (Figure 2-2a, 2-2e) as well as more spread-out diffusive movement of ferritin in the extravascular region (Figure 2-2d). For all the samples the blood vessels

were counted using the 10x objective, while the halos and the osteocytes labeled with ferritin were counted with the 20x objective.

The percentage of labeled blood vessels (i.e., labeled blood vessels/total number of blood vessels, N.Bv.La/N.Bv), the percentage of labeled osteocytes (N.Ot.La/N.Ot), and the percentage of blood vessels surrounded by halos (N.Ha/N.Bv) were calculated and analyzed using one-way ANOVA. One-way ANOVA was used because we only wanted to determine if the different processing methods could influence the percentage of blood vessels surrounded by ferritin halos; the study was not designed to determine which component of the processing methods is responsible for producing halo labeling. Statistical analysis was performed to determine differences between the histological processes using SPSS for Windows version 12.0 (SPSS Inc., Chicago, IL). For all the statistical tests, a significance level of $p < 0.05$ was used.

Results

Ferritin, localized by the Perl's reaction, was effectively delivered to the blood vessels for all treatments (Fig. 2a through 2e). However, while the ferritin was able to reach most of the bone blood vessels, there was no ferritin labeling surrounding the osteocytes. The percentage of blood vessels labeled with ferritin ranged from 79% to 95%, while the percentage of labeled osteocytes was 0% for all the treatments (Table 2-2, Figure 2-3). The percentage of labeled blood vessels for both paraffin groups was lower than the unembedded, frozen-sectioned groups.

Measurements at a magnification of 20x showed ferritin "halos" in all sections of each group. The percentage of blood vessels surrounded by halos ranged from 1.2 - 15%

(Table 2-2, Figure 2-4). The frozen-sectioned groups showed a similar percentage of blood vessels surrounded by halos (1.2 – 3.9%), while the paraffin-embedded PARA8 group was significantly larger than all other groups (15%), and the PARA3 group was significantly different from FROZ24 (Figure2- 4).

In all the sections the endosteal surface was well defined by a blue line along the perimeter, and a ferritin appositional front was also visible (Figure 2-2b, 2-2e); the edge of the periosteal surface was also stained (Figure 2*2c). Sections from the control animal that did not receive injection of ferritin did not show any characteristic blue staining occurring from the reaction of Perl's and ferritin. However, sections from the control animal that were placed in Perl's solution previously used with a sample from a ferritin-injected animal showed a marked periosteal blue line and also the presence of halos around blood vessels (Figure 2-2f).

The von Kossa method indicated that the percent mineralized area of the specimens decreased proportionally to the time placed in Perl's reagent (Figure 2-5). Samples that stayed in Perl's reagent for 1 hour showed very little demineralization. Samples that stayed longer than 5 hours in the reagent were almost completely decalcified. A total degree of decalcification was achieved by samples that stayed for 24 hours in the reagent.

Discussion

We were able to produce ferritin "halo" labeling with all the different histological treatments used. The percentage of blood vessels surrounded by halos was quite low, ranging from 1.2 – 3.9% for the samples treated with the shortest histological processes (unembedded, frozen sections) to 5.6 – 15% for the samples treated with the longest

histological processes (paraffin-embedded sections). Our measurements, taken at a magnification of 20x, are similar to those reported by other investigators (7.6% at 10x, 26% at 40x) [15].

The only significant differences between groups were found between the paraffin-embedded samples and the unembedded, frozen-sectioned samples. The groups PARA3 and PARA8 had the lowest percentage of blood vessels labeled with ferritin (Figure 2-3), and PARA8 had the highest percentage of blood vessels surrounded by halos (Figure 2-4). The differences may be explained by the differences in the embedded vs. unembedded histological processes. The frozen blocks were fixed, reacted with Perl's reagent, decalcified (groups FROZ3 and FROZ8 only) and sectioned within three days after the injection with a minimum loss of tracer. The paraffin-embedded samples were fixed, reacted with Perl's reagent, completely decalcified, washed, dehydrated in ascending grades of alcohol, cleared in xylene, embedded in paraffin, sectioned, cured in an oven, deparaffinized, and counterstained. This process took approximately nine days, in which samples were kept in solutions that greatly differ from the in vivo environment where they live and interact with physiological fluid. Such a long processing time in so many solutions might also facilitate the movement of ferritin, resulting both in a reduction of blood vessels labeled with ferritin along with the formation of "halos."

The finding of ferritin halos in the FROZ1 samples, which were treated similarly to the methods we used in our previous study that showed ferritin completely confined to the vascular pores with no "halos," [24] is probably due to the area we chose to count the blood vessels. In the present study we analyzed the ferritin distribution over the entire bone sectional area, while in our previous study we only considered the tracer distribution

in three distinct sectors of the tibia: anterior, lateral, and medial. By only considering three subareas of the cross-section, we likely overlooked the ~4% halo labeling found for the FROZ1 sections in the present study. Another difference between the present study and our previous study that could possibly affect the results was that Karnovsky's fixative was used instead of alcohol to better mimic processing by previous investigators [5,15,16,19].

While this study was only designed to test whether histological processing techniques used by other investigators could produce ferritin "halo" labeling (it was not designed to determine which portion of the histological processing produces ferritin "halos"), a possible explanation for the production of halo-like ferritin labeling is that some component of the histological processing creates structural changes in the bone matrix. Ferritin is a spherical molecule, composed of a protein-assembled shell and an iron core. In order to visualize ferritin, samples are placed in Perl's reagent, which dissolves ferritin's protein shell and reacts with the iron core to produce the characteristic Prussian blue utilized to visualize this tracer under light microscopy [4,7]. Perl's reagent is able to dissolve the protein core because it is a very strong acid (pH 0.89). To evaluate the effect of the Perl's reagent on the bone mineral, we analyzed the specimens treated with von Kossa, and it was possible to see a clear trend of bone decalcification caused by the interaction between the Perl's reagent and bone tissue (Figure 2-5). Thus the acidic activity of the reagent might influence the sieving structure of the bone: as the acidic reagent removes bone crystallites from the mineralized matrix, injected unbound ferritin may be able to penetrate the increasingly porous bone, thus creating "halos." However, it

should be noted that there was no clear trend between the length of time bone samples were placed in Perl's reagent and the percentage of blood vessels surrounded by "halos."

Another peculiarity of ferritin reacting with Perl's reagent is that during the reaction ferritin molecules are disassembled and then recombined, giving rise to a final molecule with a smaller diameter than the original one [7]. This reduction in diameter might also facilitate the propagation and diffusion of ferritin outside the vascular canal into the dissolving mineralized matrix. Moreover, the presence of halos and a ferritin appositional front found in control samples from an animal that did not receive injected ferritin but was placed in already used Perl's reagent strongly indicates the possibility of histological artifact caused by the Perl's reagent (Figure 2-2f). In this case since no ferritin was injected in vivo into the animal circulation the halo labeling could be attributed to the demineralizing action of the Perl's solution acting on the sections, and the consequent movement of ferritin present in the solution into the bone matrix. No ferritin labeling was found in control samples placed in fresh Perl's solution.

While the idea of tracking a molecule inside bone tissue is very simple, bone is a very dense yet delicate tissue, and histological processes, if not well designed, can lead to a wrong interpretation of the real bone physiology. Due to the high tissue mineral content, bone histology can be a very long and complicated process. Bone samples have to pass through many different steps before being sectioned and analyzed under the microscope. Each solution where the samples stay (i.e., acidic solutions for decalcification, dehydrating solutions, embedding media) could cause loss of biological information and, at the same time, generate unreliable results. The demineralization process might provoke an unexpected enlargement of the original pore dimensions,

allowing the passage of larger molecules such as ferritin, otherwise prohibited. Moreover, the visualization of ferritin requires a critical step, the reaction with Perl's reagent, which reacts with the iron moiety of ferritin to form Prussian blue, never accounted for as a possible source of artifact.

Previous tracer studies using ferritin have explained ferritin "halos" as being generated by a centrifugal fluid force acting in the intravascular domain, driving the ferritin outside the vascular wall and into the mineralized matrix. In addition, appositional fronts along the bone surfaces have been said to demonstrate centrifugal interstitial fluid movement from the medullary canal to the periosteal surface [5,6,9-11,15,16,19,26]. The purpose of this study was to analyze the effect of different histological processes that could lead to the presence of ferritin in the mineralized matrix and the characteristic ferritin halo labeling previously demonstrated by other investigators. We were able to demonstrate that while all processing methods produced ferritin "halos," the paraffin embedding procedure produced a higher percentage of blood vessels surrounded by halos compared to the other groups. Based on these results and the fact that "halo" labeling has not been found with any other tracer, as we seek to further delineate the movement of interstitial fluid and the role it plays in bone mechanotransduction, we believe that ferritin "halo" labeling should not be used to demonstrate physiological bone interstitial fluid flow. The use of additional tracers of dimensions comparable to ferritin will help to better understand the porosity sizes governing interstitial fluid movement in bone.

Acknowledgments

The authors would like to thank Orla O'Shea, Janane N. Diouri, Anthony Labissiere, and Dr. Francesca Orlandi for their technical support. This study was supported by research grants from the NIH (NIAMS, AR46429) and the Whitaker Foundation (RG-01-0440).

2.5 References

[1] Ayasaka N, Kondo T, Goto T, Kido MA, Nagata E, Tanaka T. Differences in the transport systems between cementocytes and osteocytes in rats using microperoxidase as a tracer. Arch Oral Biol 1992;37:363-69.

[2] Cooper RR, Milgram JW, Robinson RA. Morphology of the osteon. An electron microscopy study. J Bone Joint Surg 1966;48A:1239-1271.

[3] Cowin SC, Weinbaum S, Zeng Y. A case for bone canaliculi as the anatomical site of strain generated potentials. J Biomech 1995;28:1281-97.

[4] Cowley JM, Janney DE, Gerkin RC, Buseck PR. The structure of ferritin cores determined by electron nanodiffraction. J Struct Biol 2000;131:210-16.

[5] Dillaman RM. Movement of ferritin in the 2-day-old chick femur. Anat Rec 1984;209:445-53.

[6] Dillaman RM, Roer RD, Gay DM. Fluid movement in bone: theoretical and empirical. J Biomech 1991;24:163-77.

[7] Domínguez-Vera JM, Colacio E. Nanoparticles of prussian blue ferritin: A new route for obtaining nanomaterials. Inorg Chem 2003;42:6983-85.

[8] Doty SB, Schofield BH. Metabolic and structural changes within osteocytes of rat bone. In: Talmage RV, Munson PL, editors. Calcium, parathyroid hormone and the calcitonins. Amsterdam: Elsevier; 1972; 353-64.

[9] Hillsley MV, Frangos JA. Bone tissue engineering: the role of interstitial fluid flow. Biotechnol Bioeng 1994;43:573-81.

[10] Keanini RG, Roer RD, Dillaman RM. A theoretical model of circulatory interstitial fluid flow and species transport within porous cortical bone. J Biomech 1995;28:901-14.

[11] Kelly PJ, Montgomery RJ, Bronk JT. Reaction of the circulatory system to injury and regeneration. Clin Orthop 1990;254:275-88.

[12] Klein-Nulend J, van der Plas A, Semeins CM, Ajubi NE, Frangos JA, Nijweide PJ, Burger EH. Sensitivity of osteocytes to biomechanical stress in vitro. FASEB J 1995;9:441-45.

[13] Knothe Tate ML, Niederer P, and Knothe U. In vivo tracer transport through the lacunocanalicular system of rat bone in an environment devoid of mechanical loading. Bone 1998;22:107-17.

[14] Knothe Tate ML, Steck R, Forwood MR, Niederer, P. In vivo demonstration of load-induced fluid flow in the rat tibia and its potential implications for processes associated with functional adaptation. J Exp Biol 2000;203:2737-45.

[15] Mak AF, Qin L, Hung LK, Cheng CW, Tin CF. A histomorphometric observation of flows in cortical bone under dynamic loading. Microvasc Res 2000;59:290-300.

[16] Montgomery RJ, Sutker BD, Bronk JT, Smith SR, Kelly PJ. Interstitial fluid flow in cortical bone. Microvasc Res 1988;35:295-307.

[17] Piekarski K, Munro M. Transport mechanism operating between blood supply and osteocytes in long bones. Nature 1977;269:80-2.

[18] Presnell JK, Schreibman MP, Humason GL. Humason's animal tissue techniques. Johns Hopkins Univ. Press; 5th edition; 1997.

[19] Qin L, Mak AT, Cheng CW, Hung LK, Chan KM. Histomorphological study on pattern of fluid movement in cortical bone in goats. Anat Rec 1999;255:380-7.

[20] Quintana C, Cowley JM, Marhic C. Electron nanodiffraction and high-resolution electron microscopy studies of the structure and composition of physiological and pathological ferritin. J Struct Biol 2004;147:166-78.

[21] Squire JM, Chew M, Nneji G, Neals C, Barry J, Michel C. Quasi-periodic substructure in the microvessel endothelial glycocalyx: a possible explanation for molecular filtering? J Struct Biol 2001;136:239-55.

[22] Tami AE, Schaffler MB, Knothe Tate ML. Probing the tissue to subcellular level structure underlying bone's molecular sieving function. Biorheology 2003;40:577-90.

[23] Tanaka T, Sakano A. Differences in permeability of microperoxidase and horseradish peroxidase into the alveolar bone of developing rats. J Dent Res 1985;64: 870-6.

[24] Wang L, Ciani C, Doty SB, Fritton SP. Delineating bone's interstitial fluid flow pathway in vivo. Bone 2004;34:499-509.

[25] Weinbaum S, Cowin SC, and Zeng Y. A model for the excitation of osteocytes by mechanical loading-induced bone fluid shear stresses. J Biomech 1994;27:339-60.

[26] Winet H. A bone fluid flow hypothesis for muscle pump-driven capillary filtration: II Proposed role for exercise in erodible scaffold implant incorporation. Eur Cell Mater 2003;6:1-11.

[27] You L, Cowin SC, Schaffler MB, Weinbaum S. A model for strain amplification in the actin cytoskeleton of osteocytes due to fluid drag on pericellular matrix. J Biomech 2001;34:1375-86.

[28] You LD, Weinbaum S, Cowin SC, Schaffler MB. Ultrastructure of the osteocyte process and its pericellular matrix. Anat Rec 2004;278A:505-13.

Table 2-1. Different histological processes used.

Processing method	Fixative	Perl's reagent	Decalcification	Embedding	Sectioning method
PARA3	2 days in Karnovsky's fixative	3 hours	5 days in 10% nitric acid	Paraffin	Microtome
PARA8		8 hours	8 days in citrate formic acid		
FROZ1	2 days in Karnovsky's fixative	1 hour	24 hours in 10% nitric acid	Not embedded; cut with OCT compound	Cryostat
FROZ3		3 hours			
FROZ8		8 hours	None		
FROZ24		24 hours			

Key: PARA = paraffin-embedded section; FROZ = frozen, unembedded section.

Table 2-2: Histomorphometric measurements for the six histological methods (mean ± standard deviation).

	FROZ1	**FROZ3**	**FROZ8**	**FROZ24**	**PARA3**	**PARA8**
Total number of blood vessels labeled with ferritin (*N.Bv.La*)	210 ± 20.4	261 ± 33.6	282 ± 12.6	309 ± 28.0	249 ± 50.3	261 ± 23.2
Total number of blood vessels (*N.Bv*)	232 ± 12.6	276 ± 33.1	297 ± 9.82	331 ± 26.4	314 ± 36.1	314 ± 29.5
Total number of osteocytes labeled with ferritin (*N.Ot.La*)	0	0	0	0	0	0
Total number of ferritin halos (*N.Ha*)	9.00 ± 6.67	9.40 ± 4.39	10.2 ± 9.60	4.20 ± 8.29	17.6 ± 3.58	46.2 ± 5.93

Key: PARA = paraffin-embedded section; FROZ = frozen, unembedded section.

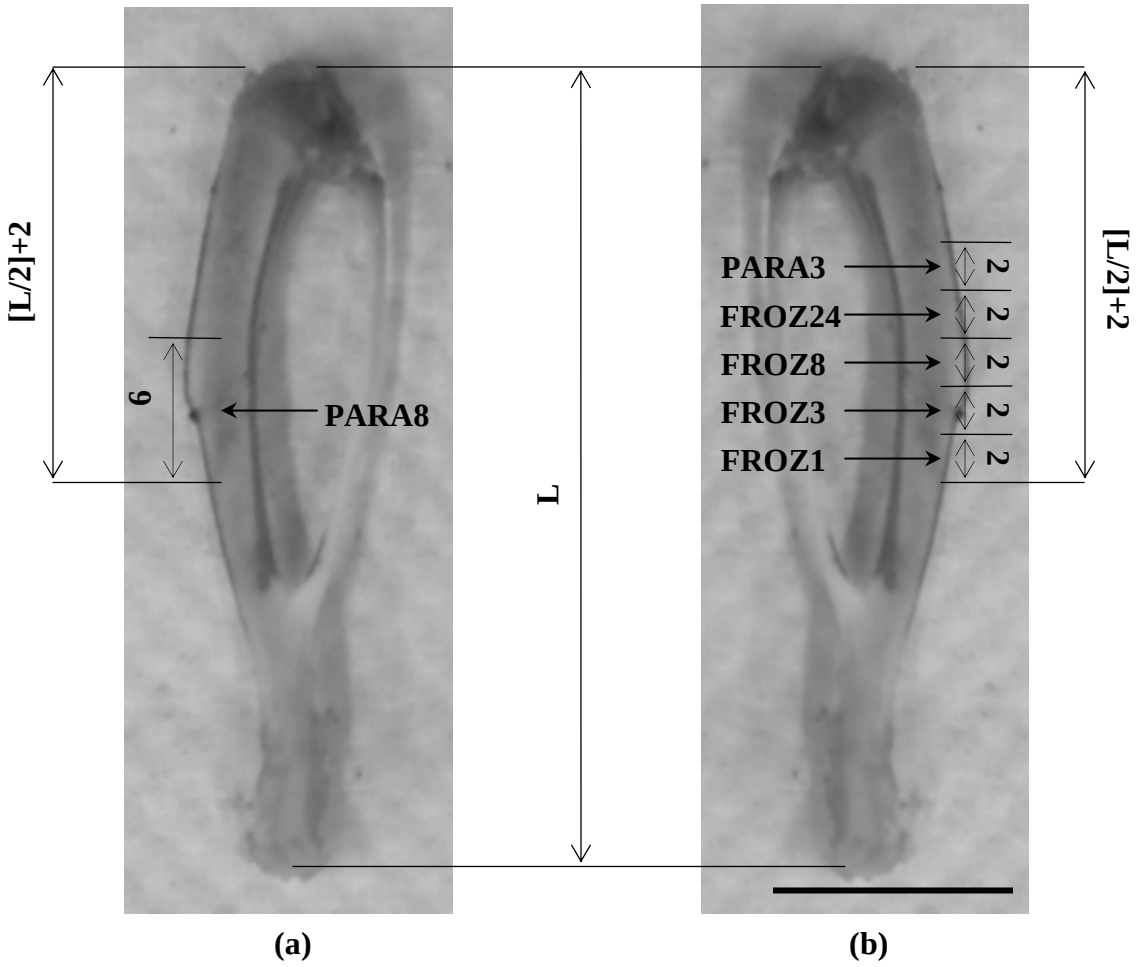

Figure 2-1. Rat right tibia (a) and left tibia (b) showing the locations where the samples where taken for the six different histological processes. The samples were named according to the histological process along with the time they were left in Perl's reagent. FROZ1, 3, 8, 24: frozen, unembedded samples left in Perl's reagent for 1, 3, 8, or 24 hours, respectively; PARA3, 8: paraffin-embedded samples left in Perl's reagent for 3 or 8 hours, respectively. L = tibia length. All dimensions are in millimeters (bar: 10 mm).

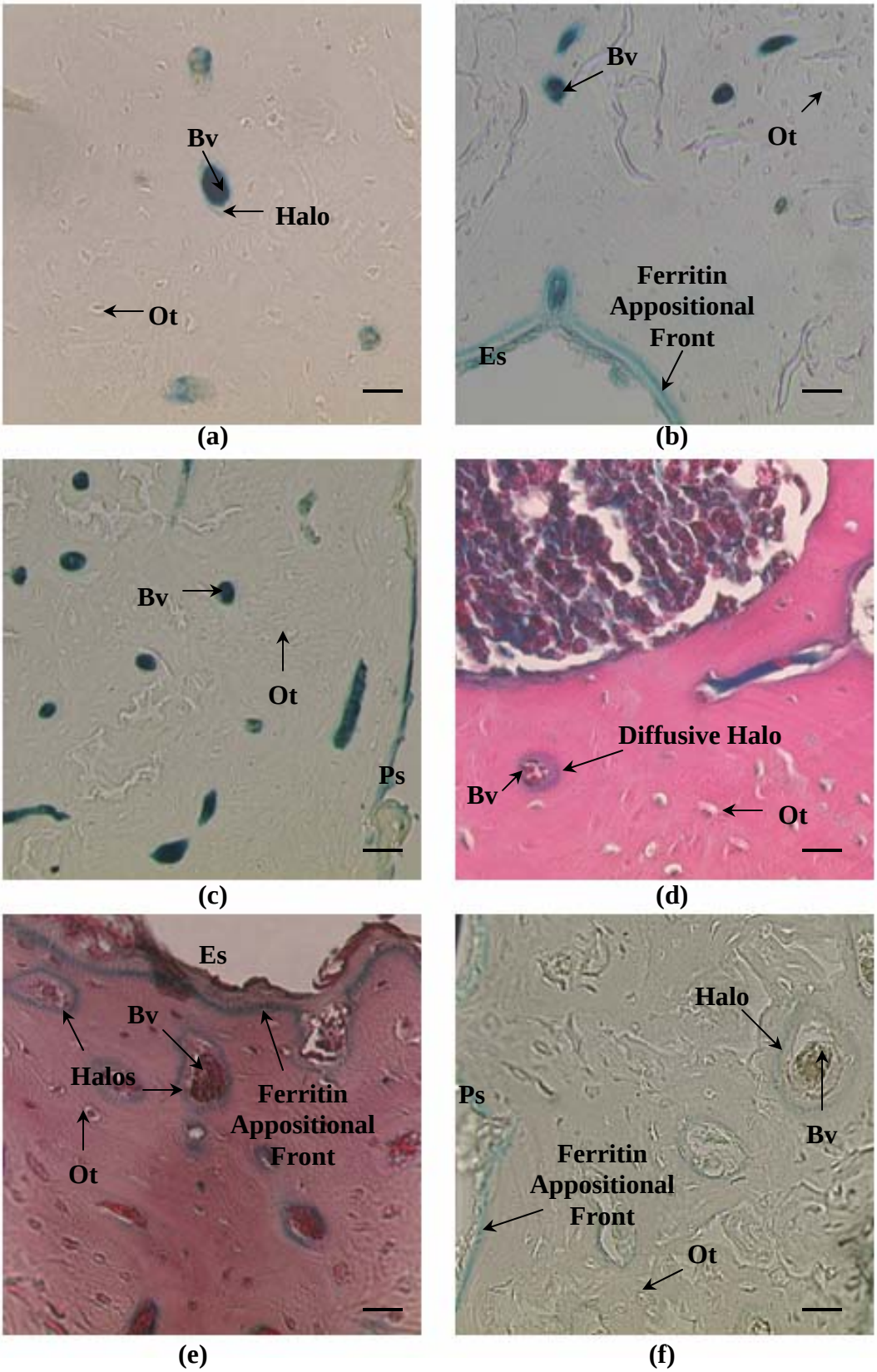
Bv
Halo
Ot
(a)
Bv
Ot
Ferritin
Appositional
Front
Es
(b)
Bv
Ot
Ps
(c)
Diffusive Halo
Bv
Ot
(d)
Es
Bv
Halos
Ferritin
Appositional
Front
Ot
(e)
Halo
Ps
Bv
Ferritin
Appositional
Front
Ot
(f)

Figure 2-2. Ferritin distribution for the different histological processes; no osteocytes (Ot) were labeled with ferritin for all the processes. (a) Group FROZ1: ferritin was primarily confined to the bone blood vessels (Bv) with the sporadic presence of ferritin "halos" surrounding blood vessels (magnification: 900x, bar: 15 μm). (b) Group FROZ3: a ferritin appositional front at the endosteal surface (Es) was clearly visible for all the histological treatments (magnification: 450x, bar: 30 μm). Group FROZ8 (not pictured) was very similar to FROZ3. (c) Group FROZ24: this group presented the lowest percentage of blood vessels surrounded by halos (magnification: 450x, bar: 30 μm). The periosteal surface (Ps) was also labeled with ferritin in all groups. (d) Group PARA3: diffusive halos were seen as more spread-out or diffusive movement of ferritin in the mineralized matrix surrounding blood vessels (magnification: 900x, bar: 15 μm). (e) Group PARA8: this group had the highest percentage of blood vessels surrounded by halos; a strong ferritin appositional front can also be seen at the endosteal surface of the bone (magnification: 900x, bar: 15 μm). (f) Halos surrounding blood vessels were also found in the control specimen after it was placed in already used Perl's solution for 24 hours; a ferritin appositional front is visible at the periosteal surface (Ps) (magnification: 10x, bar: 30 μm).

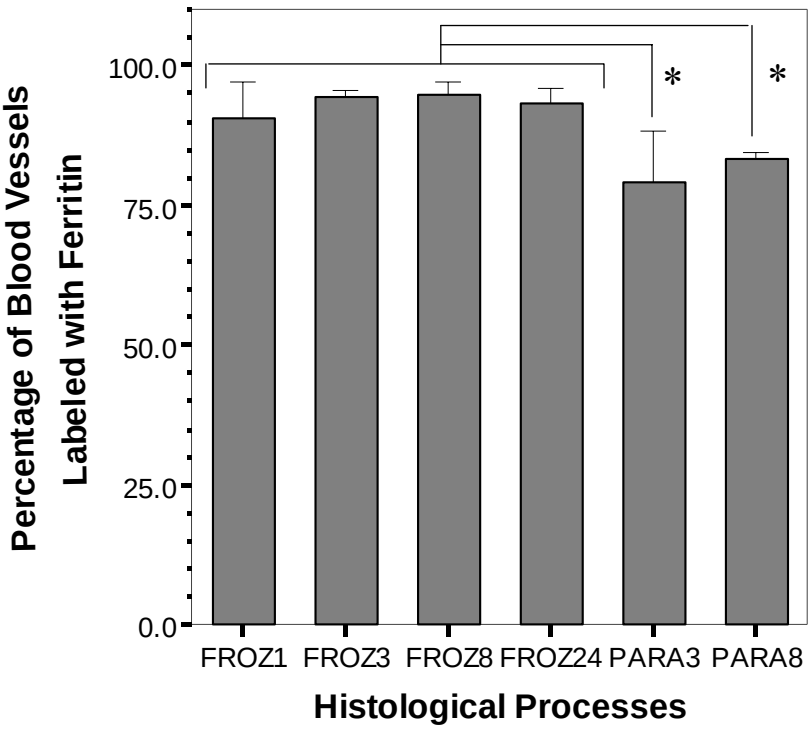

Figure 2-3. Percentage of blood vessels labeled with ferritin for the six histological processing methods (values are reported as mean ± standard deviation). The groups processed using unembedded frozen sections (FROZ) show a higher percentage of

labeled blood vessels compared to paraffin-embedded (PARA) groups. The asterisks indicate statistically significant differences between the two PARA groups and all the FROZ groups ($p < 0.05$).

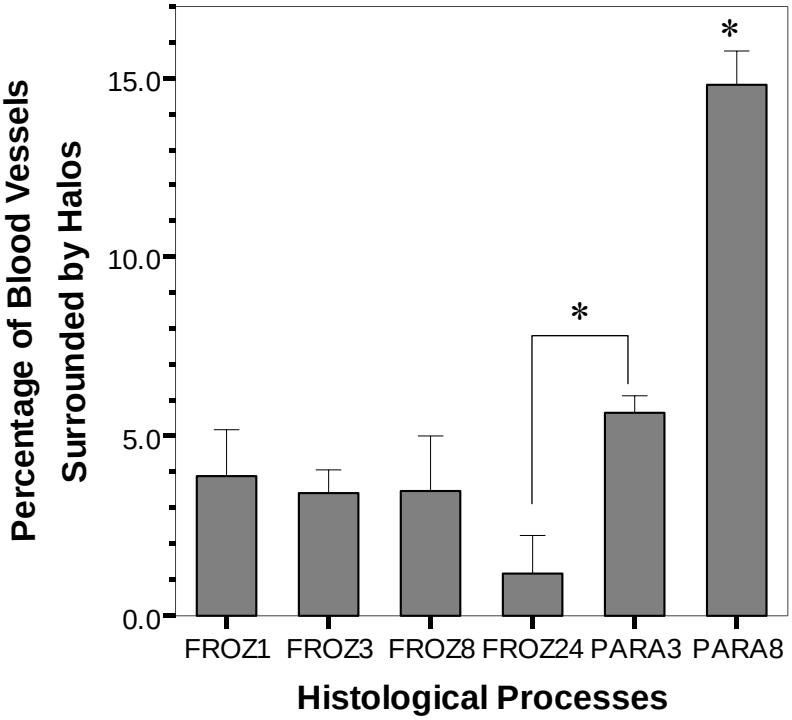

Figure 2-4. The percentage of blood vessels surrounded by halos for the six histological processing methods (values are reported as mean ± standard deviation). The paraffin-embedded group PARA8 was significantly different from all the other groups, while the paraffin-embedded PARA3 was significantly different from FROZ24 ($p < 0.05$).

Ciani et al. Fig. 5

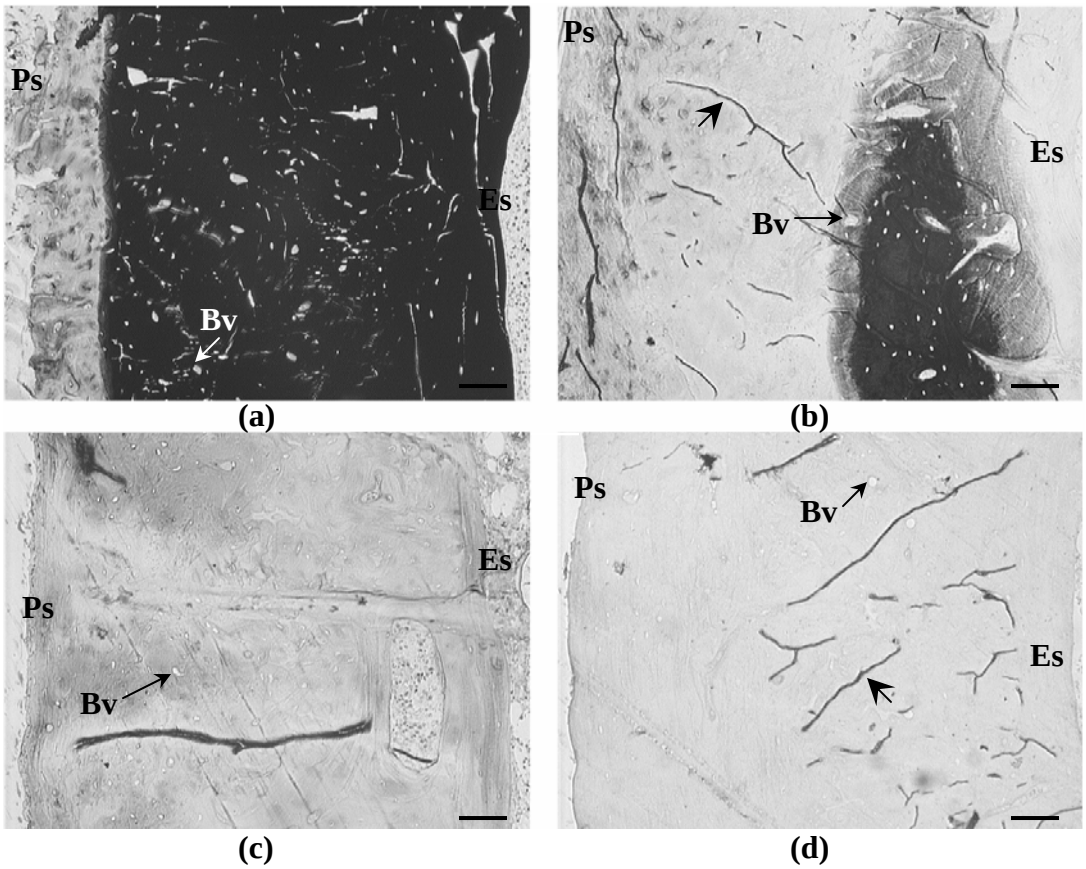

Figure 2-5. Each image shows the femoral mineral content from the periosteal surface (Ps) to the endosteal surface (Es) after the reaction for different times in Perl's reagent: (a) 1 hour; (b) 5 hours; (c) 8 hours; (d) 24 hours. The mineral content is qualitatively determined by the brown/black color (in this image by the white/black color) resulting from the reaction of the mineral present in the section and the silver nitrate in the von Kossa solution. (a) After 1 hour in Perl's the section resulted in a partial demineralization toward the periosteal surface (left side of the image), while the rest of the section was still mineralized (black color). (b) 5 hours in Perl's almost demineralized the entire section (white part of the image); the only mineral content is indicated by the black color on the right side of the image and by the varying degree of gray/black level just around it. After 8 or 24 hours in Perl's reagent (c, d) the samples did not show any mineral content. Blood vessels (Bv) are indicated along with drying artifacts (large arrowheads) caused by the embedding media used (magnification: 8x, bar: 50 μm).

Chapter 3

Effective Histological Staining Process to Visualize Bone Interstitial Fluid Space Using Confocal Microscopy

Effective Histological Staining Process to Visualize Bone Interstitial Fluid Space Using Confocal Microscopy

Cesare Ciani, Stephen B. Doty[+], Susannah P. Fritton[*]

Department of Biomedical Engineering, City College of New York / CUNY, New York, NY 10031
[+]Research Division, Hospital for Special Surgery, New York, NY 10021

*Corresponding author

Mailing address:
Department of Biomedical Engineering
City College of New York
Convent Avenue at 138th Street
New York, NY 10031

212-650-5213 (voice); 212-650-6727 (fax)
fritton@ccny.cuny.edu

Abstract

Bone is a composite porous material with two functional levels of porosity: the vascular porosity that surrounds bone blood vessels and the lacunar-canalicular porosity that surrounds the osteocytes. Both the vascular porosity and lacunar-canalicular porosity are directly involved in interstitial fluid flow, thought to play an important role in bone's maintenance. Because of the submicron dimensions of the lacunar-canalicular porosity, interstitial fluid space has been difficult to visualize and quantify. We report a new staining protocol that is reliable and easily reproducible, using fluorescein isothiocyanate (FITC) as a probe visualized by confocal microscopy. Utilizing the fluorescent properties of FITC, we also developed a methodology to reconstruct entire bone cross sections for effective visualization of cortical and cancellous bone microstructure. This new bone staining process can be used to analyze bone interstitial fluid space, including the vascular pores and the lacunar-canalicular network, providing high resolution quantification of cortical and cancellous microarchitecture.

Keywords

lacunar-canalicular porosity, staining, confocal microscopy, osteocyte, FITC

Introduction

Bone is a hard, composite porous material with two distinct levels of porosity: the vascular porosity that contains one or more blood vessels and nerves, and the submicron porosity of the lacunar-canalicular space that contains osteocytes and their processes. Although different in size and properties these two porosities share an important constituent, bone interstitial fluid, and are directly involved in load-induced interstitial bone fluid flow. This load-induced fluid displacement is thought to have two effects on bone: (a) enhancement of solute transport via convective transport mechanisms affecting maintenance of the tissue, and (b) activation of bone cells via cytoskeletal deformations, thus playing a role in bone's mechanosensory system [1-6]. To better understand the processes of bone maintenance and adaptation it is important to accurately quantify cortical and cancellous bone porosities, critical input parameters for models of interstitial fluid flow and mechanotransduction in bone.

Several groups have tried to visualize the interconnectedness of the vascular and lacunar-canalicular network and quantify bone porosities using different methods [7-9]. Unfortunately the small dimension of the lacunar-canalicular interstitial fluid space, the low resolution of the microscopic devices used, and the restricted areas analyzed have been limitations of these studies. The decalcification of bone samples used in some previous studies might also induce histological artifacts [10]. To overcome these limitations, we have developed an effective, easily reproducible technique to delineate and visualize bone interstitial fluid space.

Materials and Methods

For the protocol described rat bone is used (3-month-old male Sprague Dawley); however, the methods are not species-specific. To visualize cortical bone for this study, fresh tibial cross sections were obtained from the mid-diaphysis as well as from the metaphysis approximately 2 mm distal to the growth plate. To visualize cancellous bone, longitudinal sections were obtained from the metaphysis and epiphysis of the proximal tibia.

After harvest, bones were placed in EM fixative (0.5% gluteraldehyde, 2% paraformaldehyde in 0.05M cacodylate-sodium buffer, pH 7.4) and immediately processed to obtain fresh cortical sections and cancellous bone blocks. Cortical bone thick sections (300-400 μm) were cut with a diamond blade saw (Buehler, Lake Bluff, IL), the bone marrow washed out, and the sections placed back into EM fixative for 24 hours. The cortical sections were then ground by hand to a final thickness of 30-50 μm using Carbimet paper discs (800 and 1200 grit; Buehler), and dehydrated in ascending graded alcohols (75%, 95%, and 100%, 5 minutes each). Cancellous blocks from the metaphyseal/epiphyseal region were placed into EM fixative for 48 hours without bone marrow removal. To stain interstitial bone space we used FITC (fluorescein isothiocyanate isomer I from Sigma, product #F7250), diluted in 100% alcohol at a concentration of 1%. The solution was gently mixed in a rotator for 1 hour until clear, and then filtered. Cortical sections and cancellous blocks were then placed in 20 ml glass vials containing freshly prepared staining solution and gently mixed in a rotator for 4 hours. The cortical sections were then rinsed in 100% ETOH for 30 minutes, air dried and coverslipped with mounting media (Richard-Allan Scientific, Kalamazoo, MI). The cancellous blocks were embedded in PMMA [11], then thick sections (400-500 μm) were

cut and ground down to a final thickness of 40-80 μm using Carbimet paper discs (600 and 1200 grit; Buehler). Embedded cancellous sections were dried in ascending graded alcohols (75%, 95%, and 100%, 5 minutes each), air dried and coverslipped. During all the staining steps the sections, samples and vials were wrapped in aluminum foil to prevent loss of fluorescence.

All the sections were imaged using a confocal microscope (Leica TCS SP2, Germany) with the following parameters: 40x oil immersion lens, laser wavelength excitation of 488 nm, pinhole set at 1 Airy unit, 2048 x 2048 resolution giving a field of view of 375 x 375 μm, and laser intensity set at 12% of the full power. The gain and offset were chosen such that in the images acquired the canalicular system in both fresh and embedded sections covered the full dynamic range. A complete reconstruction of each cortical cross-section (tibia mid-diaphysis and metaphysis) was obtained using Photoshop by overlaying adjacent bone section sectors imaged with the confocal microscope.

Results

Using the simple FITC staining protocol, fresh cortical bone and PMMA-embedded cancellous bone sections show the vascular and lacunar-canalicular porosity uniformly stained, with the mineralized matrix impermeable to the fluorescent probe (Figure 3-1). The method can be used to create high-resolution images of an entire bone cross-section (file size ~ 500 MB for the mid-diaphysis sections, and ~ 1.4 GB for the metaphysis sections) that illuminate the microstructural details of the lacunar-canalicular network (Figure 3-2). The reconstructed sections do not present over- or under-stained areas, and the staining uniformity makes it possible to distinguish detailed microstructural patterns

(Figure 3-2b, c), such as compacted cancellous bone structure consisting of older cancellous bone filled in with newer compact bone (Figure 3-2c) [12].

Discussion

We have developed a consistent and effective histological method to stain bone interstitial fluid space using FITC as a fluorescent probe and confocal microscopy to visualize the bone porosities. This staining technique also appears to be an effective method to obtain high-resolution images of an entire bone cross-section, helpful when visualizing the microstructural details of the lacunar-canalicular network. Although the reconstruction process used to obtain the images of the full cross-sections is somewhat tedious, a motorized stage connected to the confocal microscope would make the reconstruction process less time-consuming. Compared to previously reported staining methods to delineate the lacunar-canalicular network and quantify bone porosity, the staining technique developed here presents several advantages: there is no need to decalcify the samples so the introduction of histological artifact is reduced; the staining technique is simple and fast, reducing the overall staining time from several days to half a day for rat bone; and finally, it does not introduce areas that are either over- or under-stained. The technique can also be used to illuminate the porosity patterns of a whole bone section without being limited to a restricted region, a factor that was not considered in the previous studies and makes this method more comprehensive.

The ability to visualize an entire cross-section makes this technique useful when analyzing and identifying bone macrostructure (e.g., compacted cancellous bone), and bone microstructure, such as regions with either high or low canalicular density. The

fluorescent properties of FITC and the high-resolution images might also be utilized to quantify the different microporosities in bone (vascular porosity and lacunar-canalicular porosity) and to obtain 3-D images to analyze bone permeability. Finally, this staining method can be easily adapted to different bone sizes, and different species.

Acknowledgments

This study was supported by a grant from the NIH (NIAMS, AR052866).

3.5 References

[1] Han Y, Cowin SC, Schaffler MB, Weinbaum S. Mechanotransduction and strain amplification in osteocyte cell processes. Proc Natl Acad Sci U S A 2004;101: 16689-94.

[2] Hillsley MV, Frangos JA. Bone tissue engineering: the role of interstitial fluid flow. Biotechnol Bioeng 1994;43: 573-81.

[3] Klein-Nulend J, van der Plas A, Semeins CM, Ajubi NE, Frangos JA, Nijweide PJ, Burger EH. Sensitivity of osteocytes to biomechanical stress in vitro. Faseb J 1995;9: 441-5.

[4] Piekarski K, Munro M. Transport mechanism operating between blood supply and osteocytes in long bones. Nature 1977;269: 80-2.

[5] Weinbaum S, Cowin SC, Zeng Y. A model for the excitation of osteocytes by mechanical loading-induced bone fluid shear stresses. J Biomech 1994;27: 339-60.

[6] You L, Cowin SC, Schaffler MB, Weinbaum S. A model for strain amplification in the actin cytoskeleton of osteocytes due to fluid drag on pericellular matrix. J Biomech 2001;34: 1375-86.

[7] Baylink DJ, Wergedal JE. Bone formation by osteocytes. Am J Physiol 1971;221: 669-78.

[8] Kusuzaki K, Kageyama N, Shinjo H, Murata H, Takeshita H, Ashihara T, Hirasawa Y. A staining method for bone canaliculi. Acta Orthop Scand 1995;66: 166-8.

[9] Li GP, Bronk JT, An KN, Kelly PJ. Permeability of cortical bone of canine tibiae. Microvasc Res 1987;34: 302-10.

[10] Ciani C, Doty SB, Fritton SP. Mapping bone interstitial fluid movement: displacement of ferritin tracer during histological processing. Bone 2005;37: 379-87.

[11] Erben RG. Embedding of bone samples in methylmethacrylate: an improved method suitable for bone histomorphometry, histochemistry, and immunohistochemistry. J Histochem Cytochem 1997;45: 307-13.

[12] Enlow DH. Principle of Bone Remodeling. Springfield, IL: Charles C. Thomas; 1963.

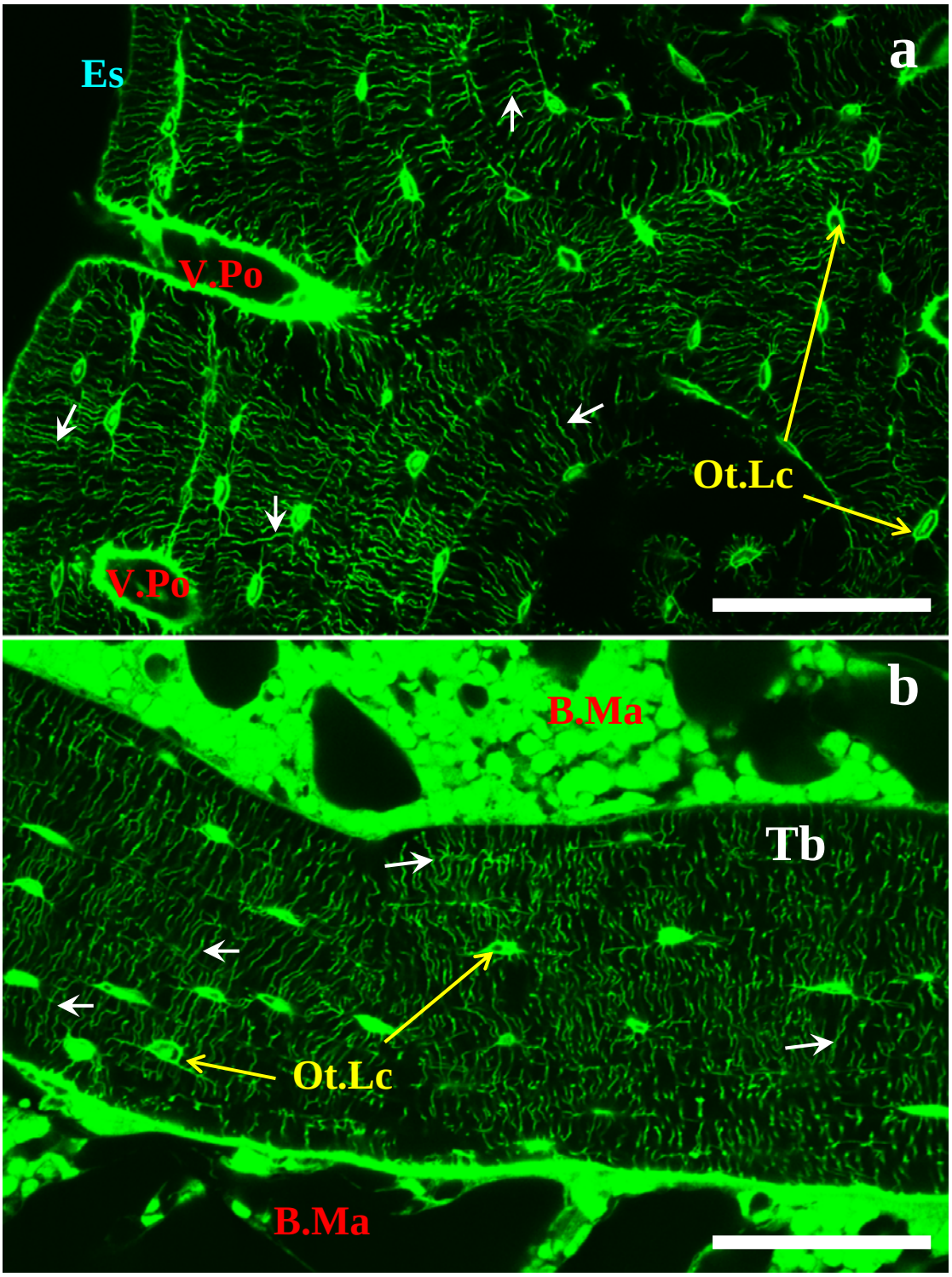

Figure 3-1. (a) Fresh cortical rat tibia diaphysis and (b) PMMA-embedded cancellous rat tibia metaphysis stained with FITC. The staining method demarcates the vascular porosity (V.Po), the canalicular porosity (small arrows), and the interstitial space surrounding the osteocyte lacunae (Ot.Lc) of both cortical and cancellous bone. Endosteal surface (Es) and bone marrow (B.Ma) are also marked; scale bars 130 μm.

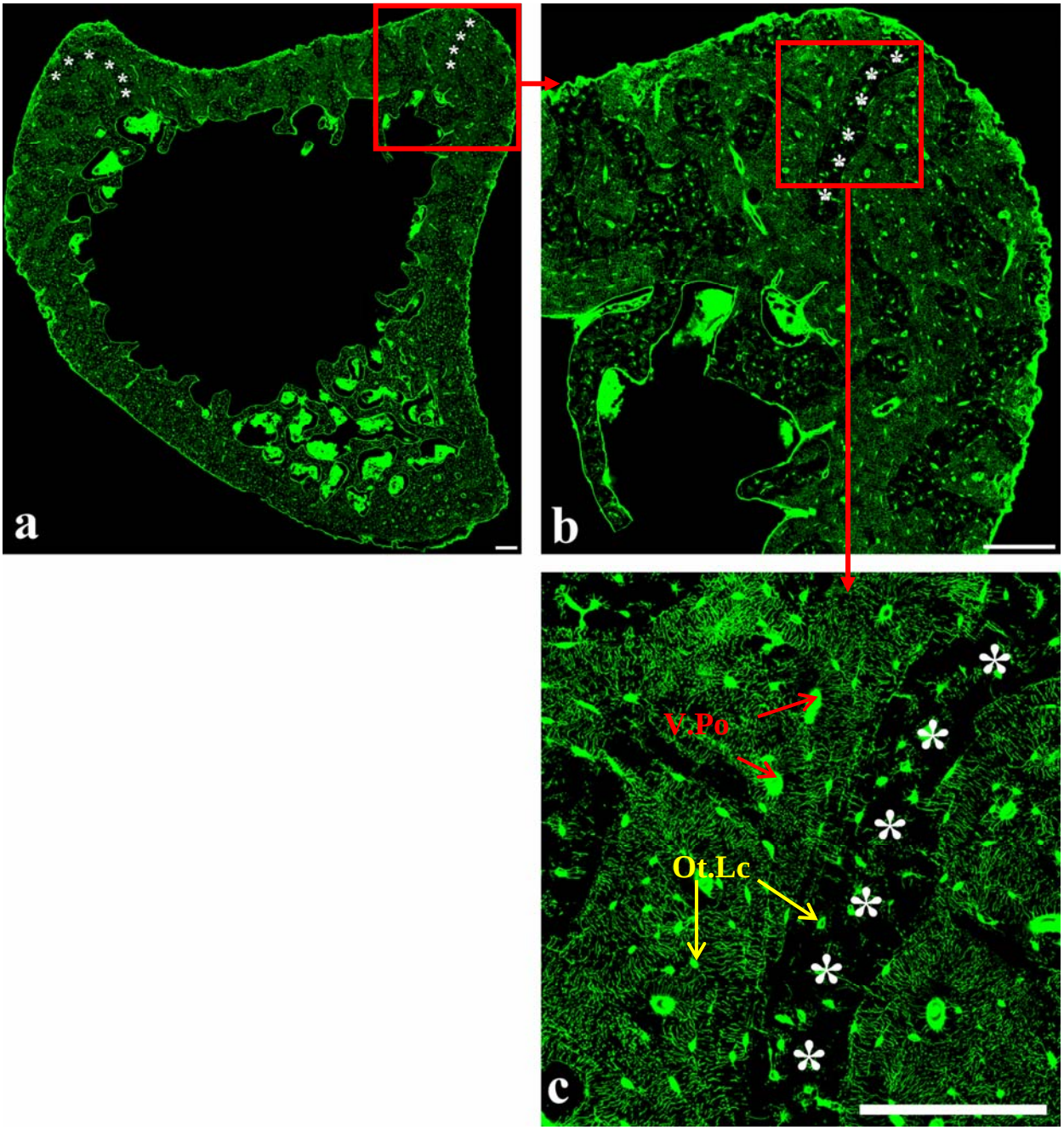

Figure 3-2. (a) Reconstructed section from the metaphyseal region of the rat tibia, and enlargement of the areas delineated by the red squares (b, c). With the reconstruction technique it is possible to visualize bone macrostructure (e.g., compacted cancellous bone), the complexity of the lacunar-canalicular system, and areas with low canalicular density (asterisks). In (c) it is possible to clearly distinguish the inhomogeneous distribution of the lacunar-canalicular system, with areas of low canalicular density in the older cancellous bone (asterisks) and areas of high canalicular density in the filled-in compact bone. Osteocyte lacunae (Ot.Lc) and vascular porosity (V.Po) are indicated in (c). Scale bars 60 μm.

Chapter 4

Increase of Vascular and Lacunar-Canalicular Porosities and Modification of Bone Microarchitecture in Ovariectomized Rats

Increase of Vascular and Lacunar-Canalicular Porosities and Modification of Bone Microarchitecture in Ovariectomized Rats

Cesare Ciani[1], Paula A. Ramirez Marin[1], Stephen B. Doty[2], Susannah P. Fritton[1*]

[1]Department of Biomedical Engineering, City College of New York / CUNY, New York, NY 10031
[2]Research Division, Hospital for Special Surgery, New York, NY 10021

*Corresponding author

Mailing address:
Department of Biomedical Engineering
City College of New York
Convent Avenue at 138th Street
New York, NY 10031

212-650-5213 (voice); 212-650-6727 (fax)
fritton@ccny.cuny.edu

Abstract

Bone is a porous material with two functional levels of porosity, the vascular porosity and the connected lacunar-canalicular porosity that surrounds the osteocytes and their processes. The application of an external load enhances the fluid transport of metabolic substances through the canalicular network, the principal site of bone's mechanosensory system. It has been proposed that diminished osteocyte viability caused by osteoporosis could modify the lacunar-canalicular network, therefore affecting bone porosities and altering the mechanical stimulus experienced by bone cells. To verify the hypothesis of microporosity changes from osteoporosis, this study measured the vascular and lacunar-canalicular porosities of normal and osteopenic bone using an ovariectomized rat model. Five-month-old female Sprague Dawley rats were divided into two groups, with one group undergoing ovariectomy (OVX, n=6) and the other used as age-matched control (CTRL, n=6). Six weeks post-ovariectomy both groups were sacrificed, tibiae were harvested, and cortical and cancellous interstitial fluid spaces were labeled using a FITC fluorescent solution. Bone sections were imaged using confocal microscopy to visualize bone porosities and backscattered scanning electron microscopy (SEM) to qualitatively determine bone mineral distribution. Results show that ovariectomy caused an increase in the vascular and lacunar-canalicular porosities in cortical bone in the metaphysis, whereas there were no significant changes in the cortical bone of the diaphysis. Ovariectomy also caused an increase in the lacunar-canalicular porosity of cancellous bone in the metaphysis, whereas there were no significant changes in the cancellous bone of the epiphysis. The high-resolution confocal images showed a compacted cancellous bone structure common to both CTRL and OVX cortical diaphysis and metaphysis

sections. Comparison of confocal and backscattered SEM images of the same regions demonstrated that higher mineralized areas corresponded to areas with a less dense, disconnected canalicular network, whereas lower mineralized areas corresponded to areas with higher canalicular density. Compacted cancellous bone from the metaphysis demonstrated a larger canalicular diameter in the OVX group compared to CTRL. These differences found due to ovariectomy demonstrate a direct influence of osteoporosis on bone microporosities and microarchitecture. Further investigation with emphasis on the fluid flow pathway will be necessary to determine how osteoporosis affects interstitial fluid flow in bone.

Keywords

osteoporosis, osteocyte, lacunar-canalicular porosity, vascular porosity, confocal microscopy, bone microstructure, bone mineral density, scanning electron microscopy

Introduction

Bone is a dense, compact, yet porous material with two functional interconnected levels of porosity, the vascular porosity and the lacunar-canalicular porosity that surrounds the osteocytes and their processes. The vascular porosity, which is associated with the blood vessels present in bone, is the largest of the two bone porosities, with dimensions on the order of 20 - 50 μm in diameter [1-3]. The lacunar-canalicular porosity is formed by a network of lacunae and canals that house the osteocytes and their cytoplasmic processes. This three-dimensional arrangement of the processes allows communication between neighboring osteocytes, osteoblasts, bone lining cells, and the vascular porosity. The dimension associated with the lacunar-canalicular porosity is on the order of 500 nm [4, 5], while the interstitial space surrounding the osteocyte processes in the canaliculi is on the order of 100 nm [6]. Within the canaliculi a pericellular fiber matrix surrounds the osteocyte processes, which are believed to be tethered to the canalicular wall [6-10].

The vascular and lacunar-canalicular porosities are filled with mobile exchangeable interstitial fluid thought to play an important role in bone maintenance. The movement of interstitial fluid in the canalicular network affects bone cells in two ways: it is believed to produce a deflection of the transverse fibers (transmembrane links between the cell cytoskeleton and the canalicular wall), which activates osteocytes via cytoskeletal deformation [7-11], and it is involved in mass transport favoring the passage of nutrients to and the removal of waste products from the osteocytes buried in the mineralized matrix [4, 12-14]. The porosities associated with the vascular and lacunar-canalicular systems

and their relative macro- and microarchitecture also contribute to the overall mechanical properties of bone tissue [15-18].

Several groups have tried to visualize the interconnectedness of the vascular and lacunar-canalicular network and quantify bone microporosities using different methodologies. However, limitations of these studies include the small dimension of the lacunar-canalicular interstitial fluid space, the low resolution of the microscopic devices used, and the restricted areas analyzed [26-30]. The necessity to decalcify bone samples might also induce histological artifacts [31]. Only recently have new techniques been developed to image the lacunar-canalicular network and quantify the submicron porosity of bone [5, 32-34]. Accurate porosity measurements and knowledge of bone microarchitecture are important factors for determining realistic bone permeability values and to understand how bone would adapt to different scenarios, such as external load or osteoporosis. These measurements can then be used in poroelastic finite elements models that assess the response of bone to its external environment.

During osteoporosis development the lack of estrogen induces a series of events such as osteocyte apoptosis, reduced communication between neighboring osteocytes, and modification of bone macroarchitecture [19-26]. An increase in bone volume fraction is frequently reported, yet there is little analysis in the literature related to changes in microstructure and microporosities during osteoporosis. Osteocytes are extremely sensitive to interstitial fluid movement produced by mechanical stress and logistically are in the best position to perceive mechanical stimuli. Therefore, any alteration of the interconnectedness of the lacunar-canalicular network, such as microporosity and

structural changes occurring during osteoporosis, might affect the mechanosensory ability of the osteocyte.

To determine how the porosities of the vascular and lacunar-canalicular networks evolve in the osteoporotic condition, the current study utilized high-resolution confocal microscopy to image the vascular and lacunar-canalicular systems of cortical and cancellous bone. Bone microporosities and microstructure were analyzed using a new fluorescent staining technique to delineate the interstitial fluid pathway in normal and osteopenic bone. Backscattered scanning electron microscopy was also used to determine mineral distribution and its correlation to lacunar-canalicular density.

Methods

Twelve 5-month-old female Sprague Dawley rats were divided into two groups, with one group undergoing ovariectomy (OVX) at 5 months of age and the other group used as age-matched controls (CTRL). Surgery for ovary removal was performed by Harlan, and permission for the study was granted by the Institutional Animal Care and Use Committee at the Hospital for Special Surgery. The animals were housed and acclimatized one week after surgery and allowed free access to food and water for one week. After one week of ad libitum food access, the OVX group was pair-fed to the average food intake of the CTRL group. Six weeks post-ovariectomy the two groups (OVX, n=6, 339 ± 20g; CTRL, n=6, 266 ± 11g) were sacrificed.

Left tibiae were harvested and put immediately in EM fixative (0.5% gluteraldehyde, 2% paraformaldehyde in 0.05M cacodylate-sodium buffer, pH 7.4). To map cortical and cancellous bone porosities, samples were taken from three different locations of the tibia

(Figure 4-1). Cortical bone sections (0.3-0.6 mm) were cut with a diamond blade saw (Buehler, Lake Bluff, IL) from the tibia diaphysis and from the metaphysis approximately 2 mm distal to the growth plate and then placed back into EM fixative for 48 hours. Cancellous bone blocks were obtained from the remaining proximal tibia containing the metaphysis and epiphysis (approximately 8–10 mm in length). Cortical sections were then rinsed in running water, ground down to a final thickness of 30-70 μm using Carbimet paper discs (600 and 1200 grit; Buehler) and dehydrated in a series of ascending graded alcohol (75%, 95%, and 100% ETOH, 5 minutes each solution), while the cancellous blocks were rinsed and dehydrated [35].

To label interstitial fluid space all the samples were stained using a newly developed staining protocol [36]. Briefly, thin cortical sections and cancellous blocks were stained for 4 hours in a 1% filtered FITC (Sigma, St. Louis, MO) solution dissolved in 100% ETOH, and rinsed in 100% ETOH for 30 minutes. The cancellous blocks were then embedded in PMMA [35], and sagittal or frontal tibial sections (0.4-0.6 mm) were cut from the plastic blocks with a diamond blade saw. Cancellous sections were then ground down to a final thickness of 40-70 μm using Carbimet paper discs (800 and 1200 grit; Buehler), and dried in ascending graded alcohol (75%, 95%, and 100%, 5 minutes each). Finally, all the cortical and cancellous sections were coverslipped with mounting media (Richard-Allan Scientific, Kalamazoo, MI).

Quantification of cortical bone porosity

To analyze the cortical bone porosity, cross-sections from the diaphysis and metaphysis were visualized using a confocal microscope (Leica TCS SP2, Germany) with

a 40x oil immersion lens (1.25 numerical aperture and pinhole set at 1 Airy unit) and wavelength excitation of 488 nm. Every image was taken at a resolution of 2048 x 2048 pixels with a field of view of 375 μm x 375 μm. A complete reconstruction of each tibial cross-section was obtained as a montage of all the field-of-view images acquired by confocal microscopy using Photoshop 7.0 (Adobe Systems, San Jose, CA). Reconstructed cross-sections ranged from ~ 104 million pixels, corresponding to ~ 900Mb for the diaphysis sections, to ~ 148 million pixels, corresponding to ~ 1.5Gb for the metaphysis sections. The images were transformed to grayscale and thresholded using Otsu's method (Image J, 1.37v, National Institutes of Health) so that the interstitial fluid space stained with FITC resulted in white pixels, whereas the impermeable area of the bone mineralized matrix was represented by black pixels.

The vascular porosity and the lacunar-canalicular porosity were quantified for the cortical diaphysis and metaphysis sections. To calculate the vascular porosity (measured as %), all the vascular pores present in each cortical section were identified, quantified, and divided by the cross-section cortical area. The lacunar-canalicular porosity (%) was calculated as the difference between the total FITC-stained interstitial fluid space (white pixels) and the pixels occupied by the vascular pores, divided by the cross-sectional area. The endosteal and periosteal surfaces were excluded when determining the cross-sectional area. For the cortical metaphysis cross-sections additional measurements were made because these sections contained a distinct compacted cancellous bone structure [37]. For the metaphysis cortical sections the percentage of cross-section having a ‘cancellous’ structure as well as the lacunar-canalicular porosity of both the ‘cancellous’ and ‘compact’ regions were quantified and compared. In addition, the vascular porosity

of the 'cancellous' regions was quantified. All measurements were obtained using Photoshop 7.0.

Quantification of cancellous bone porosity

For the metaphysis and epiphysis cancellous sections only the lacunar-canalicular porosity was quantified because the vascular porosity was not present within rat trabeculae of the proximal tibia. To determine the lacunar-canalicular porosity for the cancellous bone we analyzed 14 areas for each animal, 7 from the metaphyseal region below the growth plate and 7 from the epiphyseal region above the growth plate (Figure 4-2). These areas were visualized using the confocal microscope (Leica TCS SP2, Germany) with a 40x oil immersion lens (1.25 numerical aperture, 515 gain, 1.5 offset, and pinhole set at 1 Airy unit) and wavelength excitation of 488 nm. All the images were taken at a resolution of 2048 x 2048 pixels with a field view of 375 μm x 375 μm (Figure 4-2b, c). To quantify the lacunar-canalicular porosity the images were transformed to grayscale and thresholded using Otsu's method. The Otsu's threshold values were determined for each image over a region containing canaliculi. The lacunar-canalicular porosity was quantified as the percentage of white pixels (FITC-stained space) contained in the cancellous bone area examined, excluding marrow space or area taken up by the growth plate.

Assessment of bone mineral content

To further investigate the manifestation of osteoporosis in bone microstructure we imaged a subset of the OVX group (n=3) and the CTRL group (n=3) using scanning

electron microscopy in backscattered mode (ESEM, FEI Quanta 600, Hillsboro, Oregon). Using sections previously imaged with confocal microscopy, the backscattered images were used to qualitatively distinguish areas with different mineralization densities. Slide coverslips from cortical cross-sections from both the diaphysis and metaphysis were removed after being immersed in 100% xylene. Sections were then polished very gently with 1200 grit sandpaper to eliminate residual of either mounting media or xylene, mounted on a microscope stud holder, and visualized with SEM in backscattered mode.

Canalicular size measurements

To further investigate the effect of estrogen withdrawal on bone, we quantified the canalicular diameter for both the CTRL and OVX groups. From each group five reconstructed confocal images from the cortical metaphysis were thresholded and the mean canalicular diameter was obtained as the average of 4 measurements over the length of each canaliculus. Approximately 40 canalicular diameters were measured per section.

Because the resolution of the confocal microscope, ~ 200 nm, is of the same order of magnitude as the canalicular diameter size, ~ 500 nm, we are likely overestimating the lacunar-canalicular porosity due to partial volume effects. To investigate this overestimation, we also measured the canalicular diameter using scanning electron microscopy and compared it to the measurements obtained from confocal images. Fresh bone samples were obtained from additional age-matched control female Sprague Dawley rats (n=5, 325 ± 17g, from Harlan) that were not included in the previous porosity measurements. Fresh samples from the tibial metaphysis were harvested and

then cut using a hand saw to obtain approximately 5 x 5 mm samples. The blocks were cut longitudinally with a blade to expose the endosteal, trabecular, and cortical internal bone surfaces. To remove all cellular material samples were placed in a 20 ml aqueous solution containing 2% dimethyl sulfoxide, 2% Triton 100X, and 2% detergent that was sonicated for 40 minutes and then rinsed in running water and sonicated for 30 more minutes in fresh water. Samples were then dehydrated in 100% ETOH overnight, mounted on a sticky stub, coated with palladium (300 Å coat thickness) and finally visualized using an environmental scanning electron microscope (FEI Quanta 600). Canalicular diameters were measured using built-in microscope software on images taken at 10^4 magnification with a resolution of 1980 x 1400 pixels.

Statistical Analysis

For each location analyzed (cortical diaphysis, cortical metaphysis, cancellous metaphysis, and cancellous epiphysis) the vascular and lacunar-canalicular porosities of the CTRL group were chosen as the reference values and set equal to 1; the OVX porosities were then scaled to the CTRL reference values. This made the porosity differences between the OVX and CTRL groups easier to compare. For completeness, all the cortical and cancellous porosity measurements from the different tibial locations before and after normalization are also reported.

Vascular and lacunar-canalicular porosity cortical measurements were analyzed using two-way ANOVA repeated measurements for the two factors: group (OVX and CTRL) and location (diaphysis and metaphysis). Two-way ANOVA repeated measurements was also used to analyze the cancellous lacunar-canalicular porosity measurements for the

two factors: group (OVX and CTRL) and location (metaphysis and epiphysis). One-way ANOVA was used to analyze the canalicular diameters obtained from the confocal and scanning electron microscopy images. All the statistical analyses were performed using PRISM Statistic Package 2.0 (Graph-Pad Software Inc., San Diego, CA). For all the statistical tests, a significance level of $p < 0.05$ was used.

Results

The high-resolution confocal images illustrate the complexity of the bone microstructure in the cortical and cancellous bone of the rat tibia. All the sections showed uniform staining of the vascular and lacunar-canalicular systems, with the mineralized matrix impermeable to FITC (Figure 4-3).

Ovariectomy caused an increase in the microporosities of the cortical and cancellous bone in the metaphysis, with no significant changes in the cortical bone of the diaphysis or the cancellous bone of the epiphysis (Figure 4-4, Table 4-1). The cortical metaphysis of the OVX group had significantly higher vascular porosity (40% increase) and lacunar-canalicular porosity (16% increase) compared to CTRL (Figure 4-4a, b, Table 4-1). The lacunar-canalicular porosity of the cancellous metaphysis was also significantly higher in the OVX group compared to CTRL (56% increase) (Figure 4-4c, Table 4-1).

The high-resolution images showed a compacted cancellous bone structure [37] present in the cortical bone of the diaphysis and metaphysis in both CTRL and OVX groups (Figure 4-5). The compacted cancellous structure present in the diaphysis consisted of lamellar bone with the presence of a few randomly distributed higher mineralized endochondral spicule remnants [37]. In the metaphysis the compacted

cancellous structure consisted of older, higher mineralized 'cancellous' bone with a disconnected canalicular network surrounded by newer, lower mineralized 'compact' bone with a densely connected canalicular network [37] (Figure 4-5a-c). The percentage of the bone cross-section taken up by the 'cancellous' region, the irregular vascular porosity associated with the 'cancellous' region, and the lacunar-canalicular porosity of the 'compact' region were significantly higher in the OVX group (Table 4-2, Figure 4-6).

Comparisons of cortical bone sections imaged with both confocal microscopy and backscattered SEM demonstrated that areas with an absent or disconnected canalicular network had a higher mineralization density (Figure 4-5b-e). Conversely, areas with lower mineralization densities had a higher canalicular density (Figure 4-5b-e).

The canalicular diameter measured from the confocal images of the OVX group (697 ± 51.0 nm) was significantly larger, ~ 20%, than the canalicular diameter measured from the confocal images of the CTRL group (553 ± 32.5 nm). The canalicular diameter measured from the SEM images of age-matched normal rats (329 ± 137 nm) was significantly lower (~ 63% less) than that measured with confocal microscopy.

Discussion

The techniques used in this study, confocal and scanning electron microscopy, allowed us to obtain high-resolution images to quantify cortical and cancellous bone microporosities and illuminate the microstructural details of the lacunar-canalicular network, to visualize bone mineral distribution and correlate it to different porosity patterns, and to measure the canalicular diameter in normal and osteopenic rat bone. The vascular and lacunar-canalicular porosities of the cortical bone in the diaphysis of the rat

tibia showed no response to removal of estrogen, while the cortical bone in the metaphysis showed a 40% increase in vascular porosity and a 16% increase in lacunar-canalicular porosity. The cancellous bone in the metaphysis demonstrated a large increase (56%) in the lacunar-canalicular porosity due to ovariectomy, while the lacunar-canalicular porosity of cancellous bone in the epiphysis did not change with OVX. The lack of response to removal of estrogen in the diaphysis and epiphysis, and the active response in the metaphysis is similar to bone macroporosity changes previously reported, showing a greater and quicker response in the proximal metaphysis [38-40]. The metaphysis is also rich with compacted cancellous bone that is younger and not completely quiescent, unlike the compacted cancellous bone found in the diaphysis [37].

The microstructure of the compacted cancellous bone of the metaphysis showed several adaptations to ovary removal. Ovariectomy produced an increase in the 'cancellous' area, accompanied by an increase of the small, irregular vascular porosity associated with this particular bone structure (Figure 4-6). While this type of vasculature was present in the CTRL group, its increased presence in the OVX animals (increase of 65% compared to CTRL) must be attributed to the loss of estrogen. The lacunar-canalicular porosity also increased in the 'compact' regions of the compacted cancellous bone in the metaphysis in the OVX group. In addition, the average canalicular diameter measured in the cortical metaphysis increased by 20% in the OVX group compared to CTRL.

That the canalicular interstitial space around the osteocytes may be increased due to estrogen loss is important because such a change may affect the tethering of osteocytes to the canalicular wall, altering the effects of interstitial fluid flow due to mechanical

loading. The capability of osteocytes to adapt their lacunar wall under certain conditions was proposed by Heller-Steinberg in 1959, and named by Belanger in 1969 ‘osteolytic osteolysis’ [43, 44]. Several studies have shown that osteocytes can remodel their local environment, including lacunar and canalicular size, in response to hyperthyroidism, osteoporosis, and parathyroid hormone administration [24, 26, 45, 46]. In our study we did not quantify the change of lacunar size but we concentrated our attention on the canalicular system. The increased canalicular diameter of the OVX animals was determined over multiple measurements of the metaphysis sections; measurements were included from both the newer ‘compact’ and older ‘cancellous’ bone to have a homogeneous set of measurements related only to bone anatomical location. Further investigation to confirm the increase in canalicular size and to assess the effects on interstitial fluid flow is warranted.

Comparison of the same cortical sections imaged with confocal and backscattered scanning electron microscopy showed that bone regions with higher mineral density had lower canalicular density (endochondral spicule remnants in the diaphysis and the ‘cancellous’ regions in the metaphysis), while regions with lower mineral density had higher canalicular density (lamellar bone in the diaphysis, and newer ‘compact’ bone in the metaphysis). This type of structural development could be explained by osteocyte apoptotic activity and micropetrosis [21, 41]. The combined outcome of these two effects results in bone matrix hypermineralization of restricted areas previously occupied by apoptotic osteocytes and their dendritic processes, with consequent reduced lacunar-canalicular presence. This particular bone development has been shown to be present in bone of different age, but with higher frequency in older bone [42]. In our study the

micropetrotic nature of bone could explain the increase in 'cancellous' area in the cortical metaphysis of ovariectomized animals. It is possible that these regions increased due to osteocyte apoptosis on the borders of the regions that occurred over the six weeks of the experiment. However, this is speculation, and further studies will be needed to quantify osteocyte apoptosis and its relation to the microporosity and microarchitecture changes in the rat ovariectomy model.

While our methods are suitable for comparison between groups, a limitation of the study is that the confocal images overestimate the canalicular porosity due to partial volume effects caused by the confocal microscopy resolution (~ 200 nm). SEM measurements performed to assess the amount of overestimation of canalicular size gave an average canalicular diameter approximately 63% smaller than that measured with confocal microsopy. An important step needed to calculate bone microporosity was the thresholding, and using a more conservative threshold value would help to reduce the impact of confocal resolution over the canalicular porosity results; however, much investigation went into the choice of threshold, and the standard method chosen (Otsu's method) seemed appropriate for this application. While more advanced image processing techniques could potentially be investigated to try to account for the partial volume effects, for this study we have emphasized the relative changes in microporosities between ovariectomized and control animals without focusing on the actual porosity values measured (although these are reported for completeness). In addition, the overestimation of microporosity only applies to the canalicular porosity and not the lacunar porosity because the lacunar size, on the order of 10 μm, is well-characterized at

a resolution of 200 nm. In this study, the lacunar and canalicular porosities were quantified jointly, without separating out the lacunar and canalicular porosities.

Despite the above limitations, we conclude the following: the vascular and lacunar-canalicular porosities of bone are influenced by loss of estrogen, with osteopenic rats showing increased porosity in the cortical and cancellous bone of the metaphysis of the proximal tibia; the microarchitecture of the compacted cancellous bone in the rat metaphysis is modified due to estrogen loss; bone regions with a less dense, disconnected canalicular network are more highly mineralized, whereas regions with a higher canalicular density are less mineralized; and the canalicular diameter is increased in the metaphysis of osteopenic rats compared to controls. The increased microporosities along with the microarchitectural changes may play a role in altering the mechanosensory system as well as the mechanical properties in bone, thus contributing to the increased risk of fracture occurring during osteoporosis. Further investigation into how bone interstitial fluid flow is affected by osteoporosis will be necessary to corroborate and support the data obtained in this analysis.

4.5 References

[1] Cooper RR, Milgram JW, Robinson RA. Morphology of the osteon. An electron microscopic study. J Bone Joint Surg Am 1966;48: 1239-71.

[2] Hancox NM. Biology of Bone. Cambridge, England: Cambridge University Press; 1972.

[3] Martin R. B. DBB. Structure, Function and Adaptation of Compact Bone. New York: Raven Press; 1989.

[4] Piekarski K, Munro M. Transport mechanism operating between blood supply and osteocytes in long bones. Nature 1977;269: 80-2.

[5] Knapp HF, Reilly GC, Stemmer A, Niederer P, Knothe Tate ML. Development of preparation methods for and insights obtained from atomic force microscopy of fluid spaces in cortical bone. Scanning 2002;24: 25-33.

[6] You LD, Weinbaum S, Cowin SC, Schaffler MB. Ultrastructure of the osteocyte process and its pericellular matrix. Anat Rec A Discov Mol Cell Evol Biol 2004;278: 505-13.

[7] Weinbaum S, Cowin SC, Zeng Y. A model for the excitation of osteocytes by mechanical loading-induced bone fluid shear stresses. J Biomech 1994;27: 339-60.

[8] You L, Cowin SC, Schaffler MB, Weinbaum S. A model for strain amplification in the actin cytoskeleton of osteocytes due to fluid drag on pericellular matrix. J Biomech 2001;34: 1375-86.

[9] Han Y, Cowin SC, Schaffler MB, Weinbaum S. Mechanotransduction and strain amplification in osteocyte cell processes. Proc Natl Acad Sci U S A 2004;101: 16689-94.

[10] Wang Y, McNamara LM, Schaffler MB, Weinbaum S. A model for the role of integrins in flow induced mechanotransduction in osteocytes. Proc Natl Acad Sci U S A 2007;104: 15941-6.

[11] Cowin SC, Weinbaum S, Zeng Y. A case for bone canaliculi as the anatomical site of strain generated potentials. J Biomech 1995;28: 1281-97.

[12] Doty SB, Schofield BH. Electron microscopic localization of hydrolytic enzymes in osteoclasts. Histochem J 1972;4: 245-58.

[13] Tami AE, Schaffler MB, Knothe Tate ML. Probing the tissue to subcellular level structure underlying bone's molecular sieving function. Biorheology 2003;40: 577-90.

[14] Wang L, Ciani C, Doty SB, Fritton SP. Delineating bone's interstitial fluid pathway in vivo. Bone 2004;34: 499-509.

[15] Martin RB. Determinants of the mechanical properties of bones. J Biomech 1991;24 Suppl 1: 79-88.

[16] McCalden RW, McGeough JA, Barker MB, Court-Brown CM. Age-related changes in the tensile properties of cortical bone. The relative importance of changes in porosity, mineralization, and microstructure. J Bone Joint Surg Am 1993;75: 1193-205.

[17] Schaffler MB, Burr DB. Stiffness of compact bone: effects of porosity and density. J Biomech 1988;21: 13-6.

[18] Yeni YN, Brown CU, Wang Z, Norman TL. The influence of bone morphology on fracture toughness of the human femur and tibia. Bone 1997;21: 453-9.

[19] Knothe Tate ML, Adamson JR, Tami AE, Bauer TW. The osteocyte. Int J Biochem Cell Biol 2004;36: 1-8.

[20] Tomkinson A, Gevers EF, Wit JM, Reeve J, Noble BS. The role of estrogen in the control of rat osteocyte apoptosis. J Bone Miner Res 1998;13: 1243-50.

[21] Tomkinson A, Reeve J, Shaw RW, Noble BS. The death of osteocytes via apoptosis accompanies estrogen withdrawal in human bone. J Clin Endocrinol Metab 1997;82: 3128-35.

[22] Bagi CM, Ammann P, Rizzoli R, Miller SC. Effect of estrogen deficiency on cancellous and cortical bone structure and strength of the femoral neck in rats. Calcif Tissue Int 1997;61: 336-44.

[23] Baldock PA, Need AG, Moore RJ, Durbridge TC, Morris HA. Discordance between bone turnover and bone loss: effects of aging and ovariectomy in the rat. J Bone Miner Res 1999;14: 1442-8.

[24] Wright PH, Jowsey JO, Robb RA. Osteocyte lacunar area in normal bone, hyperparathyroidism, renal disease, and osteoporosis. Surg Forum 1978;29: 558-9.

[25] Wronski TJ, Lowry PL, Walsh CC, Ignaszewski LA. Skeletal alterations in ovariectomized rats. Calcif Tissue Int 1985;37: 324-8.

[26] Baylink DJ, Wergedal JE. Bone formation by osteocytes. Am J Physiol 1971;221: 669-78.

[27] Kusuzaki K, Kageyama N, Shinjo H, Murata H, Takeshita H, Ashihara T, Hirasawa Y. A staining method for bone canaliculi. Acta Orthop Scand 1995;66: 166-8.

[28] Li GP, Bronk JT, An KN, Kelly PJ. Permeability of cortical bone of canine tibiae. Microvasc Res 1987;34: 302-10.

[29] Ferretti M, Muglia MA, Remaggi F, Cane V, Palumbo C. Histomorphometric study on the osteocyte lacuno-canalicular network in animals of different species. II. Parallel-fibered and lamellar bones. Ital J Anat Embryol 1999;104: 121-31.

[30] Remaggi F, Cane V, Palumbo C, Ferretti M. Histomorphometric study on the osteocyte lacuno-canalicular network in animals of different species. I. Woven-fibered and parallel-fibered bones. Ital J Anat Embryol 1998;103: 145-55.

[31] Ciani C, Doty SB, Fritton SP. Mapping bone interstitial fluid movement: displacement of ferritin tracer during histological processing. Bone 2005;37: 379-87.

[32] Schneider P, Stauber M, Voide R, Stampanoni M, Donahue LR, Muller R. Ultrastructural properties in cortical bone vary greatly in two inbred strains of mice as assessed by synchrotron light based micro- and nano-CT. J Bone Miner Res 2007;22: 1557-70.

[33] Kamioka H, Honjo T, Takano-Yamamoto T. A three-dimensional distribution of osteocyte processes revealed by the combination of confocal laser scanning microscopy and differential interference contrast microscopy. Bone 2001;28: 145-9.

[34] Sugawara Y, Kamioka H, Honjo T, Tezuka K, Takano-Yamamoto T. Three-dimensional reconstruction of chick calvarial osteocytes and their cell processes using confocal microscopy. Bone 2005;36: 877-83.

[35] Erben RG. Embedding of bone samples in methylmethacrylate: an improved method suitable for bone histomorphometry, histochemistry, and immunohistochemistry. J Histochem Cytochem 1997;45: 307-13.

[36] Ciani C, Doty SB, Fritton SP. Effective Histological Staining Process Developed to Visualize Bone Interstitial Space Using Confocal Microscopy. Bone submitted, 2008.

[37] Enlow DH. Principle of Bone Remodeling. Springfield, IL: Charles C. Thomas; 1963.

[38] Frost HM, Jee WS. On the rat model of human osteopenias and osteoporoses. Bone Miner 1992;18: 227-36.

[39] Westerlind KC, Wronski TJ, Ritman EL, Luo ZP, An KN, Bell NH, Turner RT. Estrogen regulates the rate of bone turnover but bone balance in ovariectomized rats is modulated by prevailing mechanical strain. Proc Natl Acad Sci U S A 1997;94: 4199-204.

[40] Wronski TJ, Dann LM, Scott KS, Cintron M. Long-term effects of ovariectomy and aging on the rat skeleton. Calcif Tissue Int 1989;45: 360-6.

[41] Frost HM. Micropetrosis. J Bone Joint Surg Am 1960;42-A: 144-50.

[42] Remaggi F, Ferretti M, Cane V, Zaffe D. Histomorphological and chemico-physical analyses of the mineral matrix of micropetrotic human bone. Ann Anat 1996;178: 223-7.

[43] Belanger LF. Osteocytic osteolysis. Calcif Tissue Res 1969;4: 1-12.

[44] Heller-Steinberg M. Ground substance, bone salts, and cellular activity in bone formation and destruction. Am J Anat 1951;89: 347-79.

[45] Lane NE, Yao W, Balooch M, Nalla RK, Balooch G, Habelitz S, Kinney JH, Bonewald LF. Glucocorticoid-treated mice have localized changes in trabecular bone material properties and osteocyte lacunar size that are not observed in placebo-treated or estrogen-deficient mice. J Bone Miner Res 2006;21: 466-76.

[46] Tazawa K, Hoshi K, Kawamoto S, Tanaka M, Ejiri S, Ozawa H. Osteocytic osteolysis observed in rats to which parathyroid hormone was continuously administered. J Bone Miner Metab 2004;22: 524-9.

	Vascular Porosity (%)		Lacunar-canalicular porosity (%)	
	CTRL	**OVX**	**CTRL**	**OVX**
Cortical bone				
diaphysis	**2.36 ± 0.17** (1 ± 0.07)	**2.55 ± 0.24** (1.08 ± 0.1)	**19.3 ± 1** (1 ± 0.52)	**22.5 ± 5.2** (1.17 ± 0.27)
metaphysis	**2.89 ± 0.38** (1 ± 0.13)	**4.1 ± 1.01** (1.42 ± 0.35)*	**19.5 ± 2.11** (1 ± 0.11)	**22.7 ± 2.3** (1.16 ± 0.12)*
Cancellous bone				
epiphysis	not present	not present	**11.4 ± 2.09** (1 ± 0.18)	**13 ± 0.63** (1.14 ± 0.06)
metaphysis	not present	not present	**8.06 ± 1.21** (1 ± 0.15)	**12.5 ± 2.13** (1.56 ± 0.27)*

Table 4-1. Control (CTRL) and ovariectomized (OVX) vascular porosity and lacunar-canalicular porosity for the cortical diaphysis and metaphysis, and the cancellous metaphysis and epiphysis. The original measurements are reported (bold values), along with the reference values scaled to CTRL for each measurement (values in parentheses). All measurements expressed as mean ± standard deviation. *$p < 0.05$ versus CTRL.

	CTRL	OVX
'cancellous' area	**36.6 ± 5.85** (1 ± 0.16)	**43.79 ± 4.56** (1.2 ± 0.12)*
'cancellous' vascular porosity	**0.33 ± 0.06** (1 ± 0.19)	**0.55 ± 0.13** (1.65 ± 0.38)*
'cancellous' lacunar-canalicular porosity	**14.38 ± 1.3** (1 ± 0.09)	**14.53 ± 1.1** (1.01 ± 0.08)
'compact' lacunar-canalicular porosity	**27.57 ± 3.26**[a] (1 ± 0.12)	**34.18 ± 2.66**[a] (1.24 ± 0.1)*

Table 4-2. Compacted cancellous bone measurements from the cortical metaphysis sections of the control (CTRL) and ovariectomized (OVX) groups. The 'cancellous' area is the percentage of the total cross-section that taken up by the 'cancellous' regions (Figure 4-6). The original percentage measurements are reported (bold values), along with the reference values scaled to CTRL for each measurement (values in parentheses). All the measurements are expressed as mean ± standard deviation. *$p < 0.05$ versus CTRL.; [a]$p < 0.05$ for 'compact' versus 'cancellous' lacunar-canalicular porosity within the same group.

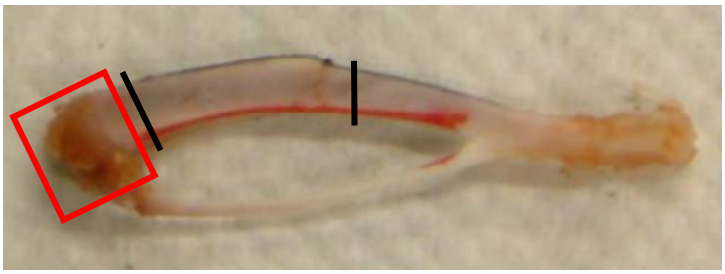

Figure 4-1. Cortical sections were obtained from the diaphysis (D) and metaphysis (M) of the rat tibia. Cancellous sections were obtained from the metaphysis and epiphysis of the proximal tibia. (square).

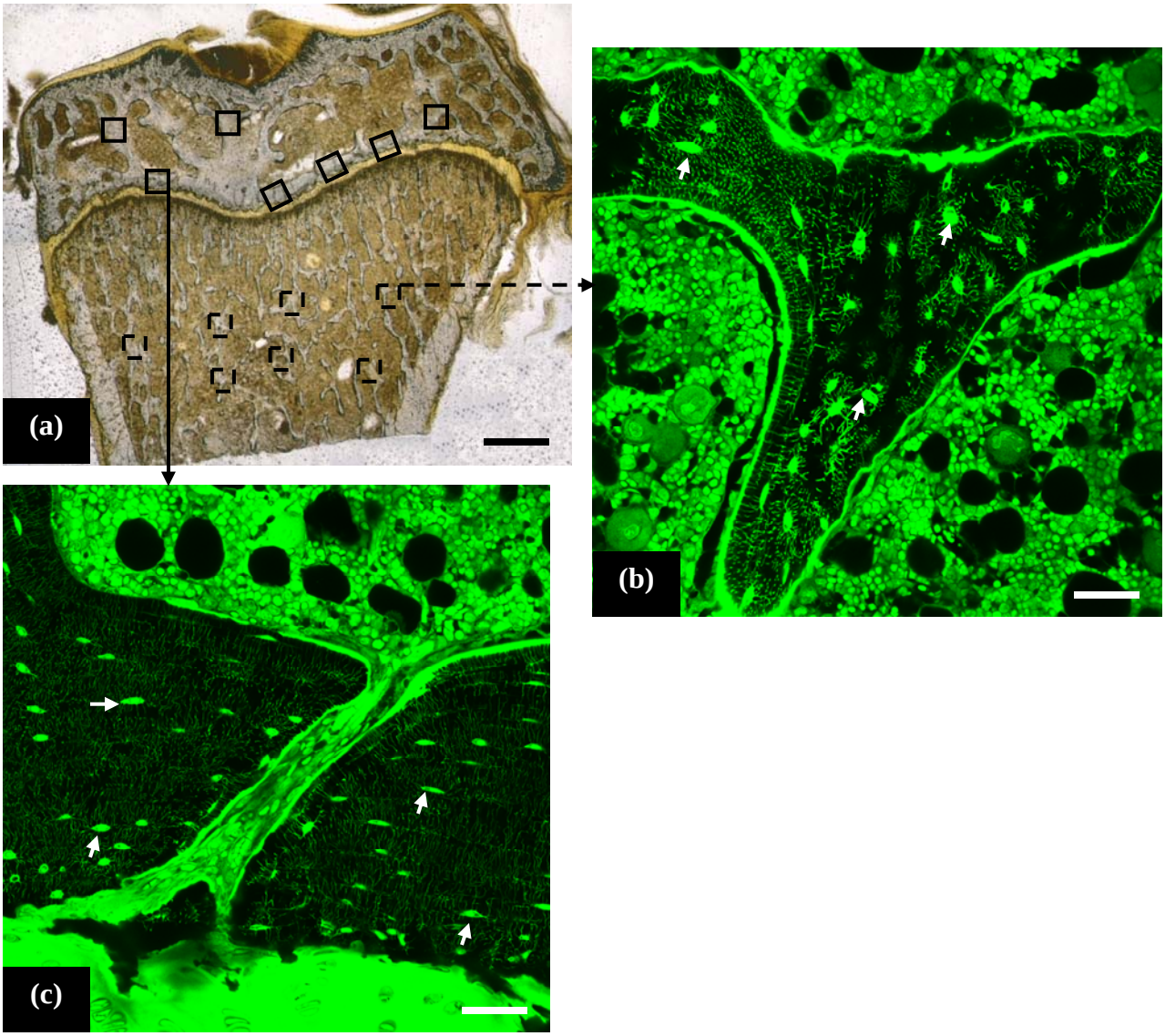

Figure 4-2. (a) A montaged light micrograph of the proximal rat tibia showing the cancellous regions sampled with 375 µm x 375 µm field of view images from the metaphysis (dashed line boxes) and the epiphysis (solid line boxes); scale bar 400 µm. Typical metaphysis (b) and (c) epiphysis (c) confocal images; osteocyte lacunae (short arrows) are indicated; scale bar 50 µm.

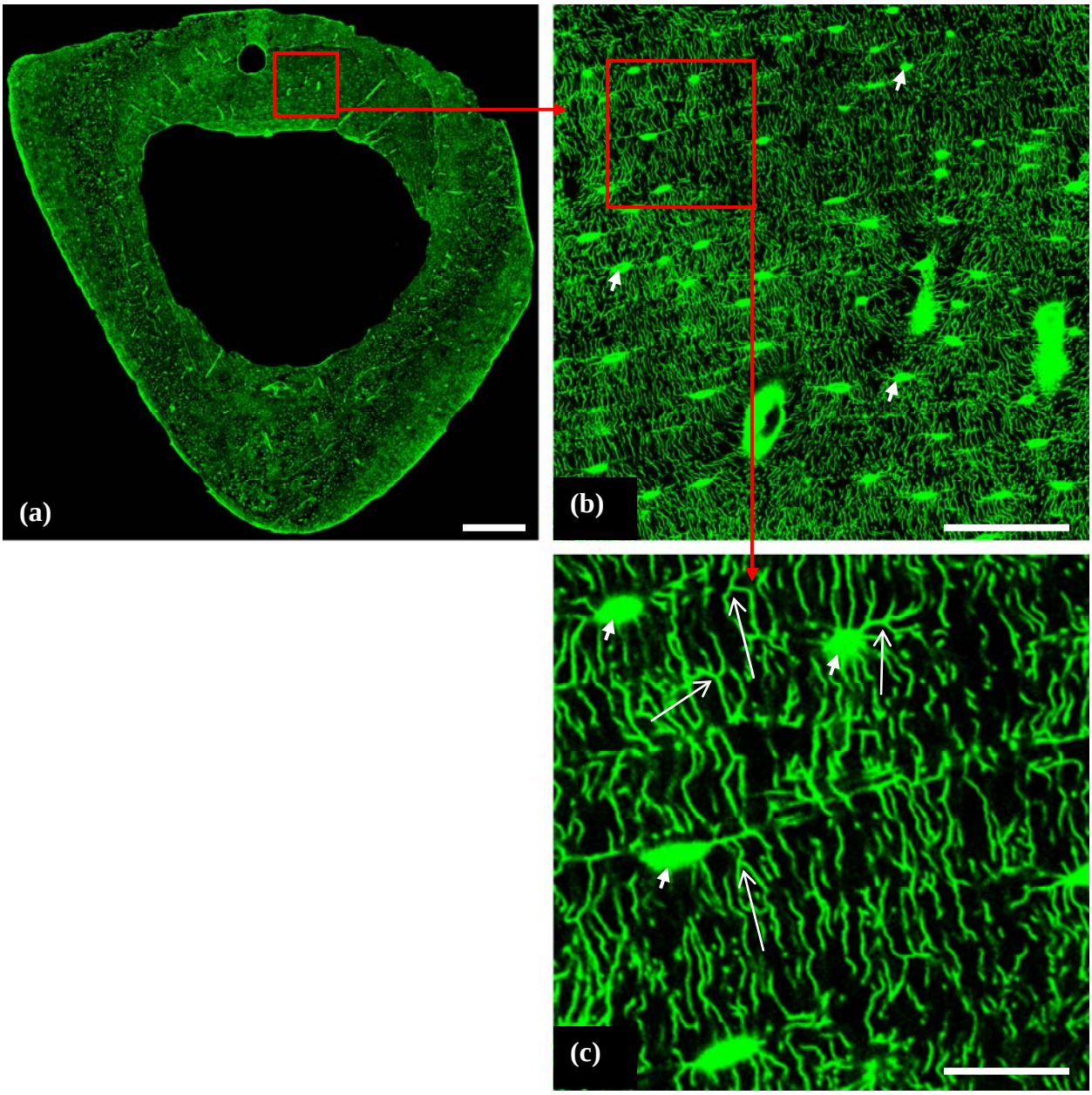

Figure 4-3. (a) A typical OVX diaphysis section created from approximately 50 montaged confocal images; scale bar 300 μm. (b) Enlarged image of square region in (a), which demonstrates the high resolution of the images; scale bar 50 μm. (c) Enlarged image of the square region in (b), further illustrating the details of the lacunar-canalicular network; scale bar 10 μm. Osteocyte lacunae (short arrows), and canalicular branching (long arrows) are indicated in (b) and (c).

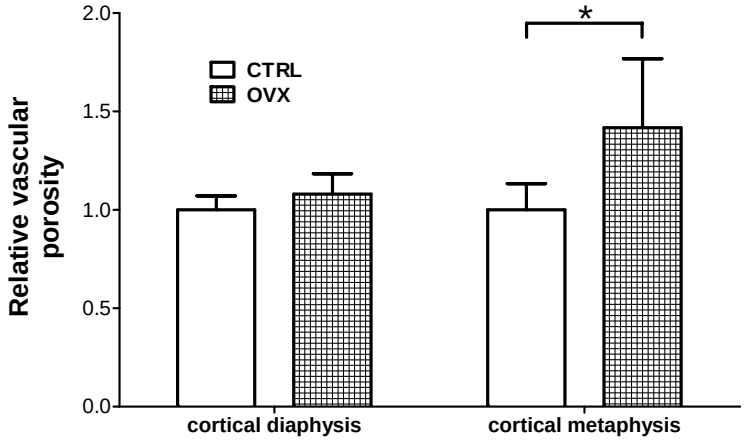

(a)

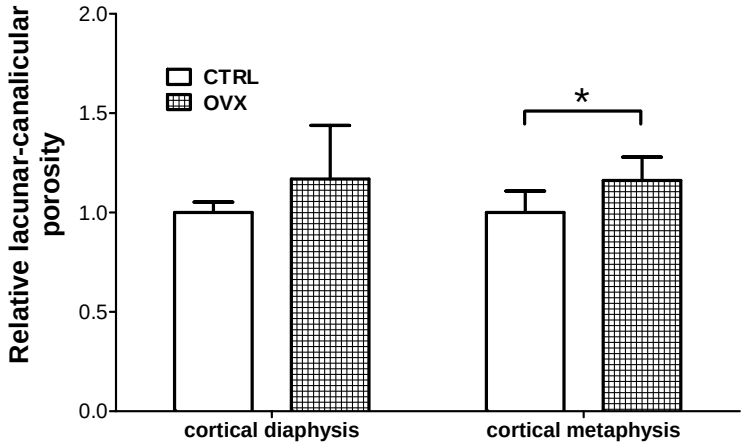

(b)

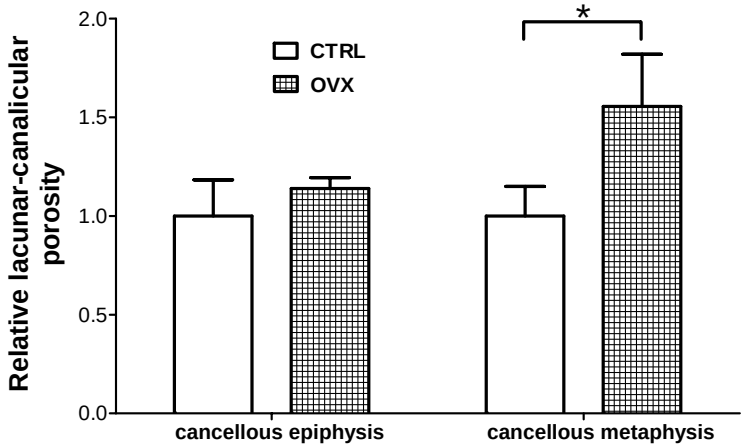

(c)

Figure 4-4. (a) Relative vascular porosities and (b) relative lacunar-canalicular porosities for the cortical diaphysis and metaphysis sections. (c) Relative lacunar-canalicular porosity for cancellous bone from the metaphysis and epiphysis of the proximal tibia. All measurements were scaled to the CTRL mean for each porosity; bars represent mean values ± standard deviations; * indicates statistical difference between groups ($p < 0.05$).

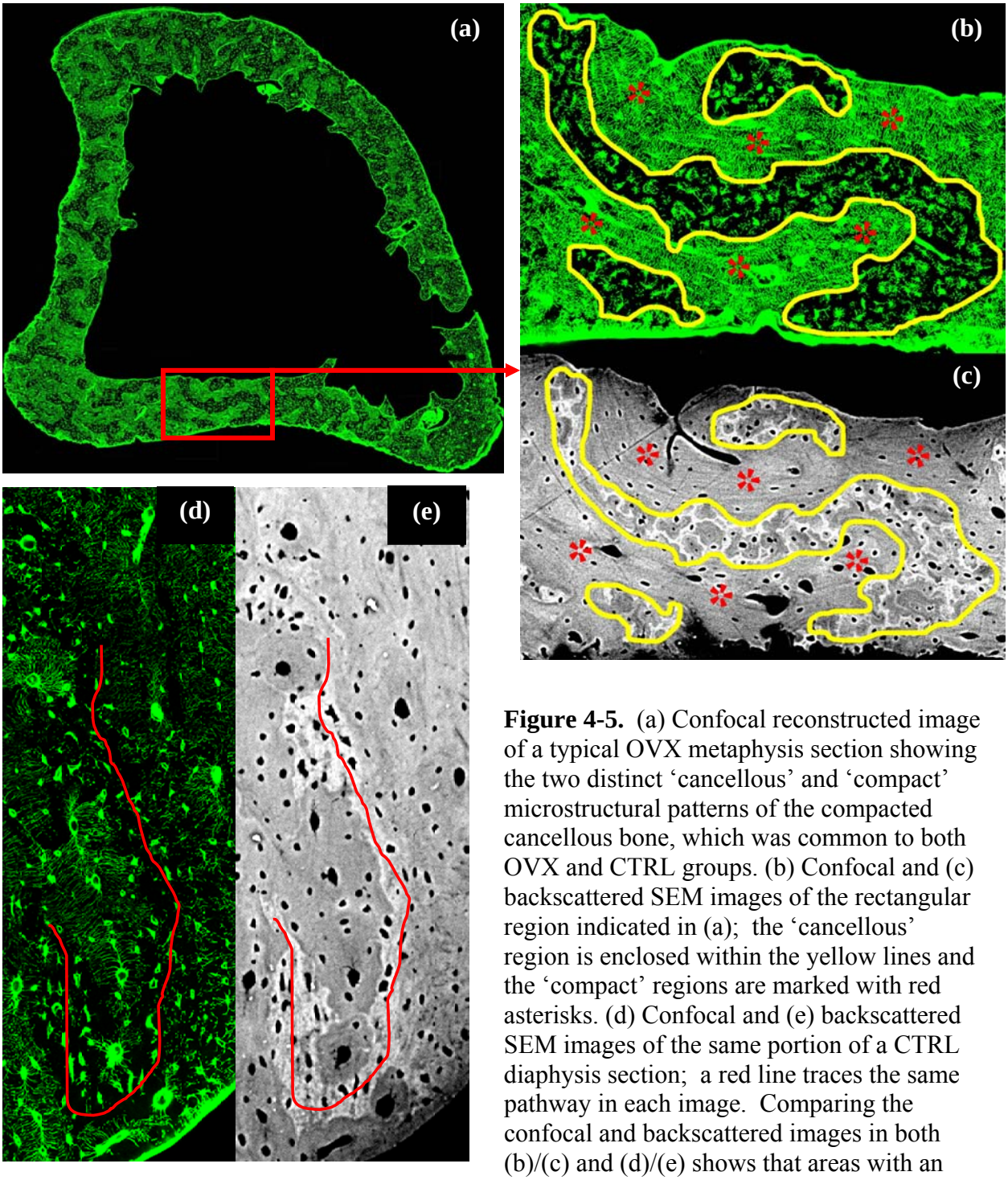

Figure 4-5. (a) Confocal reconstructed image of a typical OVX metaphysis section showing the two distinct 'cancellous' and 'compact' microstructural patterns of the compacted cancellous bone, which was common to both OVX and CTRL groups. (b) Confocal and (c) backscattered SEM images of the rectangular region indicated in (a); the 'cancellous' region is enclosed within the yellow lines and the 'compact' regions are marked with red asterisks. (d) Confocal and (e) backscattered SEM images of the same portion of a CTRL diaphysis section; a red line traces the same pathway in each image. Comparing the confocal and backscattered images in both (b)/(c) and (d)/(e) shows that areas with an absent or disconnected canalicular network regions surrounding osteocyte lacunae in the confocal images; b: enclosed within the yellow line; d: around the red line) corresponds to higher mineralization (whiter regions in the backscattered SEM images; c: enclosed within the yellow line; e: around the red line). On the contrary, higher canalicular density areas (b: red asterisks) correspond to areas of lower mineralization (c: red asterisks).

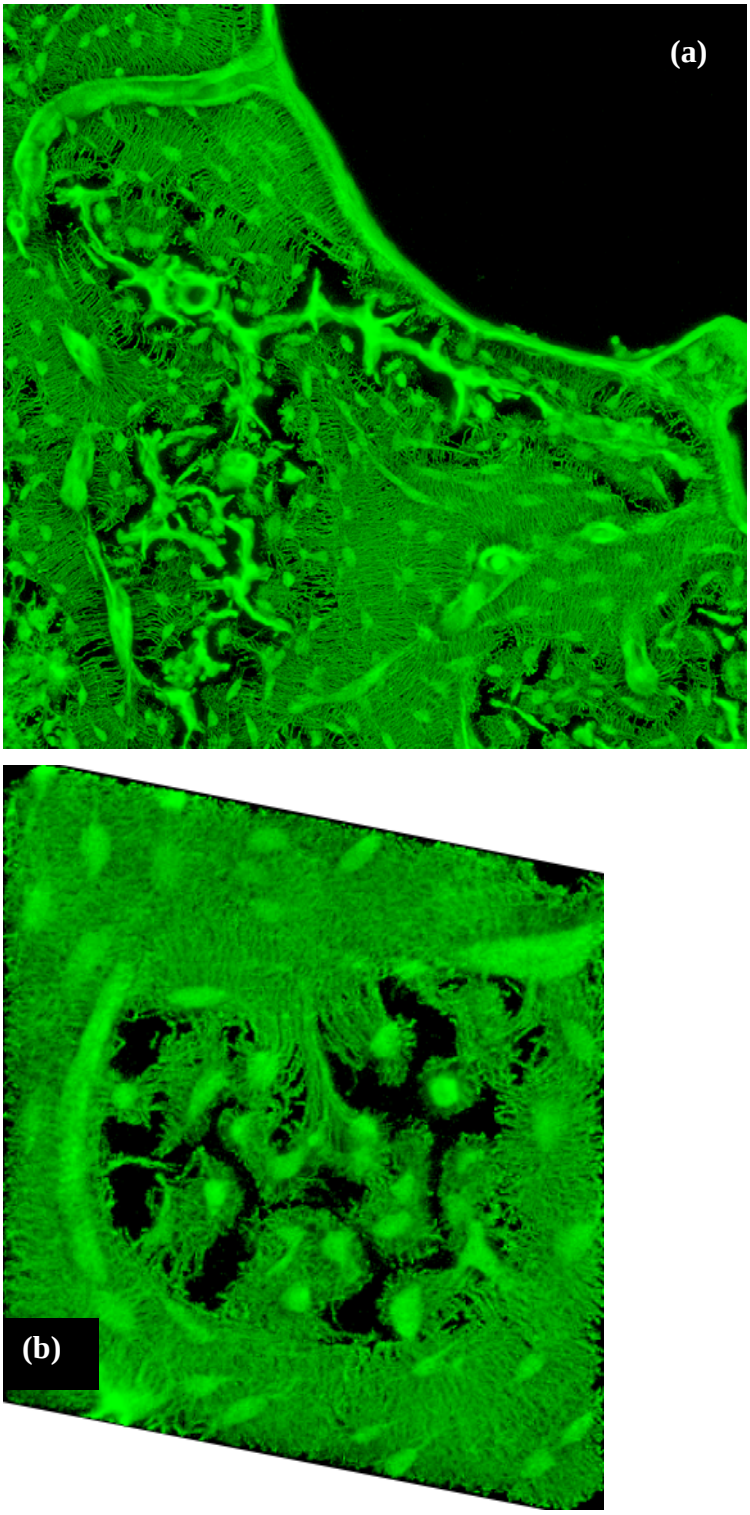

Figure 4-6. 3-D confocal stack reconstructions (approximately 20 microns thick) from compacted cancellous bone from the metaphysis. (a) OVX bone demonstrated an irregular vascular porosity associated with the 'cancellous' areas (short arrows). (b) CTRL bone demonstrated a more regular vascular porosity.

Chapter 5

Ovariectomy Enhances Mechanical Load-Induced Lacunar-Canalicular Mass Transport in Rat Tibial Cancellous Bone

Ovariectomy Enhances Mechanical Load-Induced Lacunar-Canalicular Mass Transport in Rat Tibial Cancellous Bone

Cesare Ciani[1], Adriana I. Larriera[1], Divya Sharma[1], Stephen B. Doty[2], Susannah P. Fritton[1*]

Email addresses:
cciani@gc.cuny.edu, adril84@msn.com, DotyS@hss.edu, fritton@ccny.cuny.edu

Corresponding author:
Susannah P. Fritton, Ph.D.
Department of Biomedical Engineering
The City College of New York
Convent Avenue at 138th Street
New York, NY 10031
Phone: 212-650-5213
Fax: 212-650-6727
Email: fritton@ccny.cuny.edu

Running Title:
OVARIECTOMY ENHANCES MECHANICAL LOAD-INDUCED TRANSPORT

Funding Sources:
This work was financially supported by NIH/NIAMS (AR052866).

Manuscript:	Printed pages:	**Abstract:**	279 words
	Words:		1764 characters
	Characters:		
	Black/White Figures:		
	Color Figures:		
	Tables:		
	References:		

[1]Department of Biomedical Engineering, The City College of New York / CUNY, New York, NY 10031
[2]Research Division, Hospital for Special Surgery, New York, NY 10021

Conflict of Interest Page

All the authors state that they have no conflicts of interest.

Abstract:

It has been proposed that an alteration in osteocyte viability due to osteoporosis could alter the interconnectedness of the osteocyte network, affecting interstitial fluid flow and altering the mechanical stimulus experienced by the bone cells. In this study we examined the combined effect of estrogen depletion and external loading on both cortical and cancellous bone. Female Sprague Dawley rats were divided into two groups, with one group undergoing ovariectomy (OVX, n=6) and the other group SHAM operated (n=6) at 5 months of age. Six weeks post-ovariectomy both groups were anaesthetized and injected with FITC-labeled bovine serum albumin (~ 7 nm diameter). Immediately after the tracer injection an external non-invasive physiological sinusoidal load was applied to the right tibia for 100 cycles at 1 Hz, producing approximately 500 microstrain on the proximal medial tibia. After histological processing of the proximal tibia, sections were imaged using confocal microscopy and tracer transport through the lacunar-canalicular system was quantified in cortical and cancellous bone from the metaphysis and epiphysis. The applied loading increased the percentage of osteocyte lacunae labeled with injected tracer for both groups, from an increase of 63% for the cortical metaphysis of the SHAM group, up to 327% for the cancellous epiphysis of the OVX group. Ovariectomy enhanced movement of tracer into the lacunar-canalicular porosity due to applied mechanical loading in the cancellous bone of the epiphysis and metaphysis but not in the cortical bone of the metaphysis. This study demonstrates that interstitial bone fluid flow in cancellous bone of the rat proximal tibia is increased not only through external mechanical loading but also after the development of osteopenia due to

ovariectomy, supporting the involvement of osteoporosis in bone metabolic transport and potentially in bone's mechanosensory system.

Key words: mechanical loading; cortical and cancellous bone; osteoporosis; confocal microscopy; bone interstitial fluid flow

Introduction

Bone is a porous, dynamic, and complex cellular structure that adapts to accommodate changes in its functional environment. The lacunar-canalicular porosity is a complex web of lacunae and canaliculi in the mineralized matrix that houses the osteocytes and their processes, forming a syncytium that connects osteocytes and cells located on bone surfaces [1-3]. The anatomical location of osteocytes and the extended connection to the different types of bone cells make them the ideal candidate to perceive and respond to mechanical stimuli.

When bone is mechanically loaded fluid pressure gradients are induced through bone pores, creating a load-induced interstitial fluid displacement in the lacunar-canalicular porosity [4]. Load-induced interstitial fluid movement affects osteocytes by enhancing solute transport via convective transport mechanisms to ensure the metabolic function of bone cells, which is crucial for bone maintenance and adaptation. Load-induced interstitial fluid movement is also believed to play a role in bone's mechanosensory system via the deformation of the osteocyte process cytoskeleton [16-22]. To demonstrate mass transport in the lacunar-canalicular system, several groups have performed in vivo vascular injection of different tracers, such as microperoxidase, ferritin, reactive red, and procion red [5-12]. The same experimental approach has also been used to demonstrate enhanced mass transport through the lacunar-canalicular system due to mechanical loading [13-15].

In vitro experiments have examined the capability of osteocytes to respond to fluid flow and tested how interstitial fluid flow affects bone cells. Although the flow chambers used in in vitro experiments do not replicate exactly the fluid flow environment

experienced by osteocytes in situ, they are still a useful technique to demonstrate osteocyte response to mechanical stimulation. Osteocytes respond to fluid flow with increased release of prostaglandin E2 (PGE2), osteocalcin, insulin-like growth factor (IGF), c-fos, Ca++, and NO, all anabolic agents that control normal bone remodeling [18, 23-29].

During development of osteoporosis the lack of estrogen induces osteocyte apoptosis though a decrease in osteocyte viability [30, 31]. In addition, it has been proposed that an alteration in osteocyte viability due to osteoporosis could alter the interconnectedness of the osteocyte network, affecting interstitial fluid flow and altering the mechanical stimulus experienced by the bone cells, consequently skewing the bone remodeling process towards higher osteoclastic activity [30]. The direct effect of estrogen depletion on bone microporosities was observed in our previous work where ovariectomized rats had greater lacunar-canalicular porosity in the cancellous bone of the tibial metaphysis compared to age-matched controls (Chapter 4).

Considering the higher lacunar-canalicular porosity found in our previous work with the rat ovariectomized model of osteoporosis, we hypothesize that estrogen-depleted bone offers less resistance to interstitial fluid movement, favoring the greater passage of solutes when mechanical loading is applied. To address this hypothesis we have applied an external dynamic load to the right tibia of both ovariectomized and sham-operated rats immediately after the injection of a fluorescent tracer. Cortical and cancellous tracer distribution was analyzed in the metaphysis and epiphysis of the proximal tibia, locations demonstrated to undergo bone loss due to estrogen depletion in both humans and animal models of osteoporosis [32, 33].

Methods

Permission for this in vivo study was granted by the Institutional Animal Care and Use Committee at the Hospital for Special Surgery.

Loading Device Calibration

Virgin female Sprague Dawley rats (n = 3, 310 ± 13.2g) were used to calibrate the non-invasive loading device (ElectroForce TestBench, Bose Corp., Minnetonka, MN) so that a load corresponding to 500 microstrain could be applied to the rat tibia to mimic walking activity. The animals were anaesthetized with isoflurane and the right medial proximal diaphysis of the tibia was surgically exposed. This anatomical location was chosen for its flat surface and lack of muscle attachments, which could accommodate application of a strain gage. The tibial surface was scraped with a scalpel to remove the periosteal layer, and then it was cleaned with 100% ethanol and acetone. A single-element foil gage (CEA-032UW-120, Vishay Micro-Measurements, Raleigh, NC) was aligned with the tibial long axis and attached using cyanoacrylate. The rat's right lower limb was carefully placed between the knee and foot holder of the loading device and a compressive pre-load of 1 N was applied to keep the leg in position (Figure 5-1a). Sinusoidal loads were applied at 1 Hz with magnitudes ranging from 9 to 18 N to determine the load-microstrain relationship. The applied load necessary to generate approximately 500 microstrain in the proximal rat tibia was calculated to be 14 N (Figure 5-1b).

Animal injection and loading

To assess the effects of osteoporosis on mass transport due to mechanical loading, the rat ovariectomy model was utilized to induce estrogen loss and osteopenia. Twelve 20-week-old virgin female Sprague Dawley rats were divided into two groups, with one group undergoing ovariectomy (OVX, n=6), and the other group subjected to sham surgery (SHAM, n=6), consisting of the surgical exposure of the ovaries without removal. The ovariectomy and sham surgeries were performed by Harlan. After one week recovery period the animals were shipped to the Hospital for Special Surgery where they were housed individually and the OVX group was pair-fed to the average food intake of the CTRL group for four weeks.

Before performing the loading experiment the animals were weighed and anaesthetized via an intraperitoneal injection of a mixture of ketamine (75 mg/kg body weight), and xylazine (10 mg/kg body weight). The left jugular vein was exposed surgically and a 25G5/8 needle attached to a 3-ml syringe was inserted into the vein to inject a bolus of tracer solution (fluorescent bovine serum albumin, 67 kDa, diameter ~7 nm, Sigma, St. Louis, MO) at a dosage of 0.25 mg/g body weight. Immediately after the tracer injection (injection time 2 minutes) a sinusoidal load was applied to the right tibia using the non-invasive mechanical loading device. The maximum load (14 N applied axially) corresponded to approximately 500 microstrain at the tibia proximal diaphysis based on the calibration result, and the loading duration and frequency (100 cycles at 1 Hz) were chosen to mimic a short period of walking activity. Immediately after the loading phase the rats were sacrificed with carbon dioxide inhalation and the loaded and unloaded contralateral tibiae were harvested and put into EM fixative (0.5%

gluteraldehyde, 2% paraformaldehyde in 0.05M cacodylate-sodium buffer, pH 7.4) for 48 hours. To confirm the effectiveness of the OVX procedure, ovary removal was visually verified, and the uterine horns were weighed.

Histological Processing, Imaging Techniques, and Data Collection

Cortical and cancellous bone samples were analyzed from the metaphysis and epiphysis of the proximal tibia. Tibiae blocks were cut three millimeters distal to the growth plate and embedded in PMMA after 48 hours of fixation. Either sagittal or frontal tibial sections (0.4-0.6 mm) were cut with a diamond blade saw. Sections were then ground down to a final thickness of 40-70 μm using Carbimet paper discs (800 and 1200 grit; Buehler), dried in ascending graded alcohol (75%, 95%, and 100%, 5 minutes each), and coverslipped with mounting media (Richard-Allan Scientific, Kalamazoo, MI). To visualize tracer labeling, 20 different areas were analyzed for each animal: 5 from the cancellous metaphysis, 5 from the cancellous epiphysis, and 10 from the cortical metaphysis (Figure 5-2). The cortical regions were visualized using a confocal microscope with a 40x oil immersion lens (Leica TCS SP2, Germany, 1.25 numerical aperture, 630 gain, 2.4 offset, and pinhole set at 1 Airy unit, wavelength excitation of 488 nm, and laser intensity set to 15%). All the images were taken at a resolution of 2048 x 2048 pixels with a field view of 375 μm x 375 μm. The cancellous regions were visualized using the same parameters used for the cortical regions with the only difference being a 2x factor in the objective; thus the field of view was 187.5 μm x 187.5 μm.

To determine the percentage of osteocyte lacunae labeled with the injected tracer, the total number of osteocyte lacunae was first manually counted for each confocal image using ImageJ Counting Particle plugin. The confocal images were then transformed to grayscale intensity and thresholded. For both the cortical and cancellous bone, the threshold value was determined from images of the unloaded limb and then used in the corresponding images of loaded limb. The threshold values were chosen such that the intensity of the osteocyte lacunae was neither over- nor under-stained. The osteocyte lacunae presenting at least 80% of the lacunar space labeled or 100% of the periphery of the lacuna labeled were counted as labeled (Figure 5-3). Then the percentage of osteocyte lacunae labeled was calculated by dividing by the total number of lacunae in the image. The percentage of osteocyte lacunae labeled was averaged for each anatomical location for each animal. During all these phases the analyzer was blinded.

Statistical Analyses

To examine the effects of mechanical loading and ovariectomy on tracer movement for the three anatomical locations (cortical metaphysis, cancellous metaphysis, and cancellous epiphysis) data were analyzed using a two-way ANOVA repeated measures analysis, with the within-subject factor the loading condition (unloaded and loaded tibiae) and the between-subject factor the treatment (SHAM and OVX). Bonferroni post-hoc t-tests were used to determine differences between groups. The statistical analyses were performed using PRISM 5.00 (Graph-Pad Software Inc., San Diego, CA) with a significance level of $p < 0.05$.

Results

The effectiveness of ovariectomy was verified by the absence of ovaries and by the reduced dimension and weight of the uterine horns in the OVX group (0.14 ± 0.013g) compared to the SHAM group (0.61 ± 0.054g). Despite pair-feeding, at the time of the load application the OVX rats weighed more (302 ± 7g) than the age-matched sham-operated rats (265 ± 5g).

The externally applied loading increased the percentage of osteocyte lacunae labeled with injected tracer for all three locations and both groups except for the cancellous epiphysis of the SHAM group (Table 5-1, Figures 5-4). Compared to the unloaded, contralateral tibia, loading caused an increase in percentage of osteocyte lacunae labeled ranging from 63% for the cortical metaphysis of the SHAM group to 327% for the cancellous epiphysis of the OVX group.

Ovariectomy enhanced movement of tracer into the lacunar-canalicular porosity due to applied mechanical loading in the cancellous bone of the epiphysis and metaphysis but not in the cortical bone of the metaphysic. For the cancellous bone of the metaphysis and epiphysis, the loaded tibiae of the OVX group had a higher percentage of osteocyte lacunae labeled, 66% and 142% increase, respectively, than the loaded SHAM cancellous bone from the same locations (Table 1).

Discussion

The results demonstrate that in the cancellous bone of the proximal tibia, tracer transport and thus bone interstitial fluid movement through the lacunar-canalicular porosity surrounding osteocytes is affected by both moderate external loading and

osteopenia due to ovariectomy. Cortical bone of the proximal tibia demonstrated increased tracer transport due to mechanical loading, with no enhancement due to ovariectomy.

The effects of estrogen depletion in cancellous bone of the metaphysis shown in this study correspond to previous studies that have reported decreases in bone volume fraction and other alterations in trabecular architecture in the proximal tibia of ovariectomized rats [32, 33]. The results in this study also correspond to our previous work quantifying the bone microporosities, which demonstrated that ovariectomized rats had a greater lacunar-canalicular porosity in the cancellous bone of the proximal tibia metaphysis compared to age-matched controls (Chapter 4).

'Osteocytic osteolysis,' a process describing the possible attribute of osteocytes to modify their immediate environment through micro-resorption and calcium micro-deposition, could explain the enhanced tracer labeling of osteocyte lacunae in the ovariectomized animals [34, 35]. It has been shown that under specific conditions, such as parathyroid hormone administration, hyperthyroidism, and osteoporosis, osteocytes effectively accommodate their needs to the new environmental status [36-38]. The resorption of the lacunar and canalicular surfaces surrounding osteocytes would result in a broadening of the lacunar and canalicular spaces, and the larger pores would allow a larger volume of fluid to move during cyclic or pulsatile loading. Thus, molecular transport would be enhanced through the lacunar-canalicular network, with consequent increase in the number of osteocyte lacunae labeled with injected tracer.

Mechanosensitivity of osteocytes might also be affected by an increase in lacunar-canalicular pore size. The action of interstitial fluid movement on osteocytes is

considered one of the best candidates to describe the ability of bone to respond to mechanical stimulation. When bone is mechanically loaded, interstitial fluid displacements are created, and fluid flows through the lacunar-canalicular porosity. Analysis of the canalicular structure and the position of the osteocyte processes throughout the canalicular length has shown that osteocyte processes occupy the center part of the canaliculus core [39]. This is possible because the dendrites are physically hooked to the canalicular wall through tethering elements and conical structures that protrude from the canalicular wall [19, 39]. The function of these structures is not only to hold the dendrites in place, but essentially to work as cellular strain amplifier that is activated during flow movement. The increasing canalicular diameter seen in osteopenic rat bone could cause the disruption of the tethering elements and the detachment of the conical protrusions from the processes, impairing the capability of the osteocyte to perceive mechanical stimuli and eventually leading to osteocyte apoptosis.

Although many investigators have related the beneficial effect of loading to osteoporosis and to bone macrostructure, this study was designed to analyze changes in interstitial fluid transport caused by estrogen depletion. The increased cancellous bone interstitial transport quantified in the lacunar-canalicular network due to ovariectomy is another important factor to take into consideration if we want to fully understand and completely assemble the complex osteoporosis puzzle. Further investigations as to how interstitial fluid flow changes might impair the capability of osteocytes to be sensitive to mechanical loading and to function as the bone mechanotransducer are needed.

5.5 Reference

[1] Cooper RR, Milgram JW, Robinson RA. Morphology of the osteon. An electron microscopic study. J Bone Joint Surg Am 1966;48: 1239-71.

[2] Hancox NM. Biology of Bone. Cambridge, England: Cambridge University Press; 1972.

[3] Martin R. B. DBB. Structure, Function and Adaptation of Compact Bone. New York: Raven Press; 1989.

[4] Qin YX, Kaplan T, Saldanha A, Rubin C. Fluid pressure gradients, arising from oscillations in intramedullary pressure, is correlated with the formation of bone and inhibition of intracortical porosity. J Biomech 2003;36: 1427-37.

[5] Ciani C, Doty SB, Fritton SP. Mapping bone interstitial fluid movement: displacement of ferritin tracer during histological processing. Bone 2005;37: 379-87.

[6] Doty SB, Schofield BH. Electron microscopic localization of hydrolytic enzymes in osteoclasts. Histochem J 1972;4: 245-58.

[7] Knothe Tate ML, Knothe U, Niederer P. Experimental elucidation of mechanical load-induced fluid flow and its potential role in bone metabolism and functional adaptation. Am J Med Sci 1998;316: 189-95.

[8] Knothe Tate ML, Niederer P, Knothe U. In vivo tracer transport through the lacunocanalicular system of rat bone in an environment devoid of mechanical loading. Bone 1998;22: 107-17.

[9] Montgomery RJ, Sutker BD, Bronk JT, Smith SR, Kelly PJ. Interstitial fluid flow in cortical bone. Microvasc Res 1988;35: 295-307.

[10] Qin L, Mak AT, Cheng CW, Hung LK, Chan KM. Histomorphological study on pattern of fluid movement in cortical bone in goats. Anat Rec 1999;255: 380-7.

[11] Tanaka T, Sakano A. Differences in permeability of microperoxidase and horseradish peroxidase into the alveolar bone of developing rats. J Dent Res 1985;64: 870-6.

[12] Wang L, Ciani C, Doty SB, Fritton SP. Delineating bone's interstitial fluid pathway in vivo. Bone 2004;34: 499-509.

[13] Knothe Tate ML, Knothe U. An ex vivo model to study transport processes and fluid flow in loaded bone. J Biomech 2000;33: 247-54.

[14] Mak AF, Qin L, Hung LK, Cheng CW, Tin CF. A histomorphometric observation of flows in cortical bone under dynamic loading. Microvasc Res 2000;59: 290-300.

[15] Tami AE, Schaffler MB, Knothe Tate ML. Probing the tissue to subcellular level structure underlying bone's molecular sieving function. Biorheology 2003;40: 577-90.

[16] Burger EH, Klein-Nulend J. Mechanotransduction in bone--role of the lacuno-canalicular network. Faseb J 1999;13 Suppl: S101-12.

[17] Cowin SC, Weinbaum S, Zeng Y. A case for bone canaliculi as the anatomical site of strain generated potentials. J Biomech 1995;28: 1281-97.

[18] Klein-Nulend J, van der Plas A, Semeins CM, Ajubi NE, Frangos JA, Nijweide PJ, Burger EH. Sensitivity of osteocytes to biomechanical stress in vitro. Faseb J 1995;9: 441-5.

[19] Wang Y, McNamara LM, Schaffler MB, Weinbaum S. A model for the role of integrins in flow induced mechanotransduction in osteocytes. Proc Natl Acad Sci U S A 2007;104: 15941-6.

[20] Weinbaum S, Cowin SC, Zeng Y. A model for the excitation of osteocytes by mechanical loading-induced bone fluid shear stresses. J Biomech 1994;27: 339-60.

[21] You L, Cowin SC, Schaffler MB, Weinbaum S. A model for strain amplification in the actin cytoskeleton of osteocytes due to fluid drag on pericellular matrix. J Biomech 2001;34: 1375-86.

[22] Han Y, Cowin SC, Schaffler MB, Weinbaum S. Mechanotransduction and strain amplification in osteocyte cell processes. Proc Natl Acad Sci U S A 2004;101: 16689-94.

[23] Ajubi NE, Klein-Nulend J, Alblas MJ, Burger EH, Nijweide PJ. Signal transduction pathways involved in fluid flow-induced PGE2 production by cultured osteocytes. Am J Physiol 1999;276: E171-8.

[24] Ajubi NE, Klein-Nulend J, Nijweide PJ, Vrijheid-Lammers T, Alblas MJ, Burger EH. Pulsating fluid flow increases prostaglandin production by cultured chicken osteocytes--a cytoskeleton-dependent process. Biochem Biophys Res Commun 1996;225: 62-8.

[25] Klein-Nulend J, Roelofsen J, Sterck JG, Semeins CM, Burger EH. Mechanical loading stimulates the release of transforming growth factor-beta activity by cultured mouse calvariae and periosteal cells. J Cell Physiol 1995;163: 115-9.

[26] Lean JM, Mackay AG, Chow JW, Chambers TJ. Osteocytic expression of mRNA for c-fos and IGF-I: an immediate early gene response to an osteogenic stimulus. Am J Physiol 1996;270: E937-45.

[27] Mikuni-Takagaki Y, Suzuki Y, Kawase T, Saito S. Distinct responses of different populations of bone cells to mechanical stress. Endocrinology 1996;137: 2028-35.

[28] Skerry TM, Bitensky L, Chayen J, Lanyon LE. Early strain-related changes in enzyme activity in osteocytes following bone loading in vivo. J Bone Miner Res 1989;4: 783-8.

[29] Pavalko FM, Chen NX, Turner CH, Burr DB, Atkinson S, Hsieh YF, Qiu J, Duncan RL. Fluid shear-induced mechanical signaling in MC3T3-E1 osteoblasts requires cytoskeleton-integrin interactions. Am J Physiol 1998;275: C1591-601.

[30] Tomkinson A, Gevers EF, Wit JM, Reeve J, Noble BS. The role of estrogen in the control of rat osteocyte apoptosis. J Bone Miner Res 1998;13: 1243-50.

[31] Tomkinson A, Reeve J, Shaw RW, Noble BS. The death of osteocytes via apoptosis accompanies estrogen withdrawal in human bone. J Clin Endocrinol Metab 1997;82: 3128-35.

[32] Frost HM, Jee WS. On the rat model of human osteopenias and osteoporoses. Bone Miner 1992;18: 227-36.

[33] Wronski TJ, Dann LM, Scott KS, Cintron M. Long-term effects of ovariectomy and aging on the rat skeleton. Calcif Tissue Int 1989;45: 360-6.

[34] Belanger LF. Osteocytic osteolysis. Calcif Tissue Res 1969;4: 1-12.

[35] Heller-Steinberg M. Ground substance, bone salts, and cellular activity in bone formation and destruction. Am J Anat 1951;89: 347-79.

[36] Baylink DJ, Wergedal JE. Bone formation by osteocytes. Am J Physiol 1971;221: 669-78.

[37] Tazawa K, Hoshi K, Kawamoto S, Tanaka M, Ejiri S, Ozawa H. Osteocytic osteolysis observed in rats to which parathyroid hormone was continuously administered. J Bone Miner Metab 2004;22: 524-9.

[38] Wright PH, Jowsey JO, Robb RA. Osteocyte lacunar area in normal bone, hyperparathyroidism, renal disease, and osteoporosis. Surg Forum 1978;29: 558-9.

[39] You LD, Weinbaum S, Cowin SC, Schaffler MB. Ultrastructure of the osteocyte process and its pericellular matrix. Anat Rec A Discov Mol Cell Evol Biol 2004;278: 505-13.

	Percentage of osteocyte lacunae labeled		
	Unloaded (left)	**Loaded (right)**	**% increase**
SHAM cortical metaphysis	15.7 ± 8.16	25.5 ± 11.8[a]	62.7
SHAM cancellous metaphysis	13.8 ± 8.9	38.2 ± 14.4[a]	178
SHAM cancellous epiphysis	3.01 ±1.66	10.3 ± 5.68	--
OVX cortical metaphysis	11.3 ± 11.7	24.8 ± 13.0[a]	120
OVX cancellous metaphysis	25.9 ± 4.81	63.5 ± 8.91[a,b]	145
OVX cancellous epiphysis	5.84 ± 2.01	24.9 ± 10.2[a,b]	327

Table 5-1. Percentage of osteocyte lacunae labeled with injected tracer for the three analyzed regions (cortical metaphysis, cancellous metaphysis, and cancellous epiphysis) for both unloaded (left) and loaded (right) tibiae. SHAM = sham-operated group; OVX = ovariectomized group. [a]$p < 0.05$ compared to unloaded tibia at same anatomical region; [b]$p < 0.05$ compared to loaded SHAM at same anatomical region.

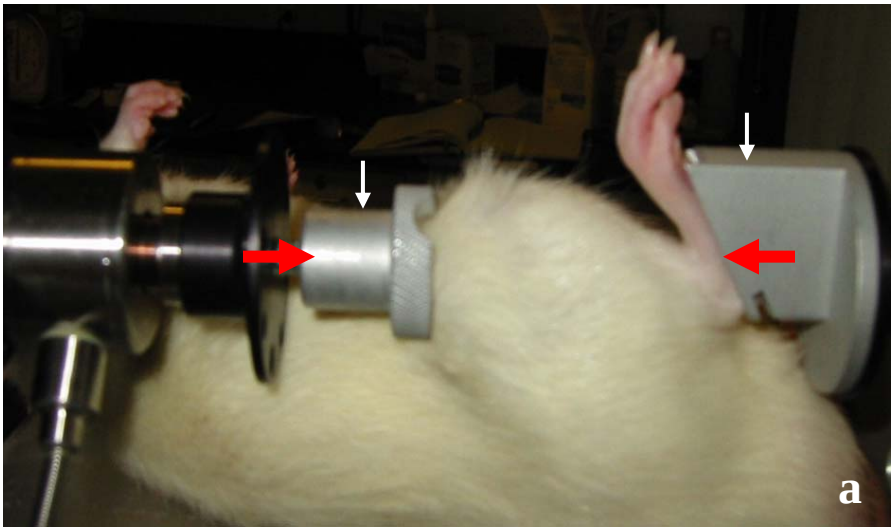

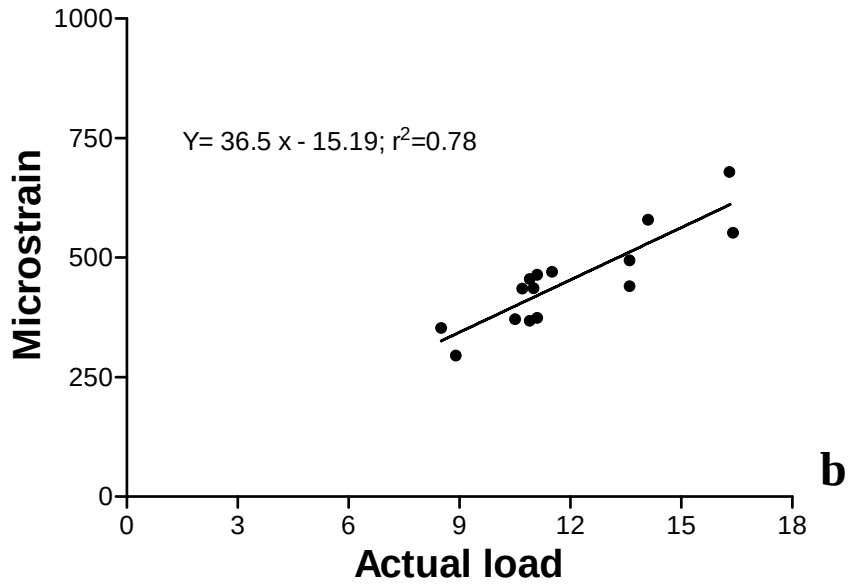

Figure 5-1. (a) Sinusoidal loading was applied non-invasively to the rat tibia, which was constrained between the knee cup and foot holder (small vertical arrows). The loading direction is indicated by the big arrows. (b) Calibration of loading device illustrating the relationship between applied load (N) and tibial microstrain. An applied load of 14 N

engenders approximately 500 microstrain in the proximal medial tibia, as measured with strain gages (n=3).

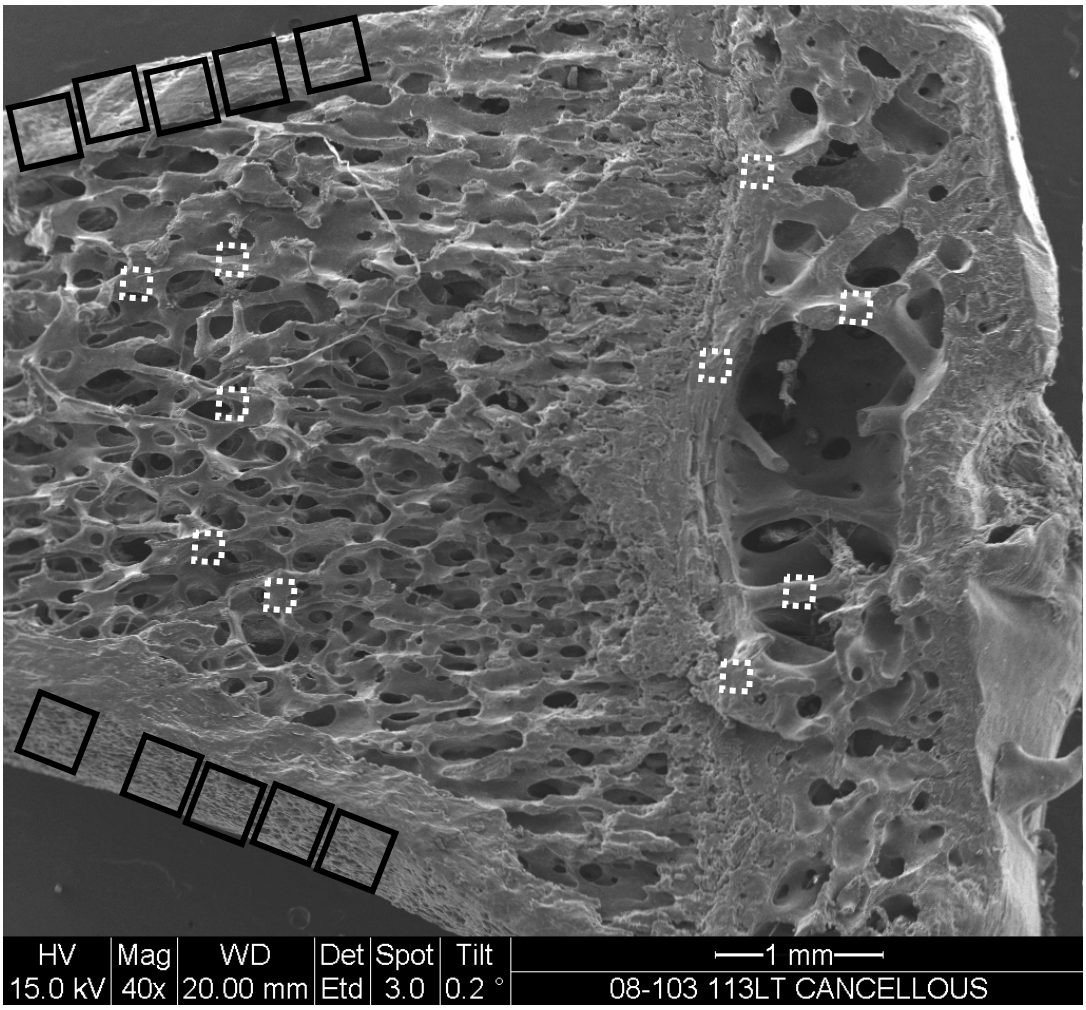

Figure 5-2. Scanning electron microscopy image of a rat tibia frontal section taken to illustrate the locations from where the cortical and cancellous bone images were taken. To map cortical and cancellous interstitial fluid movement, ten 375 x 375 μm regions from the cortex regions were imaged (black boxes), and ten 187.5 x 187.5 μm regions, 5 from the metaphysis and 5 from the epiphysis (white dotted boxes) were imaged. The locations were chosen not to include the primary spongiosa.

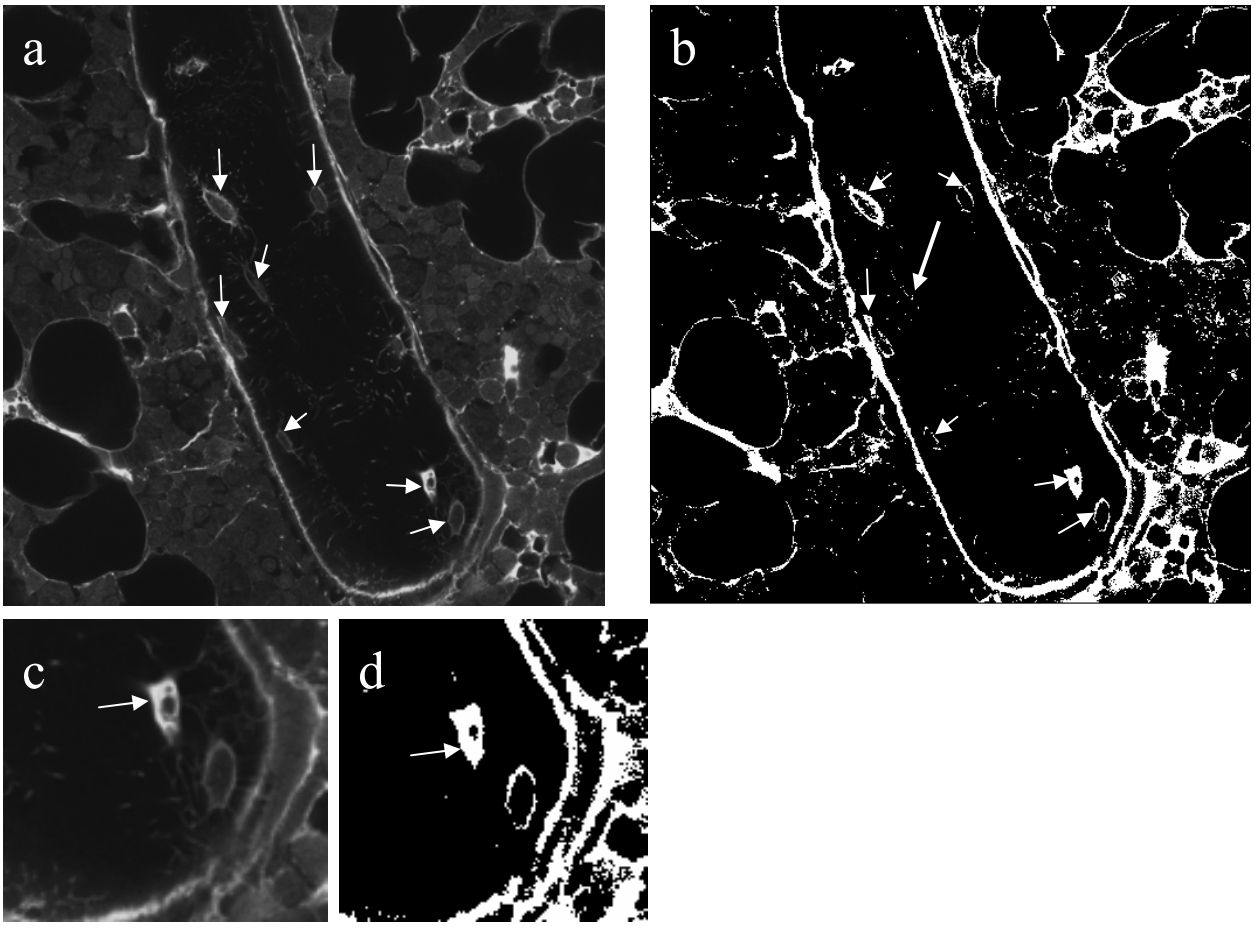

Figure 5-3. (a) Typical appearance of a grayscale image of cancellous bone of the metaphysis. The trabecula is surrounded by bone marrow, and the visible osteocytes are indicated with white arrows. (b) Same image after thresholding; labeled osteocyte lacunae are marked with small arrows and an osteocyte lacuna that disappears after thresholding is marked with a big arrow. (c) Higher magnification of the image in (a) showing two osteocytes, and (d) same image after thresholding. The arrow in (d) indicates the osteocyte chosen that satisfies the criteria to be considered as labeled (osteocyte lacunae presenting at least 80% of the lacunar space labeled or 100% of the periphery of the lacuna labeled).

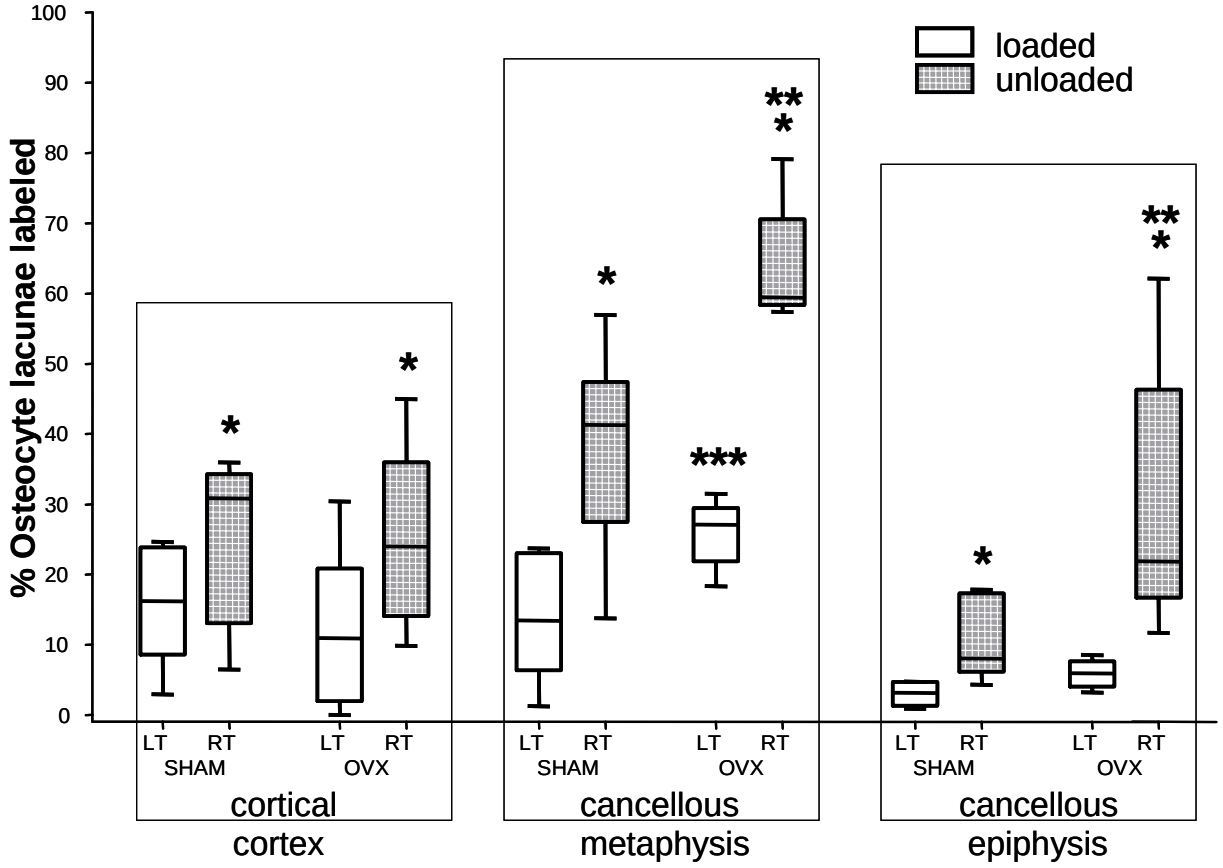

Figure 5-4. Box plots of the percentage of osteocyte lacunae labeled with injected tracer for the SHAM and OVX groups for the three anatomical locations: cortical metaphysis and cancellous metaphysis and epiphysis and for the loaded right tibia (RT) and contralateral, unloaded left tibia (LT).
* significant difference compared to unloaded ($p < 0.05$);
** significant difference compared to loaded SHAM ($p < 0.05$);
*** significant difference compared to unloaded SHAM ($p < 0.05$).

Chapter 6

Concluding Remarks

6.1 Introduction

The present work aimed to better understand bone's interstitial fluid flow pathway and determine the effect that conditions such as osteoporosis and external load produce on bone interstitial fluid movement. It is important to understand load-induced interstitial fluid flow because it plays a role in bone adaptation and maintenance of the tissue, and it is believed to play a role in bone's mechanosensory system. This chapter summarizes the major accomplishments, limitations, and future directions of the present study.

6.2 Accomplishments

In Chapter 2 we challenged using the tracer ferritin to explain normal interstitial fluid movement in bone. In vivo tracer studies have shown that ferritin (~ 12 nm diameter) forms halo-shaped labeling that appears to enter the mineralized matrix around blood vessels [1-4]. This ferritin labeling is widely used to explain normal interstitial fluid movement in bone: the halos are said to demonstrate bulk centrifugal interstitial fluid movement away from a highly pressurized vascular porosity [1-8]. A model by Keanini et al. suggested that the halos are a convective front of the tracer that passes through the unmineralized collagen-proteoglycan matrix [9]. Our previous tracer study revealed that ferritin was confined exclusively to the vascular canals and blood vessels and did not enter the lacunar-canalicular porosity [10]. The study described in Chapter 2 analyzed the effect of different histological processes on the presence of ferritin in the mineralized matrix and the characteristic ferritin 'halo' labeling previously demonstrated by other investigators. Using the histological processing techniques developed by previous investigators we were able to produce ferritin halos [11]. Based on these results and the

fact that halo labeling has not been found with any other tracer, from this study we can draw two major conclusions: (a) ferritin labeling should not be used to demonstrate physiological bone interstitial fluid flow, and (b) molecules larger than ferritin (~ 12 nm) are too big to pass into the lacunar-canalicular system.

In the seek to further delineate the movement of interstitial fluid and the role it plays in bone mechanotransduction, we developed a new staining protocol to visualize bone interstitial fluid spaces (Chapter 3). We created a reliable and easily reproducible staining technique using fluorescein isothiocyanate (FITC) as a probe visualized by confocal microscopy. This staining technique is an effective method to obtain high-resolution images that illuminate the details of the lacunar-canalicular network. The ability to visualize an entire cross-section makes this technique useful when analyzing and identifying bone macrostructure (e.g., compacted cancellous bone [12]), and bone microstructure, such as regions with either high or low canalicular density. The fluorescent properties of FITC and the high-resolution images can also be utilized to quantify the different microporosities in bone and to obtain 3-D images to analyze bone permeability.

Taking advantage of the staining protocol described in Chapter 3, in Chapter 4 we characterized bone interstitial fluid spaces of control (CTRL) and ovariectomized (OVX) rats. As reported in the literature, during osteoporosis development the lack of estrogen induces a series of events such as osteocyte apoptosis, reduced communication between neighboring osteocytes, and modification of bone macroarchitecture, yet there is little analysis related to changes in microstructure and microporosities during osteoporosis [13-

18]. This study was designed to determine how the porosities of the vascular and lacunar-canalicular networks evolve in the osteoporotic condition.

The techniques used in the study described in Chapter 4, confocal and scanning electron microscopy, allowed us to obtain high-resolution images to quantify cortical and cancellous bone microporosities and illuminate the microstructural details of the lacunar-canalicular network, to visualize bone mineral distribution and correlate it to different porosity patterns, and to measure the canalicular diameter in normal and osteopenic rat bone. The major findings of this study were: (a) the cortical bone in the metaphysis showed a 40% increase in vascular porosity and a 16% increase in lacunar-canalicular porosity; (b) the cancellous bone in the metaphysis demonstrated a large increase (56%) in the lacunar-canalicular porosity due to ovariectomy, while the lacunar-canalicular porosity of cancellous bone in the epiphysis did not change with ovariectomy; (c) the metaphysis is also rich with compacted cancellous bone that is younger and not completely quiescent, unlike the compacted cancellous bone found in the diaphysis [12]; (d) the average canalicular diameter measured in the cortical metaphysis increased by 20% in the OVX group compared to CTRL; and (e) bone regions with higher mineral density had lower canalicular density (endochondral spicule remnants in the diaphysis and the ‘cancellous’ regions in the metaphysis), while regions with lower mineral density had higher canalicular density (lamellar bone in the diaphysis, and newer ‘compact’ bone in the metaphysis). Osteocytes are very sensitive to interstitial fluid movement produced by mechanical stress, and the increased microporosities induced in this study by lack of estrogen may play an important a role in altering the mechanosensory ability of the osteocyte. The microarchitectural changes occurring after osteopenia development might

also decrease the mechanical properties in bone, thus contributing to the increased risk of fracture occurring during osteoporosis.

Further investigation into how load-induced interstitial fluid flow is affected by osteoporosis was necessary to corroborate and support the data obtained in the study described in Chapter 4. Chapter 5 was designed to analyze changes in interstitial fluid transport caused by estrogen depletion. We hypothesized that estrogen-depleted bone offers less resistance to interstitial fluid movement, favoring the greater passage of solutes when mechanical loading is applied. To address this hypothesis we applied an external dynamic load to the right tibia of both ovariectomized (OVX) and sham-operated (SHAM) rats immediately after the injection of a fluorescent tracer. Cortical and cancellous tracer distribution was analyzed in the metaphysis and epiphysis of the proximal tibia, locations demonstrated to undergo bone loss due to estrogen depletion in both humans and animal models of osteoporosis [19, 20]. The results demonstrated that in the cancellous bone of the proximal tibia, tracer transport and thus bone interstitial fluid movement through the lacunar-canalicular porosity surrounding osteocytes is affected by both moderate external loading and osteopenia due to ovariectomy. Cortical bone of the proximal tibia demonstrated increased tracer transport due to mechanical loading, with no enhancement due to ovariectomy. These findings corroborate the data of Chapter 4, where ovariectomized rats had a greater lacunar-canalicular porosity in the cancellous bone of the proximal tibia metaphysis compared to age-matched controls. The ability of osteocytes to modify their immediate environment has been called ’osteocytic osteolysis’ [21]. It is possible that the increased canalicular diameter in the ovariectomized animals demonstrated in Chapter 4 is caused by osteocytic osteolysis,

which would allow a larger volume of fluid to move during cyclic or pulsatile loading, as shown in Chapter 5.

Mechanosensitivity of osteocytes might also be affected by an increase in lacunar-canalicular pore size. Osteocytes are very sensitive to interstitial fluid movement and are considered to be the primary mechanosensor in bone. When bone is mechanically loaded, interstitial fluid displacements are created, and fluid flows through the lacunar-canalicular porosity. Analysis of the canalicular structure has shown that osteocyte processes occupy the center part of the canaliculus core [22]. This is possible because the dendrites are believed to be physically hooked to the canalicular wall through tethering elements and conical structures that protrude from the canalicular wall [22, 23]. The function of these structures is not only to hold the dendrites in place, but to work as a cellular strain amplifier that is activated during flow movement. The increasing canalicular diameter seen in osteopenic rat bone could cause the disruption of the tethering elements and the detachment of the conical protrusions from the processes, impairing the capability of the osteocyte to perceive mechanical stimuli and eventually leading to osteocyte apoptosis.

Together, the data and results of this dissertation have helped to better understand and delineate bone interstitial fluid movement and its role in mechanostransduction for both normal and osteopenic bone. In summary, we can draw the following conclusions:

- ferritin “halo” labeling should not be used to demonstrate physiological bone interstitial fluid flow (Chapter 2);

- interstitial bone fluid flow in cancellous bone of the rat proximal tibia is increased not only through external mechanical loading but also after the development of osteopenia due to ovariectomy (Chapter 5);
- ovariectomy-induced osteopenia influences bone microporosities and microstructure, possibly impairing the capability of osteocytes to perform efficiently as mechanotranducers (Chapters 4 and 5).

6.3 Limitations and Future Directions

There are several limitations to the work presented in this dissertation. A common limitation to all the studies is the employment of an animal model to describe bone interstitial fluid movement, bone porosities, and osteoporosis in humans. Although the rat provides a useful and well-established model to investigate a variety of clinically related problems, one must always consider the role that species differences might have on experimental results.

A limitation of the ferritin study described in Chapter 2 is related to histological processing. Although reduced to a minimum, bone samples still remained in different types of solution for extended periods of time. This might be a cause of tracer displacement and artifact that could not be identified. An obvious solution would be to visualize interstitial fluid movement in vivo [24]. Confocal laser scanning microscopy and dual photon microscopy allow this type of experimentation, and it would be of great interest to develop this approach to quantify interstitial fluid movement.

The major limitation of Chapter 4 regards the maximum resolution of confocal microscopy. Because the canalicular diameter size (~ 500 nm), and the maximum

resolution of confocal microscopy (~ 200 nm) are of the same order, it is likely that the confocal images overestimate the canalicular porosity due to partial volume effects. Scanning electron microscopy measurements performed to assess the amount of overestimation of canalicular size gave an average canalicular diameter approximately 60% smaller than that measured with confocal microscopy. The choice of confocal settings used during image acquisition, such as detector gain, amplifier gain, laser intensity, pinhole size, and thresholding all effected the canalicular measurements. The choice of threshold in particular has a strong effect on the canalicular quantification. Using a more conservative threshold value would help to reduce the impact of confocal resolution on the canalicular porosity results; however, much investigation went into the choice of threshold, and the standard method chosen (Otsu's method) seemed appropriate for this application. In addition, the overestimation of microporosity only applies to the canalicular porosity and not the lacunar porosity because the lacunar size, on the order of 10 μm, is well-characterized at a resolution of 200 nm. In this study, the lacunar and canalicular porosities were quantified jointly, but we are developing a protocol to calculate the lacunar porosity separately from the canalicular porosity. This differentiation will help to reduce the overestimation of the lacunar-canalicular porosity.

In the last study presented (Chapter 5), we only applied one loading regime to induce interstitial fluid displacement. This decision was made because we were interested in the effect that a simple, physiological loading regime would have on interstitial fluid movement. Varying the magnitude, frequency, and duration of the applied loading will help to better understand the relationship between osteoporosis, bone mechanostransduction, and bone adaptation.

To extend the work described in this thesis future studies will include: quantification of lacunar size of normal and osteopenic rat bone; characterization of the number of canaliculi emanating from osteocyte lacunae in osteopenic bone; injection of different sized tracers in the osteoporosis rat model to determine if estrogen withdrawal affects the molecular sieve of the osteocyte pericellular matrix; characterization of canalicular dimension in ovariectomized rats using scanning electron microscopy as was done for normal rats in this work; further analysis of the vascular changes documented in ovariectomized rats using both micro-CT and 3D confocal reconstructions; and finally, characterization of osteocyte viability in ovariectomized rats through measurement of apoptotis in situ and correlation with the microstructural results found in this work. These continued studies should help to elucidate the role that interstitial fluid flow may play in the development of osteoporosis, knowledge that could be used to treat and possibly prevent the disease.

6.4 References

[1] Dillaman RM. Movement of ferritin in the 2-day-old chick femur. Anat Rec 1984;209: 445-53.

[2] Mak AF, Qin L, Hung LK, Cheng CW, Tin CF. A histomorphometric observation of flows in cortical bone under dynamic loading. Microvasc Res 2000;59: 290-300.

[3] Montgomery RJ, Sutker BD, Bronk JT, Smith SR, Kelly PJ. Interstitial fluid flow in cortical bone. Microvasc Res 1988;35: 295-307.

[4] Qin L, Mak AT, Cheng CW, Hung LK, Chan KM. Histomorphological study on pattern of fluid movement in cortical bone in goats. Anat Rec 1999;255: 380-7.

[5] Dillaman RM, Roer RD, Gay DM. Fluid movement in bone: theoretical and empirical. J Biomech 1991;24 Suppl 1: 163-77.

[6] Hillsley MV, Frangos JA. Bone tissue engineering: the role of interstitial fluid flow. Biotechnol Bioeng 1994;43: 573-81.

[7] Kelly PJ, Montgomery RJ, Bronk JT. Reaction of the circulatory system to injury and regeneration. Clin Orthop Relat Res 1990: 275-88.

[8] Winet H. A bone fluid flow hypothesis for muscle pump-driven capillary filtration: II. Proposed role for exercise in erodible scaffold implant incorporation. Eur Cell Mater 2003;6: 1-10; discussion 10-1.

[9] Keanini RG, Roer RD, Dillaman RM. A theoretical model of circulatory interstitial fluid flow and species transport within porous cortical bone. J Biomech 1995;28: 901-14.

[10] Wang L, Ciani C, Doty SB, Fritton SP. Delineating bone's interstitial fluid pathway in vivo. Bone 2004;34: 499-509.

[11] Ciani C, Doty SB, Fritton SP. Mapping bone interstitial fluid movement: displacement of ferritin tracer during histological processing. Bone 2005;37: 379-87.

[12] Enlow DH. Principle of Bone Remodeling. Springfield, IL: Charles C. Thomas; 1963.

[13] Baldock PA, Need AG, Moore RJ, Durbridge TC, Morris HA. Discordance between bone turnover and bone loss: effects of aging and ovariectomy in the rat. J Bone Miner Res 1999;14: 1442-8.

[14] Baylink DJ, Wergedal JE. Bone formation by osteocytes. Am J Physiol 1971;221: 669-78.

[15] Tomkinson A, Gevers EF, Wit JM, Reeve J, Noble BS. The role of estrogen in the control of rat osteocyte apoptosis. J Bone Miner Res 1998;13: 1243-50.

[16] Tomkinson A, Reeve J, Shaw RW, Noble BS. The death of osteocytes via apoptosis accompanies estrogen withdrawal in human bone. J Clin Endocrinol Metab 1997;82: 3128-35.

[17] Wright PH, Jowsey JO, Robb RA. Osteocyte lacunar area in normal bone, hyperparathyroidism, renal disease, and osteoporosis. Surg Forum 1978;29: 558-9.

[18] Wronski TJ, Lowry PL, Walsh CC, Ignaszewski LA. Skeletal alterations in ovariectomized rats. Calcif Tissue Int 1985;37: 324-8.

[19] Frost HM, Jee WS. On the rat model of human osteopenias and osteoporoses. Bone Miner 1992;18: 227-36.

[20] Wronski TJ, Dann LM, Scott KS, Cintron M. Long-term effects of ovariectomy and aging on the rat skeleton. Calcif Tissue Int 1989;45: 360-6.

[21] Belanger LF. Osteocytic osteolysis. Calcif Tissue Res 1969;4: 1-12.

[22] You LD, Weinbaum S, Cowin SC, Schaffler MB. Ultrastructure of the osteocyte process and its pericellular matrix. Anat Rec A Discov Mol Cell Evol Biol 2004;278: 505-13.

[23] Wang Y, McNamara LM, Schaffler MB, Weinbaum S. A model for the role of integrins in flow induced mechanotransduction in osteocytes. Proc Natl Acad Sci U S A 2007;104: 15941-6.

[24] Wang L, Wang Y, Han Y, Henderson SC, Majeska RJ, Weinbaum S, Schaffler MB. In situ measurement of solute transport in the bone lacunar-canalicular system. Proc Natl Acad Sci U S A l2005;102: 1911-6.

Bibliography

Chapter 1

[1] Burger EH, Klein-Nulend J. Mechanotransduction in bone--role of the lacuno-canalicular network. Faseb J 1999;13 Suppl: S101-12.

[2] Klein-Nulend J, van der Plas A, Semeins CM, Ajubi NE, Frangos JA, Nijweide PJ, Burger EH. Sensitivity of osteocytes to biomechanical stress in vitro. Faseb J 1995;9: 441-5.

[3] Chow JW, Wilson AJ, Chambers TJ, Fox SW. Mechanical loading stimulates bone formation by reactivation of bone lining cells in 13-week-old rats. J Bone Miner Res 1998;13: 1760-7.

[4] Hauge EM, Qvesel D, Eriksen EF, Mosekilde L, Melsen F. Cancellous bone remodeling occurs in specialized compartments lined by cells expressing osteoblastic markers. J Bone Miner Res 2001;16: 1575-82.

[5] Miller SC, de Saint-Georges L, Bowman BM, Jee WS. Bone lining cells: structure and function. Scanning Microsc 1989;3: 953-60; discussion 960-1.

[6] Norimatsu H, Yamamoto T, Ozawa H, Talmage RV. Changes in calcium phosphate on bone surfaces and in lining cells after the administration of parathyroid hormone or calcitonin. Clin Orthop Relat Res 1982: 271-8.

[7] Rubinacci A, Villa I, Dondi Benelli F, Borgo E, Ferretti M, Palumbo C, Marotti G. Osteocyte-bone lining cell system at the origin of steady ionic current in damaged amphibian bone. Calcif Tissue Int 1998;63: 331-9.

[8] Cooper RR, Milgram JW, Robinson RA. Morphology of the osteon. An electron microscopic study. J Bone Joint Surg Am 1966;48: 1239-71.

[9] Cowin SC. Bone poroelasticity. J Biomech l1999;32: 217-38.

[10] Mohsin S, Taylor D, Lee TC. Three-dimensional reconstruction of Haversian systems in ovine compact bone. Eur J Morphol 2002;40: 309-15.

[11] You LD, Weinbaum S, Cowin SC, Schaffler MB. Ultrastructure of the osteocyte process and its pericellular matrix. Anat Rec A Discov Mol Cell Evol Biol 2004;278: 505-13.

[12] Wang Y, McNamara LM, Schaffler MB, Weinbaum S. A model for the role of integrins in flow induced mechanotransduction in osteocytes. Proc Natl Acad Sci U S A 2007;104: 15941-6.

[13] Weinbaum S, Cowin SC, Zeng Y. A model for the excitation of osteocytes by mechanical loading-induced bone fluid shear stresses. J Biomech 1994;27: 339-60.
[14] You L, Cowin SC, Schaffler MB, Weinbaum S. A model for strain amplification in the actin cytoskeleton of osteocytes due to fluid drag on pericellular matrix. J Biomech 2001;34: 1375-86.

[15] Cowin SC, Weinbaum S, Zeng Y. A case for bone canaliculi as the anatomical site of strain generated potentials. J Biomech 1995;28: 1281-97.

[16] Squire JM, Chew M, Nneji G, Neal C, Barry J, Michel C. Quasi-periodic substructure in the microvessel endothelial glycocalyx: a possible explanation for molecular filtering? J Struct Biol 2001;136: 239-55.

[17] Ciani C, Doty SB, Fritton SP. Mapping bone interstitial fluid movement: displacement of ferritin tracer during histological processing. Bone 2005;37: 379-87.

[18] Knothe Tate ML, Knothe U. An ex vivo model to study transport processes and fluid flow in loaded bone. J Biomech 2000;33: 247-54.

[19] Knothe Tate ML, Knothe U, Niederer P. Experimental elucidation of mechanical load-induced fluid flow and its potential role in bone metabolism and functional adaptation. Am J Med Sci 1998;316: 189-95.

[20] Montgomery RJ, Sutker BD, Bronk JT, Smith SR, Kelly PJ. Interstitial fluid flow in cortical bone. Microvasc Res 1988;35: 295-307.

[21] Tami AE, Schaffler MB, Knothe Tate ML. Probing the tissue to subcellular level structure underlying bone's molecular sieving function. Biorheology 2003;40: 577-90.

[22] Wang L, Ciani C, Doty SB, Fritton SP. Delineating bone's interstitial fluid pathway in vivo. Bone 2004;34: 499-509.

[23] Neuman WF, Neuman MW. The chemical dynamics of bone. Chigago; 1958.

[24] Neuman WF, Toriba TY, Mulrvan BJ. The surface chemistry of bone. J Am Chem Soc 1953;75: 4239-4242.

[25] Martin RB. Determinants of the mechanical properties of bones. J Biomech 1991;24 Suppl 1: 79-88.

[26] McCalden RW, McGeough JA, Barker MB, Court-Brown CM. Age-related changes in the tensile properties of cortical bone. The relative importance of changes in porosity, mineralization, and microstructure. J Bone Joint Surg Am 1993;75: 1193-205.

[27] Schaffler MB, Burr DB. Stiffness of compact bone: effects of porosity and density. J Biomech 1988;21: 13-6.

[28] Yeni YN, Brown CU, Wang Z, Norman TL. The influence of bone morphology on fracture toughness of the human femur and tibia. Bone 1997;21: 453-9.

[29] Li GP, Bronk JT, An KN, Kelly PJ. Permeability of cortical bone of canine tibiae. Microvasc Res 1987;34: 302-10.

[30] Morris MA, Lopez-Curto JA, Hughes SP, An KN, Bassingthwaighte JB, Kelly PJ. Fluid spaces in canine bone and marrow. Microvasc Res 1982;23: 188-200.

[31] Sugawara Y, Kamioka H, Honjo T, Tezuka K, Takano-Yamamoto T. Three-dimensional reconstruction of chick calvarial osteocytes and their cell processes using confocal microscopy. Bone 2005;36: 877-83.

[32] Beno T, Ciani C, Doty SB, Fritton SP. Structural measurements of osteocyte lacunae and canaliculi using confocal microscopy. In: Proceedings of the 2005 Summer Bioengineering Conference abstract 92348; 2005.

[33] Qin YX, Kaplan T, Saldanha A, Rubin C. Fluid pressure gradients, arising from oscillations in intramedullary pressure, is correlated with the formation of bone and inhibition of intracortical porosity. J Biomech 2003;36: 1427-37.

[34] Hillsley MV, Frangos JA. Bone tissue engineering: the role of interstitial fluid flow. Biotechnol Bioeng 1994;43: 573-81.

[35] Han Y, Cowin SC, Schaffler MB, Weinbaum S. Mechanotransduction and strain amplification in osteocyte cell processes. Proc Natl Acad Sci U S A 2004;101: 16689-94.

[36] Piekarski K, Munro M. Transport mechanism operating between blood supply and osteocytes in long bones. Nature 1977;269: 80-2.

[37] Ayasaka N, Kondo T, Goto T, Kido MA, Nagata E, Tanaka T. Differences in the transport systems between cementocytes and osteocytes in rats using microperoxidase as a tracer. Arch Oral Biol 1992;37: 363-9.

[38] Dillaman RM. Movement of ferritin in the 2-day-old chick femur. Anat Rec 1984;209: 445-53.

[39] Dillaman RM, Roer RD, Gay DM. Fluid movement in bone: theoretical and empirical. J Biomech 1991;24 Suppl 1: 163-77.

[40] Doty SB, Schofield BH. Electron microscopic localization of hydrolytic enzymes in osteoclasts. Histochem J 1972;4: 245-58.

[41] Qin L, Mak AT, Cheng CW, Hung LK, Chan KM. Histomorphological study on pattern of fluid movement in cortical bone in goats. Anat Rec 1999;255: 380-7.

[42] Tanaka T, Sakano A. Differences in permeability of microperoxidase and horseradish peroxidase into the alveolar bone of developing rats. J Dent Res 1985;64: 870-6.

[43] Quintana C, Cowley JM, Marhic C. Electron nanodiffraction and high-resolution electron microscopy studies of the structure and composition of physiological and pathological ferritin. J Struct Biol 2004;147: 166-78.

[44] Mak AF, Qin L, Hung LK, Cheng CW, Tin CF. A histomorphometric observation of flows in cortical bone under dynamic loading. Microvasc Res 2000;59: 290-300.

[45] Kelly PJ, Montgomery RJ, Bronk JT. Reaction of the circulatory system to injury and regeneration. Clin Orthop Relat Res 1990: 275-88.

[46] Winet H. A bone fluid flow hypothesis for muscle pump-driven capillary filtration: II. Proposed role for exercise in erodible scaffold implant incorporation. Eur Cell Mater 2003;6: 1-10; discussion 10-1.

[47] Ajubi NE, Klein-Nulend J, Nijweide PJ, Vrijheid-Lammers T, Alblas MJ, Burger EH. Pulsating fluid flow increases prostaglandin production by cultured chicken osteocytes--a cytoskeleton-dependent process. Biochem Biophys Res Commun 1996;225: 62-8.

[48] Jiang JX, Cherian PP. Hemichannels formed by connexin 43 play an important role in the release of prostaglandin E(2) by osteocytes in response to mechanical strain. Cell Commun Adhes 2003;10: 259-64.

[49] Kamioka H, Sugawara Y, Honjo T, Yamashiro T, Takano-Yamamoto T. Terminal differentiation of osteoblasts to osteocytes is accompanied by dramatic changes in the distribution of actin-binding proteins. J Bone Miner Res 2004;19: 471-8.

[50] Pavalko FM, Chen NX, Turner CH, Burr DB, Atkinson S, Hsieh YF, Qiu J, Duncan RL. Fluid shear-induced mechanical signaling in MC3T3-E1 osteoblasts requires cytoskeleton-integrin interactions. Am J Physiol 1998;275: C1591-601.

[51] Reilly GC, Haut TR, Yellowley CE, Donahue HJ, Jacobs CR. Fluid flow induced PGE2 release by bone cells is reduced by glycocalyx degradation whereas calcium signals are not. Biorheology 2003;40: 591-603.

[52] Chrischilles EA, Butler CD, Davis CS, Wallace RB. A model of lifetime osteoporosis impact. Arch Intern Med 1991;151: 2026-32.

[53] Martin RB, Butcher RL, Sherwood LL, Buckendahl P, Boyd RD, Farris D, Sharkey N, Dannucci G. Effects of ovariectomy in beagle dogs. Bone 1987;8: 23-31.

[54] Snow GR, Anderson C. The effects of 17 beta-estradiol and progestagen on trabecular bone remodeling in oophorectomized dogs. Calcif Tissue Int 1986;39: 198-205.

[55] Snow GR, Karambolova KK, Anderson C. Bone remodeling in the lumbar vertebrae of young adult beagles. Am J Vet Res 1986;47: 1275-7.

[56] Turner AS, Alvis M, Myers W, Stevens ML, Lundy MW. Changes in bone mineral density and bone-specific alkaline phosphatase in ovariectomized ewes. Bone 1995;17: 395S-402S.

[57] Turner AS, Mallinckrodt CH, Alvis MR, Bryant HU. Dual-energy X-ray absorptiometry in sheep: experiences with in vivo and ex vivo studies. Bone 1995;17: 381S-387S.

[58] Frost HM, Jee WS. On the rat model of human osteopenias and osteoporoses. Bone Miner 1992;18: 227-36.

[59] Wronski TJ, Dann LM, Scott KS, Cintron M. Long-term effects of ovariectomy and aging on the rat skeleton. Calcif Tissue Int 1989;45: 360-6.

[60] Wronski TJ, Lowry PL, Walsh CC, Ignaszewski LA. Skeletal alterations in ovariectomized rats. Calcif Tissue Int 1985;37: 324-8.

[61] Jordan VC, Phelps E, Lindgren JU. Effects of anti-estrogens on bone in castrated and intact female rats. Breast Cancer Res Treat 1987;10: 31-5.

[62] Kalu DN, Liu CC, Hardin RR, Hollis BW. The aged rat model of ovarian hormone deficiency bone loss. Endocrinology 1989;124: 7-16.

[63] Turner RT, Vandersteenhoven JJ, Bell NH. The effects of ovariectomy and 17 beta-estradiol on cortical bone histomorphometry in growing rats. J Bone Miner Res 1987;2: 115-22.

[64] Wronski TJ, Walsh CC, Ignaszewski LA. Histologic evidence for osteopenia and increased bone turnover in ovariectomized rats. Bone 1986;7: 119-23.

[65] Westerlind KC, Wronski TJ, Ritman EL, Luo ZP, An KN, Bell NH, Turner RT. Estrogen regulates the rate of bone turnover but bone balance in ovariectomized rats is modulated by prevailing mechanical strain. Proc Natl Acad Sci U S A 1997;94: 4199-204.

[66] Ke HZ, Jee WS, Ito H, Setterberg RB, Li M, Lin BY, Liang XG, Ma YF. Greater bone formation induction occurred in aged than young cancellous bone sites. Bone 1993;14: 481-5.

[67] Wronski TJ, Dann LM, Horner SL. Time course of vertebral osteopenia in ovariectomized rats. Bone l1989;10: 295-301.

[68] Pawley JB. Handbook of Biological Confocal Microscopy. Wisconsin: Springer; 1995.

[69] Colopy SA, Benz-Dean J, Barrett JG, Sample SJ, Lu Y, Danova NA, Kalscheur VL, Vanderby R, Jr., Markel MD, Muir P. Response of the osteocyte syncytium adjacent to and distant from linear microcracks during adaptation to cyclic fatigue loading. Bone 2004;35: 881-91.

[70] Muir P, Sample SJ, Barrett JG, McCarthy J, Vanderby R, Jr., Markel MD, Prokuski LJ, Kalscheur VL. Effect of fatigue loading and associated matrix microdamage on bone blood flow and interstitial fluid flow. Bone 2007;40: 948-56.

[71] Wang L, Wang Y, Han Y, Henderson SC, Majeska RJ, Weinbaum S, Schaffler MB. In situ measurement of solute transport in the bone lacunar-canalicular system. Proc Natl Acad Sci U S A 2005;102: 11911-6.

[72] Schatten H, Pawley JB. Biological Low Voltage Field Emission Scanning Electron Microscopy. 2007.

[73] Boyde A, Hobdell M. Scanning electron microscopy of bone. Calcif Tissue Res 1968: Suppl:4-4B.

[74] Miller SC, Wronski TJ. Long-term osteopenic changes in cancellous bone structure in ovariectomized rats. Anat Rec 1993;236: 433-41.

[75] Rohanizadeh R, LeGeros RZ, Bohic S, Pilet P, Barbier A, Daculsi G. Ultrastructural properties of bone mineral of control and tiludronate-treated osteoporotic rat. Calcif Tissue Int 2000;67: 330-6.

[76] Whitehouse WJ, Dyson ED, Jackson CK. The scanning electron microscope in studies of trabecular bone from a human vertebral body. J Anat 1971;108: 481-96.

[77] Davies JE, Baldan N. Scanning electron microscopy of the bone-bioactive implant interface. J Biomed Mater Res 1997;36: 429-40.

[78] Ciani C, Doty SB, Fritton SP. Transport of different sized probes into bone's lacunar-canalicular porosity. In: Transactions of the 51st Meeting of the Orthopedic Research Society; 2005. p. 1644.

[79] da Vinci L, O'Malley CD. Leonardo on the Human Boby. Dover: Courrier Dover Publications; 1983.

[80] Jee WSS. The skeletal tissues, in Cells and Tissue Biology, A Textbook of Histology. Baltimore: Urban and Schwarzenberg; 1988.

[81] Chicago LU. Stritch School of Medicine website. In.

[82] Zeiss. Confocal Laser Scanning Microscopy. In; 2007.

[83] University P. Radiological & Environmental Management www.purdue.edu/REM/rs/sem.htm.

Chapter2

[1] Ayasaka N, Kondo T, Goto T, Kido MA, Nagata E, Tanaka T. Differences in the transport systems between cementocytes and osteocytes in rats using microperoxidase as a tracer. Arch Oral Biol 1992;37:363-69.

[2] Cooper RR, Milgram JW, Robinson RA. Morphology of the osteon. An electron microscopy study. J Bone Joint Surg 1966;48A:1239-1271.

[3] Cowin SC, Weinbaum S, Zeng Y. A case for bone canaliculi as the anatomical site of strain generated potentials. J Biomech 1995;28:1281-97.

[4] Cowley JM, Janney DE, Gerkin RC, Buseck PR. The structure of ferritin cores determined by electron nanodiffraction. J Struct Biol 2000;131:210-16.

[5] Dillaman RM. Movement of ferritin in the 2-day-old chick femur. Anat Rec 1984;209:445-53.

[6] Dillaman RM, Roer RD, Gay DM. Fluid movement in bone: theoretical and empirical. J Biomech 1991;24:163-77.

[7] Domínguez-Vera JM, Colacio E. Nanoparticles of prussian blue ferritin: A new route for obtaining nanomaterials. Inorg Chem 2003;42:6983-85.

[8] Doty SB, Schofield BH. Metabolic and structural changes within osteocytes of rat bone. In: Talmage RV, Munson PL, editors. Calcium, parathyroid hormone and the calcitonins. Amsterdam: Elsevier; 1972; 353-64.

[9] Hillsley MV, Frangos JA. Bone tissue engineering: the role of interstitial fluid flow. Biotechnol Bioeng 1994;43:573-81.

[10] Keanini RG, Roer RD, Dillaman RM. A theoretical model of circulatory interstitial fluid flow and species transport within porous cortical bone. J Biomech 1995;28:901-14.

[11] Kelly PJ, Montgomery RJ, Bronk JT. Reaction of the circulatory system to injury and regeneration. Clin Orthop 1990;254:275-88.

[12] Klein-Nulend J, van der Plas A, Semeins CM, Ajubi NE, Frangos JA, Nijweide PJ, Burger EH. Sensitivity of osteocytes to biomechanical stress in vitro. FASEB J 1995;9:441-45.

[13] Knothe Tate ML, Niederer P, and Knothe U. In vivo tracer transport through the lacunocanalicular system of rat bone in an environment devoid of mechanical loading. Bone 1998;22:107-17.

[14] Knothe Tate ML, Steck R, Forwood MR, Niederer, P. In vivo demonstration of load-induced fluid flow in the rat tibia and its potential implications for processes associated with functional adaptation. J Exp Biol 2000;203:2737-45.

[15] Mak AF, Qin L, Hung LK, Cheng CW, Tin CF. A histomorphometric observation of flows in cortical bone under dynamic loading. Microvasc Res 2000;59:290-300.

[16] Montgomery RJ, Sutker BD, Bronk JT, Smith SR, Kelly PJ. Interstitial fluid flow in cortical bone. Microvasc Res 1988;35:295-307.

[17] Piekarski K, Munro M. Transport mechanism operating between blood supply and osteocytes in long bones. Nature 1977;269:80-2.

[18] Presnell JK, Schreibman MP, Humason GL. Humason's animal tissue techniques. Johns Hopkins Univ. Press; 5th edition; 1997.

[19] Qin L, Mak AT, Cheng CW, Hung LK, Chan KM. Histomorphological study on pattern of fluid movement in cortical bone in goats. Anat Rec 1999;255:380-7.

[20] Quintana C, Cowley JM, Marhic C. Electron nanodiffraction and high-resolution electron microscopy studies of the structure and composition of physiological and pathological ferritin. J Struct Biol 2004;147:166-78.

[21] Squire JM, Chew M, Nneji G, Neals C, Barry J, Michel C. Quasi-periodic substructure in the microvessel endothelial glycocalyx: a possible explanation for molecular filtering? J Struct Biol 2001;136:239-55.

[22] Tami AE, Schaffler MB, Knothe Tate ML. Probing the tissue to subcellular level structure underlying bone's molecular sieving function. Biorheology 2003;40:577-90.

[23] Tanaka T, Sakano A. Differences in permeability of microperoxidase and horseradish peroxidase into the alveolar bone of developing rats. J Dent Res 1985;64: 870-6.

[24] Wang L, Ciani C, Doty SB, Fritton SP. Delineating bone's interstitial fluid flow pathway in vivo. Bone 2004;34:499-509.

[25] Weinbaum S, Cowin SC, and Zeng Y. A model for the excitation of osteocytes by mechanical loading-induced bone fluid shear stresses. J Biomech 1994;27:339-60.

[26] Winet H. A bone fluid flow hypothesis for muscle pump-driven capillary filtration: II Proposed role for exercise in erodible scaffold implant incorporation. Eur Cell Mater 2003;6:1-11.

[27] You L, Cowin SC, Schaffler MB, Weinbaum S. A model for strain amplification in the actin cytoskeleton of osteocytes due to fluid drag on pericellular matrix. J Biomech 2001;34:1375-86.

[28] You LD, Weinbaum S, Cowin SC, Schaffler MB. Ultrastructure of the osteocyte process and its pericellular matrix. Anat Rec 2004;278A:505-13.

Chapter3

[1] Han Y, Cowin SC, Schaffler MB, Weinbaum S. Mechanotransduction and strain amplification in osteocyte cell processes. Proc Natl Acad Sci U S A 2004;101: 16689-94.

[2] Hillsley MV, Frangos JA. Bone tissue engineering: the role of interstitial fluid flow. Biotechnol Bioeng 1994;43: 573-81.

[3] Klein-Nulend J, van der Plas A, Semeins CM, Ajubi NE, Frangos JA, Nijweide PJ, Burger EH. Sensitivity of osteocytes to biomechanical stress in vitro. Faseb J 1995;9: 441-5.

[4] Piekarski K, Munro M. Transport mechanism operating between blood supply and osteocytes in long bones. Nature 1977;269: 80-2.

[5] Weinbaum S, Cowin SC, Zeng Y. A model for the excitation of osteocytes by mechanical loading-induced bone fluid shear stresses. J Biomech 1994;27: 339-60.

[6] You L, Cowin SC, Schaffler MB, Weinbaum S. A model for strain amplification in the actin cytoskeleton of osteocytes due to fluid drag on pericellular matrix. J Biomech 2001;34: 1375-86.

[7] Baylink DJ, Wergedal JE. Bone formation by osteocytes. Am J Physiol 1971;221: 669-78.

[8] Kusuzaki K, Kageyama N, Shinjo H, Murata H, Takeshita H, Ashihara T, Hirasawa Y. A staining method for bone canaliculi. Acta Orthop Scand 1995;66: 166-8.

[9] Li GP, Bronk JT, An KN, Kelly PJ. Permeability of cortical bone of canine tibiae. Microvasc Res 1987;34: 302-10.

[10] Ciani C, Doty SB, Fritton SP. Mapping bone interstitial fluid movement: displacement of ferritin tracer during histological processing. Bone 2005;37: 379-87.

[11] Erben RG. Embedding of bone samples in methylmethacrylate: an improved method suitable for bone histomorphometry, histochemistry, and immunohistochemistry. J Histochem Cytochem 1997;45: 307-13.

[12] Enlow DH. Principle of Bone Remodeling. Springfield, IL: Charles C. Thomas; 1963.

Chapter4

[1] Cooper RR, Milgram JW, Robinson RA. Morphology of the osteon. An electron microscopic study. J Bone Joint Surg Am 1966;48: 1239-71.

[2] Hancox NM. Biology of Bone. Cambridge, England: Cambridge University Press; 1972.

[3] Martin R. B. DBB. Structure, Function and Adaptation of Compact Bone. New York: Raven Press; 1989.

[4] Piekarski K, Munro M. Transport mechanism operating between blood supply and osteocytes in long bones. Nature 1977;269: 80-2.

[5] Knapp HF, Reilly GC, Stemmer A, Niederer P, Knothe Tate ML. Development of preparation methods for and insights obtained from atomic force microscopy of fluid spaces in cortical bone. Scanning 2002;24: 25-33.

[6] You LD, Weinbaum S, Cowin SC, Schaffler MB. Ultrastructure of the osteocyte process and its pericellular matrix. Anat Rec A Discov Mol Cell Evol Biol 2004;278: 505-13.

[7] Weinbaum S, Cowin SC, Zeng Y. A model for the excitation of osteocytes by mechanical loading-induced bone fluid shear stresses. J Biomech 1994;27: 339-60.

[8] You L, Cowin SC, Schaffler MB, Weinbaum S. A model for strain amplification in the actin cytoskeleton of osteocytes due to fluid drag on pericellular matrix. J Biomech 2001;34: 1375-86.

[9] Han Y, Cowin SC, Schaffler MB, Weinbaum S. Mechanotransduction and strain amplification in osteocyte cell processes. Proc Natl Acad Sci U S A 2004;101: 16689-94.

[10] Wang Y, McNamara LM, Schaffler MB, Weinbaum S. A model for the role of integrins in flow induced mechanotransduction in osteocytes. Proc Natl Acad Sci U S A 2007;104: 15941-6.

[11] Cowin SC, Weinbaum S, Zeng Y. A case for bone canaliculi as the anatomical site of strain generated potentials. J Biomech 1995;28: 1281-97.

[12] Doty SB, Schofield BH. Electron microscopic localization of hydrolytic enzymes in osteoclasts. Histochem J 1972;4: 245-58.

[13] Tami AE, Schaffler MB, Knothe Tate ML. Probing the tissue to subcellular level structure underlying bone's molecular sieving function. Biorheology 2003;40: 577-90.

[14] Wang L, Ciani C, Doty SB, Fritton SP. Delineating bone's interstitial fluid pathway in vivo. Bone 2004;34: 499-509.

[15] Martin RB. Determinants of the mechanical properties of bones. J Biomech 1991;24 Suppl 1: 79-88.

[16] McCalden RW, McGeough JA, Barker MB, Court-Brown CM. Age-related changes in the tensile properties of cortical bone. The relative importance of changes in porosity, mineralization, and microstructure. J Bone Joint Surg Am 1993;75: 1193-205.

[17] Schaffler MB, Burr DB. Stiffness of compact bone: effects of porosity and density. J Biomech 1988;21: 13-6.

[18] Yeni YN, Brown CU, Wang Z, Norman TL. The influence of bone morphology on fracture toughness of the human femur and tibia. Bone 1997;21: 453-9.

[19] Knothe Tate ML, Adamson JR, Tami AE, Bauer TW. The osteocyte. Int J Biochem Cell Biol 2004;36: 1-8.

[20] Tomkinson A, Gevers EF, Wit JM, Reeve J, Noble BS. The role of estrogen in the control of rat osteocyte apoptosis. J Bone Miner Res 1998;13: 1243-50.

[21] Tomkinson A, Reeve J, Shaw RW, Noble BS. The death of osteocytes via apoptosis accompanies estrogen withdrawal in human bone. J Clin Endocrinol Metab 1997;82: 3128-35.

[22] Bagi CM, Ammann P, Rizzoli R, Miller SC. Effect of estrogen deficiency on cancellous and cortical bone structure and strength of the femoral neck in rats. Calcif Tissue Int 1997;61: 336-44.

[23] Baldock PA, Need AG, Moore RJ, Durbridge TC, Morris HA. Discordance between bone turnover and bone loss: effects of aging and ovariectomy in the rat. J Bone Miner Res 1999;14: 1442-8.

[24] Wright PH, Jowsey JO, Robb RA. Osteocyte lacunar area in normal bone, hyperparathyroidism, renal disease, and osteoporosis. Surg Forum 1978;29: 558-9.

[25] Wronski TJ, Lowry PL, Walsh CC, Ignaszewski LA. Skeletal alterations in ovariectomized rats. Calcif Tissue Int 1985;37: 324-8.

[26] Baylink DJ, Wergedal JE. Bone formation by osteocytes. Am J Physiol 1971;221: 669-78.

[27] Kusuzaki K, Kageyama N, Shinjo H, Murata H, Takeshita H, Ashihara T, Hirasawa Y. A staining method for bone canaliculi. Acta Orthop Scand 1995;66: 166-8.

[28] Li GP, Bronk JT, An KN, Kelly PJ. Permeability of cortical bone of canine tibiae. Microvasc Res 1987;34: 302-10.

[29] Ferretti M, Muglia MA, Remaggi F, Cane V, Palumbo C. Histomorphometric study on the osteocyte lacuno-canalicular network in animals of different species. II. Parallel-fibered and lamellar bones. Ital J Anat Embryol 1999;104: 121-31.

[30] Remaggi F, Cane V, Palumbo C, Ferretti M. Histomorphometric study on the osteocyte lacuno-canalicular network in animals of different species. I. Woven-fibered and parallel-fibered bones. Ital J Anat Embryol 1998;103: 145-55.

[31] Ciani C, Doty SB, Fritton SP. Mapping bone interstitial fluid movement: displacement of ferritin tracer during histological processing. Bone 2005;37: 379-87.

[32] Schneider P, Stauber M, Voide R, Stampanoni M, Donahue LR, Muller R. Ultrastructural properties in cortical bone vary greatly in two inbred strains of mice as assessed by synchrotron light based micro- and nano-CT. J Bone Miner Res 2007;22: 1557-70.

[33] Kamioka H, Honjo T, Takano-Yamamoto T. A three-dimensional distribution of osteocyte processes revealed by the combination of confocal laser scanning microscopy and differential interference contrast microscopy. Bone 2001;28: 145-9.

[34] Sugawara Y, Kamioka H, Honjo T, Tezuka K, Takano-Yamamoto T. Three-dimensional reconstruction of chick calvarial osteocytes and their cell processes using confocal microscopy. Bone 2005;36: 877-83.

[35] Erben RG. Embedding of bone samples in methylmethacrylate: an improved method suitable for bone histomorphometry, histochemistry, and immunohistochemistry. J Histochem Cytochem 1997;45: 307-13.

[36] Ciani C, Doty SB, Fritton SP. Effective Histological Staining Process Developed to Visualize Bone Interstitial Space Using Confocal Microscopy. Bone submitted, 2008.

[37] Enlow DH. Principle of Bone Remodeling. Springfield, IL: Charles C. Thomas; 1963.

[38] Frost HM, Jee WS. On the rat model of human osteopenias and osteoporoses. Bone Miner 1992;18: 227-36.

[39] Westerlind KC, Wronski TJ, Ritman EL, Luo ZP, An KN, Bell NH, Turner RT. Estrogen regulates the rate of bone turnover but bone balance in ovariectomized rats is modulated by prevailing mechanical strain. Proc Natl Acad Sci U S A 1997;94: 4199-204.

[40] Wronski TJ, Dann LM, Scott KS, Cintron M. Long-term effects of ovariectomy and aging on the rat skeleton. Calcif Tissue Int 1989;45: 360-6.

[41] Frost HM. Micropetrosis. J Bone Joint Surg Am 1960;42-A: 144-50.

[42] Remaggi F, Ferretti M, Cane V, Zaffe D. Histomorphological and chemico-physical analyses of the mineral matrix of micropetrotic human bone. Ann Anat 1996;178: 223-7.

[43] Belanger LF. Osteocytic osteolysis. Calcif Tissue Res 1969;4: 1-12.

[44] Heller-Steinberg M. Ground substance, bone salts, and cellular activity in bone formation and destruction. Am J Anat 1951;89: 347-79.

[45] Lane NE, Yao W, Balooch M, Nalla RK, Balooch G, Habelitz S, Kinney JH, Bonewald LF. Glucocorticoid-treated mice have localized changes in trabecular bone material properties and osteocyte lacunar size that are not observed in placebo-treated or estrogen-deficient mice. J Bone Miner Res 2006;21: 466-76.

[46] Tazawa K, Hoshi K, Kawamoto S, Tanaka M, Ejiri S, Ozawa H. Osteocytic osteolysis observed in rats to which parathyroid hormone was continuously administered. J Bone Miner Metab 2004;22: 524-9.

Chapter5

[1] Cooper RR, Milgram JW, Robinson RA. Morphology of the osteon. An electron microscopic study. J Bone Joint Surg Am 1966;48: 1239-71.

[2] Hancox NM. Biology of Bone. Cambridge, England: Cambridge University Press; 1972.

[3] Martin R. B. DBB. Structure, Function and Adaptation of Compact Bone. New York: Raven Press; 1989.

[4] Qin YX, Kaplan T, Saldanha A, Rubin C. Fluid pressure gradients, arising from oscillations in intramedullary pressure, is correlated with the formation of bone and inhibition of intracortical porosity. J Biomech 2003;36: 1427-37.

[5] Ciani C, Doty SB, Fritton SP. Mapping bone interstitial fluid movement: displacement of ferritin tracer during histological processing. Bone 2005;37: 379-87.

[6] Doty SB, Schofield BH. Electron microscopic localization of hydrolytic enzymes in osteoclasts. Histochem J 1972;4: 245-58.

[7] Knothe Tate ML, Knothe U, Niederer P. Experimental elucidation of mechanical load-induced fluid flow and its potential role in bone metabolism and functional adaptation. Am J Med Sci 1998;316: 189-95.

[8] Knothe Tate ML, Niederer P, Knothe U. In vivo tracer transport through the lacunocanalicular system of rat bone in an environment devoid of mechanical loading. Bone 1998;22: 107-17.

[9] Montgomery RJ, Sutker BD, Bronk JT, Smith SR, Kelly PJ. Interstitial fluid flow in cortical bone. Microvasc Res 1988;35: 295-307.

[10] Qin L, Mak AT, Cheng CW, Hung LK, Chan KM. Histomorphological study on pattern of fluid movement in cortical bone in goats. Anat Rec 1999;255: 380-7.

[11] Tanaka T, Sakano A. Differences in permeability of microperoxidase and horseradish peroxidase into the alveolar bone of developing rats. J Dent Res 1985;64: 870-6.

[12] Wang L, Ciani C, Doty SB, Fritton SP. Delineating bone's interstitial fluid pathway in vivo. Bone 2004;34: 499-509.

[13] Knothe Tate ML, Knothe U. An ex vivo model to study transport processes and fluid flow in loaded bone. J Biomech 2000;33: 247-54.

[14] Mak AF, Qin L, Hung LK, Cheng CW, Tin CF. A histomorphometric observation of flows in cortical bone under dynamic loading. Microvasc Res 2000;59: 290-300.

[15] Tami AE, Schaffler MB, Knothe Tate ML. Probing the tissue to subcellular level structure underlying bone's molecular sieving function. Biorheology 2003;40: 577-90.

[16] Burger EH, Klein-Nulend J. Mechanotransduction in bone--role of the lacuno-canalicular network. Faseb J 1999;13 Suppl: S101-12.

[17] Cowin SC, Weinbaum S, Zeng Y. A case for bone canaliculi as the anatomical site of strain generated potentials. J Biomech 1995;28: 1281-97.

[18] Klein-Nulend J, van der Plas A, Semeins CM, Ajubi NE, Frangos JA, Nijweide PJ, Burger EH. Sensitivity of osteocytes to biomechanical stress in vitro. Faseb J 1995;9: 441-5.

[19] Wang Y, McNamara LM, Schaffler MB, Weinbaum S. A model for the role of integrins in flow induced mechanotransduction in osteocytes. Proc Natl Acad Sci U S A 2007;104: 15941-6.

[20] Weinbaum S, Cowin SC, Zeng Y. A model for the excitation of osteocytes by mechanical loading-induced bone fluid shear stresses. J Biomech 1994;27: 339-60.

[21] You L, Cowin SC, Schaffler MB, Weinbaum S. A model for strain amplification in the actin cytoskeleton of osteocytes due to fluid drag on pericellular matrix. J Biomech 2001;34: 1375-86.

[22] Han Y, Cowin SC, Schaffler MB, Weinbaum S. Mechanotransduction and strain amplification in osteocyte cell processes. Proc Natl Acad Sci U S A 2004;101: 16689-94.

[23] Ajubi NE, Klein-Nulend J, Alblas MJ, Burger EH, Nijweide PJ. Signal transduction pathways involved in fluid flow-induced PGE2 production by cultured osteocytes. Am J Physiol 1999;276: E171-8.

[24] Ajubi NE, Klein-Nulend J, Nijweide PJ, Vrijheid-Lammers T, Alblas MJ, Burger EH. Pulsating fluid flow increases prostaglandin production by cultured chicken osteocytes--a cytoskeleton-dependent process. Biochem Biophys Res Commun 1996;225: 62-8.

[25] Klein-Nulend J, Roelofsen J, Sterck JG, Semeins CM, Burger EH. Mechanical loading stimulates the release of transforming growth factor-beta activity by cultured mouse calvariae and periosteal cells. J Cell Physiol 1995;163: 115-9.

[26] Lean JM, Mackay AG, Chow JW, Chambers TJ. Osteocytic expression of mRNA for c-fos and IGF-I: an immediate early gene response to an osteogenic stimulus. Am J Physiol 1996;270: E937-45.

[27] Mikuni-Takagaki Y, Suzuki Y, Kawase T, Saito S. Distinct responses of different populations of bone cells to mechanical stress. Endocrinology 1996;137: 2028-35.

[28] Skerry TM, Bitensky L, Chayen J, Lanyon LE. Early strain-related changes in enzyme activity in osteocytes following bone loading in vivo. J Bone Miner Res 1989;4: 783-8.

[29] Pavalko FM, Chen NX, Turner CH, Burr DB, Atkinson S, Hsieh YF, Qiu J, Duncan RL. Fluid shear-induced mechanical signaling in MC3T3-E1 osteoblasts requires cytoskeleton-integrin interactions. Am J Physiol 1998;275: C1591-601.

[30] Tomkinson A, Gevers EF, Wit JM, Reeve J, Noble BS. The role of estrogen in the control of rat osteocyte apoptosis. J Bone Miner Res 1998;13: 1243-50.

[31] Tomkinson A, Reeve J, Shaw RW, Noble BS. The death of osteocytes via apoptosis accompanies estrogen withdrawal in human bone. J Clin Endocrinol Metab 1997;82: 3128-35.

[32] Frost HM, Jee WS. On the rat model of human osteopenias and osteoporoses. Bone Miner 1992;18: 227-36.

[33] Wronski TJ, Dann LM, Scott KS, Cintron M. Long-term effects of ovariectomy and aging on the rat skeleton. Calcif Tissue Int 1989;45: 360-6.

[34] Belanger LF. Osteocytic osteolysis. Calcif Tissue Res 1969;4: 1-12.

[35] Heller-Steinberg M. Ground substance, bone salts, and cellular activity in bone formation and destruction. Am J Anat 1951;89: 347-79.

[36] Baylink DJ, Wergedal JE. Bone formation by osteocytes. Am J Physiol 1971;221: 669-78.

[37] Tazawa K, Hoshi K, Kawamoto S, Tanaka M, Ejiri S, Ozawa H. Osteocytic osteolysis observed in rats to which parathyroid hormone was continuously administered. J Bone Miner Metab 2004;22: 524-9.

[38] Wright PH, Jowsey JO, Robb RA. Osteocyte lacunar area in normal bone, hyperparathyroidism, renal disease, and osteoporosis. Surg Forum 1978;29: 558-9.

[39] You LD, Weinbaum S, Cowin SC, Schaffler MB. Ultrastructure of the osteocyte process and its pericellular matrix. Anat Rec A Discov Mol Cell Evol Biol 2004;278: 505-13.

Chapter6

[1] Dillaman RM. Movement of ferritin in the 2-day-old chick femur. Anat Rec 1984;209: 445-53.

[2] Mak AF, Qin L, Hung LK, Cheng CW, Tin CF. A histomorphometric observation of flows in cortical bone under dynamic loading. Microvasc Res 2000;59: 290-300.

[3] Montgomery RJ, Sutker BD, Bronk JT, Smith SR, Kelly PJ. Interstitial fluid flow in cortical bone. Microvasc Res 1988;35: 295-307.

[4] Qin L, Mak AT, Cheng CW, Hung LK, Chan KM. Histomorphological study on pattern of fluid movement in cortical bone in goats. Anat Rec 1999;255: 380-7.

[5] Dillaman RM, Roer RD, Gay DM. Fluid movement in bone: theoretical and empirical. J Biomech 1991;24 Suppl 1: 163-77.

[6] Hillsley MV, Frangos JA. Bone tissue engineering: the role of interstitial fluid flow. Biotechnol Bioeng 1994;43: 573-81.

[7] Kelly PJ, Montgomery RJ, Bronk JT. Reaction of the circulatory system to injury and regeneration. Clin Orthop Relat Res 1990: 275-88.

[8] Winet H. A bone fluid flow hypothesis for muscle pump-driven capillary filtration: II. Proposed role for exercise in erodible scaffold implant incorporation. Eur Cell Mater 2003;6: 1-10; discussion 10-1.

[9] Keanini RG, Roer RD, Dillaman RM. A theoretical model of circulatory interstitial fluid flow and species transport within porous cortical bone. J Biomech 1995;28: 901-14.

[10] Wang L, Ciani C, Doty SB, Fritton SP. Delineating bone's interstitial fluid pathway in vivo. Bone 2004;34: 499-509.

[11] Ciani C, Doty SB, Fritton SP. Mapping bone interstitial fluid movement: displacement of ferritin tracer during histological processing. Bone 2005;37: 379-87.

[12] Enlow DH. Principle of Bone Remodeling. Springfield, IL: Charles C. Thomas; 1963.

[13] Baldock PA, Need AG, Moore RJ, Durbridge TC, Morris HA. Discordance between bone turnover and bone loss: effects of aging and ovariectomy in the rat. J Bone Miner Res 1999;14: 1442-8.

[14] Baylink DJ, Wergedal JE. Bone formation by osteocytes. Am J Physiol 1971;221: 669-78.

[15] Tomkinson A, Gevers EF, Wit JM, Reeve J, Noble BS. The role of estrogen in the control of rat osteocyte apoptosis. J Bone Miner Res 1998;13: 1243-50.

[16] Tomkinson A, Reeve J, Shaw RW, Noble BS. The death of osteocytes via apoptosis accompanies estrogen withdrawal in human bone. J Clin Endocrinol Metab 1997;82: 3128-35.

[17] Wright PH, Jowsey JO, Robb RA. Osteocyte lacunar area in normal bone, hyperparathyroidism, renal disease, and osteoporosis. Surg Forum 1978;29: 558-9.

[18] Wronski TJ, Lowry PL, Walsh CC, Ignaszewski LA. Skeletal alterations in ovariectomized rats. Calcif Tissue Int 1985;37: 324-8.

[19] Frost HM, Jee WS. On the rat model of human osteopenias and osteoporoses. Bone Miner 1992;18: 227-36.

[20] Wronski TJ, Dann LM, Scott KS, Cintron M. Long-term effects of ovariectomy and aging on the rat skeleton. Calcif Tissue Int 1989;45: 360-6.

[21] Belanger LF. Osteocytic osteolysis. Calcif Tissue Res 1969;4: 1-12.

[22] You LD, Weinbaum S, Cowin SC, Schaffler MB. Ultrastructure of the osteocyte process and its pericellular matrix. Anat Rec A Discov Mol Cell Evol Biol 2004;278: 505-13.

[23] Wang Y, McNamara LM, Schaffler MB, Weinbaum S. A model for the role of integrins in flow induced mechanotransduction in osteocytes. Proc Natl Acad Sci U S A 2007;104: 15941-6.

[24] Wang L, Wang Y, Han Y, Henderson SC, Majeska RJ, Weinbaum S, Schaffler MB. In situ measurement of solute transport in the bone lacunar-canalicular system. Proc Natl Acad Sci U S A l2005;102: 1911-6.